Diss. No. 20813

Catalytic urea decomposition, side-reactions and urea evaporation in the selective catalytic reduction of NO$_x$

A dissertation submitted to

ETH ZURICH

for the degree of

Doctor of Sciences

presented by

ANDREAS MANUEL BERNHARD

M.Sc., University of Berne

Born April 29th, 1984

citizen of Seeberg

accepted on the recommendation of

Prof. Dr. A. Wokaun, examiner

Prof. Dr. J. A. van Bokhoven, co-examiner

Dr. O. Kröcher, co-examiner

2012

Acknowledgements

Table of contents

Summary

Nitrogen oxides (NO_x) from lean combustion processes are an important pollutant in industrialized countries. A widely used technology to reduce NO_x emissions is the selective catalytic reduction (SCR) with ammonia. SCR has been applied in fossil power plants since the 1970s. Today, SCR is also established in trucks, where is has been applied for about one decade, and its application in diesel passenger cars is emerging. SCR is likely to become a key technology to comply with the upcoming Euro 6 legislation. An important drawback of the SCR process is the need for the toxic reducing agent ammonia. In mobile applications, ammonia is usually replaced by safe aqueous urea solution (AdBlue®), which is dosed into the hot exhaust gas to release ammonia upon decomposition.

Urea decomposition is a two-step reaction. The first step is the urea thermolysis into ammonia and isocyanic acid. Thermolysis is usually thought to be a solely thermal reaction. The second step is isocyanic acid hydrolysis, which takes place on the SCR catalyst or on a dedicated hydrolysis catalyst. Since the exhaust gas temperature and the residence time in the exhaust pipe is insufficient for complete thermal urea decomposition, a major fraction of the dosed urea remains intact before it enters the catalyst. Intact urea or decomposition byproducts may form solid deposits in the exhaust pipe and on the catalyst. In spite of the commercial relevance of urea-SCR, little is known about the catalytic decomposition of urea and byproducts.

In the presented thesis, urea thermolysis, the first step of urea decomposition, was found to be a catalytic reaction. A water-free catalyst screening showed the activity order anatase TiO_2 > H-ZSM-5 $\approx$ Al_2O_3 >

Summary

$ZrO_2 > SiO_2$. The urea hydrolysis activities exhibited a different order: ZrO_2 > anatase TiO_2 > Al_2O_3 > H-ZSM-5 > SiO_2. The high urea hydrolysis activity of the ZrO_2 catalyst in spite of its low thermolysis activity suggests that urea hydrolyzes directly on ZrO_2 without intermediate isocyanic acid formation. The hydrolysis of pure isocyanic acid was much faster than urea hydrolysis; hence catalytic urea thermolysis must be the rate-determining step in catalytic urea hydrolysis on anatase TiO_2, Al_2O_3 and H-ZSM-5.

An investigation of the side-reactions on anatase TiO_2 showed that the undesired byproducts biuret, cyanuric acid and melamine can also be catalytically hydrolyzed. TiO_2 was chosen for these experiments because TiO_2 is used as a dedicated hydrolysis catalyst in some commercial SCR systems.

In the absence of a catalyst, urea was found to sublime from an inert monolith impregnated with urea. The high carrier gas flow rate relative to the amount of urea present on the monolith and the large geometric surface area of the monolith allowed urea sublimation to be faster than urea thermolysis. This result suggests that urea evaporation is relevant to the urea-SCR process, too. Urea was confirmed to exist in the gas phase in monomolecular form at atmospheric pressure by Fourier transform infrared (FTIR) spectroscopy. Moreover, a method to quantify gaseous urea by FTIR spectroscopy was developed.

Considering urea evaporation and catalytic urea decomposition is likely to improve future computer models used to design SCR systems.

Zusammenfassung

Stickoxide (NO_x) aus mageren Verbrennungsprozessen sind ein in Industrieländern bedeutender Schadstoff. Für die NO_x-Reduktion ist die selektive katalytische Reduktion (SCR) mit Ammoniak weit verbreitet. SCR wird seit den 1970er Jahren in fossilen Kraftwerken eingesetzt. Heute ist SCR für Lastwagen etabliert, wo dieses Verfahren seit etwa zehn Jahren eingesetzt wird, und Anwendungen in Personenwagen nehmen zu. Wahrscheinlich wird SCR für die Einhaltung der bevorstehenden Euro 6 Abgasvorschrift eine Schlüsselrolle spielen. Ein bedeutender Nachteil des SCR Verfahrens ist der Bedarf nach dem giftigen Reduktionsmittel Ammoniak. Für mobile Anwendungen wird Ammoniak meistens durch eine harmlose wässrige Harnstofflösung (AdBlue®) ersetzt, welche sich im heissen Abgas zu Ammoniak zersetzt.

Die Harnstoffzersetzung läuft in zwei Reaktionsschritten ab. Der erste Schritt ist die Thermolyse zu Ammoniak und Isocyansäure. Die Thermolyse gilt in der Regel als eine rein thermische Reaktion. Der zweite Schritt ist die Hydrolyse der Isocyansäure auf dem SCR Katalysator oder auf einem dezidierten Hydrolysekatalysator. Da die Abgastemperatur und die Aufenthaltszeit im Auspuff nicht ausreichen für eine vollständige thermische Zersetzung, erreicht ein grosser Teil des dosierten Harnstoffs den Katalysator. Intakter Harnstoff oder Nebenprodukte der Zersetzung können im Abgasrohr und auf dem Katalysator feste Ablagerungen bilden. Über die katalytische Zersetzung von Harnstoff und Nebenprodukten ist jedoch trotz der wirtschaftlichen Bedeutung des SCR Verfahrens nur wenig bekannt.

Zusammenfassung

Die vorliegende Arbeit zeigt, dass die Harnstoffthermolyse eine katalytische Reaktion ist. In einem wasserfreien Katalysatorscreening wurden folgende Thermolyseaktivitäten gefunden: Anatas TiO_2 > H-ZSM-5 $\approx$ Al_2O_3 > ZrO_2 > SiO_2. Die Hydrolyseaktivitäten zeigten eine andere Reihenfolge: ZrO_2 > Anatas TiO_2 > Al_2O_3 > H-ZSM-5 > SiO_2. Die hohe Hydrolyse-, aber geringe Thermolyseaktivität des ZrO_2 Katalysators weist darauf hin, dass Harnstoff auf ZrO_2 direkt hydrolysiert, ohne intermediär Isocyansäure zu bilden. Die Hydrolyse reiner Isocyansäure war wesentlich schneller als die Harnstoffhydrolyse, folglich muss die katalytische Harnstoffthermolyse auf Anatas TiO_2, Al_2O_3 und H-ZSM-5 geschwindigkeitsbestimmend sein.

Eine Untersuchung der Nebenreaktionen auf Anatas TiO_2 hat gezeigt, dass auch die Hydrolyse der unerwünschten Nebenprodukte Biuret, Cyanursäure und Melamin katalysiert wird.

Ohne Katalysator konnte Harnstoff von einem inerten, mit Harnstoff imprägnierten Monolithen sublimiert werden. Der hohe Trägergasfluss relativ zu der Harnstoffmenge auf dem Monolithen, und die grosse Oberfläche des Monolithen ermöglichten es der Harnstoffsublimation schneller abzulaufen als der Harnstoffzersetzung. Mittels Fourier-Transformations-Infrarotspektroskopie (FTIR) konnte nachgewiesen werden, dass gasförmiger Harnstoff bei Atmosphärendruck in monomolekularer Form vorliegt. Ausserdem wurde eine Quantifizierungsmethode für gasförmigen Harnstoff mittels FTIR Spektroskopie bei Atmosphärendruck entwickelt.

Die Berücksichtigung der katalytischen Harnstoffzersetzung und der Harnstoffverdampfung sollte zukünftige Computermodelle verbessern, welche für die Auslegung von SCR Systemen eingesetzt werden.

Abbreviations and general formulae

α	$\alpha = NH_3/NO_x$ or $\alpha = 2\times urea/NO_x$
CFD	computational fluid dynamic
CYA	cyanuric acid, IUPAC name: 1,3,5-Triazinane-2,4,6-trione
$DeNO_x$	$DeNO_x = (NO_{x,in} - NO_{x,out})/NO_{x,in}$
DFT	density functional theory
DRIFT	diffuse reflectance infrared Fourier transform
DSC	differential scanning calorimetry
EtOH	ethanol
FTIR	Fourier transform infrared
GHSV	Gas hourly space velocity
	= gas volume flow at STP per catalyst volume
HNCO	isocyanic acid
MeOH	methanol
NO_x	nitrogen oxides, $NO_x = NO + NO_2$
STP	standard temperature and pressure: 0°C, 1013 mbar
TGA	thermogravimetric analysis
TPD	temperature programmed desorption

1. Introduction

1.1. Background

Nitrogen oxide (NO_x) is an important pollutant in industrialized countries. NO_x itself is toxic; moreover, it contributes to high ground-level ozone (O_3) concentrations and to acid rain [1, 2]. The main sources of NO_x are combustion processes [3], where NO_x is formed by N_2 oxidation at high temperature (thermal NO_x), by oxidation of nitrogen contained in the fuel (fuel NO_x) or by reactions of N_2 with intermediate hydrocarbon (HC) fragments from fuel combustion (prompt NO_x) [4]. In diesel engines, thermal NO_x formation is predominant with NO being the main constituent of the NO_x [4]. Besides, smaller amounts of NO_2 are formed, whereas other nitrogen oxides like N_2O, N_2O_5, NO_3^- are usually negligible [4]. Thermal NO formation is described by the well accepted Zeldovich mechanism [5]:

Zeldovich two-step mechanism: $N_2 + O \rightarrow NO + N$

Zeldovich two-step mechanism: $N + O_2 \rightarrow NO + O$

Extended Zeldovich mechanism: $N + OH \rightarrow NO + H$
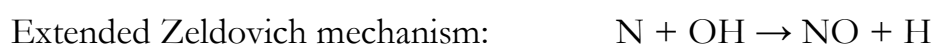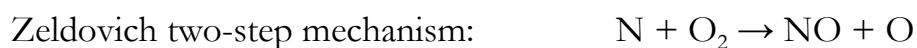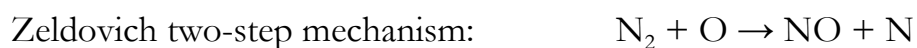
Diesel engines are widely used in trucks, busses, construction machines, ships, and so forth. Also, the market share of passenger cars equipped with diesel engines is increasing. Diesel engines offer better fuel economy than gasoline engines [6]. On the other hand, diesel engines require a sophisticated exhaust aftertreatment system. Unfortunately, the tree-way-catalyst, which reduces three classes of pollutants in the gasoline exhaust, namely CO, NO_x and HC, is not applicable for diesel exhaust because of

the presence of excess O_2. Diesel engines combust a lean air-fuel mixture ($\lambda>1$), whereas most gasoline engines combust a stoichiometric air-fuel mixture ($\lambda=1$). In the presence of excess O_2, the tree-way catalyst cannot reduce the NO_x, because the CO, which would preferentially react with NO_x rather than O_2 traces in gasoline exhaust, is immediately oxidized with O_2.

Concerns about health effects of diesel exhaust have lead to the introduction of emission standards, which in turn have induced progress in diesel technology. Table 1-1 shows recent and upcoming emission standards in the European Union. Quite similar regulations apply in many industrialized countries outside Europe.

Table 1-1. EU emission standards for gasoline and diesel engines, table adapted from [7, 8].

Stage	Date	CO	HC	HC + NO$_x$	NO$_x$	PM[a]	PN[b]
Passenger cars with gasoline engine, g/km (#/km for PN)							
Euro 3	01/2000	2.3	0.2	-	0.15	-	-
Euro 4	01/2005	1	0.1	-	0.08	-	-
Euro 5	09/2009	1	0.1[c]	-	0.06	0.005[d]	-
Euro 6	09/2014	1	0.1[c]	-	0.06	0.005[d]	$6.0\times10^{11, d}$
Passenger cars with diesel engine, g/km (#/km for PN)							
Euro 3	01/2000	0.64	-	0.56	0.5	0.05	-
Euro 4	01/2005	0.5	-	0.3	0.25	0.025	-
Euro 5a	09/2000	0.5	-	0.23	0.18	0.005	-
Euro 5b	09/2011	0.5	-	0.23	**0.18**	0.005	6.0×10^{11}
Euro 6	09/2014	0.5	-	0.17	**0.08**	0.005	6.0×10^{11}
Heavy-duty applications with diesel engine, g/kWh, smoke in m^{-1}							
	Date	CO	HC		NO$_x$	PM	Smoke
Euro IV	10/2005	1.5	0.46		3.5	0.02	0.5
Euro V	10/2008	1.5	0.46		**2**	0.02	0.5
Euro VI	10/2013	1.5	0.13		**0.4**	0.01	

a: PM: particulate matter
b: PN: number of particles
c: non-methane HC = 0.068 g/km
d: applicable only to vehicles using direct injection engines

Important measures to reduce the pollutant levels in diesel exhaust include engine improvements like the use of exhaust gas recirculation (EGR), the use of ultra-low sulfur diesel fuel and exhaust aftertreatment like oxidative catalysts, wallflow particulate filters (DPF) [9] and NO_x reduction catalysts.

Among all the regulated emissions, the NO_x emission will be reduced most strongly by the upcoming Euro 6 and Euro VI regulations (Table 1-1). The required reduction of NO_x levels is not likely to be achieved by further optimization of the combustion process alone. Moreover, optimizing a diesel engine for low NO_x emissions increases its soot emissions and its fuel consumption, since a trade-off exists between these properties as shown in Fig. 1-1 [1, 10, 11].
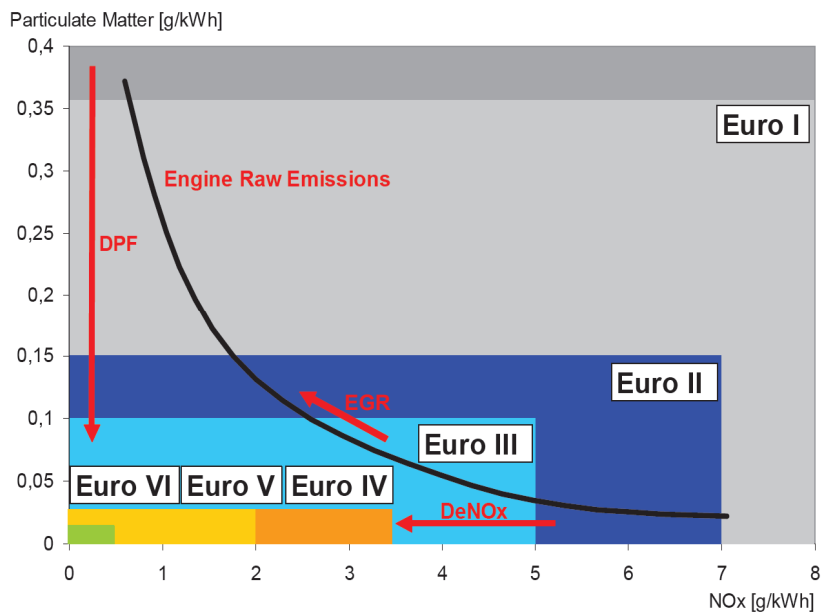
Fig. 1-1. Trade-off between soot and NO_x emission for a heavy-duty diesel engine. Abbreviations: DPF: diesel particulate filter. Figure adapted from [12].

For these reasons, exhaust aftertreatment systems for NO_x in the presence of excess O_2 are likely to come into wide application. A common and

efficient technique for this purpose is the selective catalytic reduction (SCR) with ammonia (NH_3).

1.2. Selective catalytic reduction of NO_x

The SCR process was first used in the 1970s for NO_x reduction in the flue gas of power plants [2]. Today, SCR is also established for smaller-scale applications including heavy duty diesel engines, and it is seen as one of the most promising technologies for adhering to the upcoming Euro VI NO_x emission standard [13].

In the SCR process, NH_3 is added to the exhaust as a reducing agent. NH_3 preferentially reacts with NO_x rather than O_2 due to the selective activity of the catalyst:

Standard-SCR: $4\,NO + 4\,NH_3 + O_2 \rightarrow 4\,N_2 + 6\,H_2O$

Fast-SCR: $2\,NO + 2\,NO_2 + 4\,NH_3 \rightarrow 4\,N_2 + 6\,H_2O$
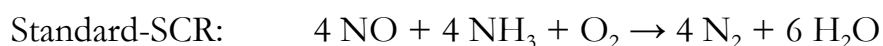
NH_3 can also be oxidized to N_2O and NO in unwanted side-reactions [14]. N_2O is a potent greenhouse gas and NO formation can outbalance the NO_x reduction at very inappropriate operating conditions. The impact of these side-reactions is minimized by optimizing the SCR catalyst and by avoiding too high operating temperatures.

The most widespread class of SCR catalysts is V_2O_5/WO_3-TiO_2, since it is quite inexpensive and exhibits a good activity at moderate temperatures as well as a good sulfur resistance. V_2O_5 provides the redox activity; its concentration is a compromise between activity and selectivity. WO_3 improves the stability of the TiO_2 support towards the anatase-to-rutile phase transition and increases the surface acidity [15]. The typical

formulation for mobile applications is 2 wt% V_2O_5 and 8 wt% WO_3. Surface acidity is a key aspect of an SCR catalyst to achieve efficient adsorption of the reducing agent NH_3, so that as much as possible of the dosed NH_3 is used for NO_x reduction. An SCR catalyst with low surface acidity would only achieve high NO_x conversions in the presence of excess NH_3, which would mean large NH_3 emissions. A large emission of NH_3 cannot be accepted due to its toxicity; furthermore large NH_3 emissions would bring along a high NH_3 consumption. NH_3 emissions are not regulated by emission standards (Table 1-1), but for practical use they are typically limited to a tailpipe concentration of 10 ppm [10]. In some cases, an oxidizing NH_3-slip catalyst is placed downstream of the SCR catalyst to comply with the aim of low NH_3-slip. An important drawback of V_2O_5-based catalysts is the possibility of toxic vanadia emission at very high temperatures. Today, V_2O_5-based SCR catalysts are used for on-road application in the European Union, but not in the USA and in Japan [16].

Another important class of SCR catalysts is metal ion-exchanged zeolites. Cu-exchanged zeolite catalysts provide high low-temperature activity [17] and Fe-exchanged zeolite catalysts maintain their selectivity up to high temperatures [18]. Of course, zeolite SCR catalysts cannot produce toxic vanadia emissions. On the other hand, zeolite SCR catalysts are more expensive than V_2O_5-based SCR catalysts and are therefore rarely used for off-road applications.

1.2.1. NH_3-slip vs. $DeNO_x$ curves

Recording NH_3-slip vs. $DeNO_x$ curves is an elegant method to evaluate SCR performance. The aim of the presented thesis was to investigate urea decomposition, not to evaluate the $DeNO_x$ performance of SCR catalysts.

However, NH_3-slip vs. $DeNO_x$ curves were recorded to evaluate the spray quality of our experimental setup, see chapter 2.1.9. Hence, NH_3-slip vs. $DeNO_x$ curves are introduced here in the context of SCR performance. For a fast test, one may measure the SCR performance at a fixed NH_3 to NO_x ratio of 1 ($\alpha=1$) at different temperatures. However, the NO_x reduction achieved at $\alpha=1$ is not application-relevant because the NH_3-slip should amount to <10 ppm. To determine the $DeNO_x$ at 10 ppm NH_3-slip, α has to be varied. The results obtained with different α-values at one temperature can be plotted as a NH_3-slip vs. $DeNO_x$ curve, where the $DeNO_x$ at 10 ppm NH_3-slip can be obtained by interpolation. Notably, NH_3-slip vs. $DeNO_x$ curves do not only provide the $DeNO_x$ at 10 ppm NH_3-slip, they also allow conclusions on catalyst characteristics like surface acidity. An ideal (nonexistent) SCR catalyst would show a rectangular NH_3-slip vs. $DeNO_x$ curve that goes from 0% to 100% $DeNO_x$ horizontally along the x-axis without any NH_3-slip (diamonds in Fig. 1-2). Only overdosing of the reducing agent would lead to an NH_3-slip, the curve would then rise vertically. A good SCR catalyst operated at its optimal temperature and at low space velocity comes close to the optimal NH_3-slip vs. $DeNO_x$ curve. An SCR catalyst can be poisoned or sintered. Changes in the NH_3-slip vs. $DeNO_x$ curve help to understand such aging processes. For instance, the curve may be bent from a rectangular towards a diagonal shape by poisoning with alkali metals due to a loss of surface acidity (squares in Fig. 1-2) [19], whereas sintering will shift the curve to the left due to decreased redox activity (triangles in Fig. 1-2).
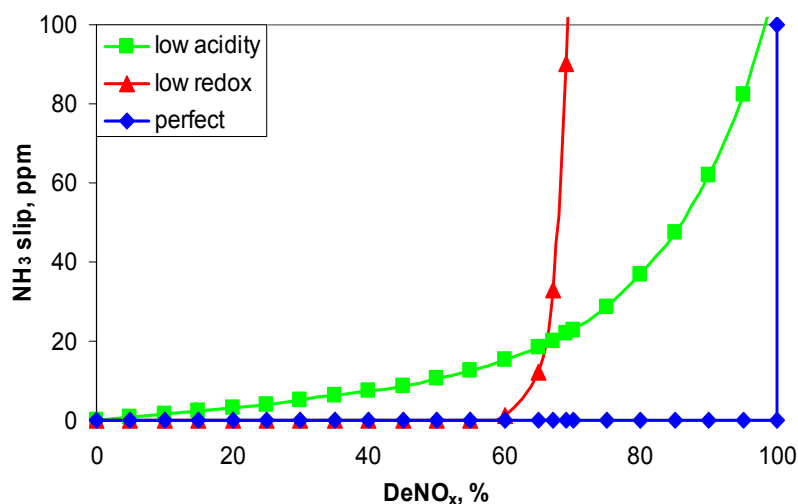
Fig. 1-2. Idealized NH₃-slip vs. DeNOₓ curves.

1.3. NH₃-supply

The reducing agent NH_3 has to be added to the exhaust gas to accomplish NO_x reduction on the SCR catalyst. Unfortunately, pure NH_3 is so toxic that its use is restricted to large-scale stationary applications. For smaller-scale and mobile applications, NH_3 is usually replaced by a non-toxic aqueous urea solution, which releases NH_3 upon decomposition. Urea decomposition will be introduced in the chapters 1.4-1.6.

Before urea solution came into wide application, several other NH_3-precursors were proposed like solid cyanuric acid (CYA), solid urea and aqueous NH_3 solution [20, 21]. In the context of SCR for power plants, inorganic ammonium salts, urea or CYA were mentioned as NH_3-precursors in a Japanese patent in 1977 already [7, 21]. In 1986, a publication by Perry and Siebers about NO_x reduction by CYA received much attention [21, 22]. The authors assumed that isocyanic acid (HNCO), which was reliably produced by CYA decomposition, was the actual

reducing agent, but a later study showed that HNCO was first hydrolyzed to NH_3 [21, 23].

Today, aqueous urea solution is the predominant NH_3-precursor. Urea is inexpensive because it is produced in large amounts in industry as a nitrogen-fertilizer, it is non-toxic, non-corrosive and its aqueous solution can be stored, dosed and decomposed quite easily. 32.5 wt% urea solution exhibits an eutectic melting point at -11°C [14] and is marketed under the trade name AdBlue®. Other names are diesel exhaust fluid (DEF) and aqueous urea solution (AUS). For ships, 40% urea solution is used, because the solution is not exposed to low temperatures in the ships engine room [21]. Despite its advantages, the use of AdBlue® has associated problems like the tendency to form deposits of condensed urea and decomposition byproducts, the need for an expensive heating system to avoid freezing of the solution below -11°C, the limited stability when stored at elevated temperature (shelf life when stored between 30-35°C: 6 months [21, 24]) and the rather low NH_3 storage density of 0.22 kg NH_3 per liter [25]. Formation and decomposition of byproducts will be discussed in chapter 4. Moreover, urea evaporation (chapters 2.1.11 and 3) and catalytic urea decomposition (chapter 5 and 6) will be discussed. The freezing stability, the stability when stored at elevated temperature and/or the NH_3 storage density may be improved by using alternative NH_3-precursor compounds like methanamide, ammonium formate and guanidinium formate (GuFo). The catalytic decomposition of these alternative compounds was previously investigated in our group by Daniel Peitz in his PhD thesis [26]. Another option that completely eliminates freezing issues and provides a high NH_3 storage density, is using solid precursors that release NH_3 upon heating like ammonium carbamate (NH_4COONH_2) and metal ammine salts [21]. The

Danish company Amminex is marketing electrically heated cartouches, containing the metal ammine salt $Sr(NH_3)_XCl_2$, under the name AdAmmine^{TM}.

1.4. Urea thermolysis and evaporation[A]

The predominant NH_3-precursor compound urea decomposes in the hot exhaust gas via a two-step reaction to yield the actual SCR reducing agent NH_3 [14].

Urea thermolysis: $$CO(NH_2)_2 \rightarrow NH_3 + HNCO \tag{1}$$

HNCO hydrolysis: $$HNCO + H_2O \rightarrow NH_3 + CO_2 \tag{2}$$
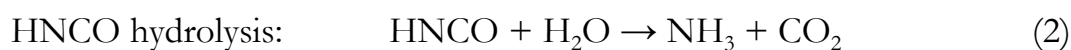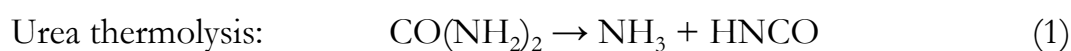
Before these chemical reactions occur, a dosed urea solution aerosol is heated up by the surrounding exhaust gas and the contained water evaporates. The exact state of aggregation of urea during decomposition is still uncertain [27, 28]. Two recent theoretical studies [29, 30] relying on experimental data [8, 31-33] point towards urea evaporation from liquid aerosols and thermolysis in the gas phase. However, another recent study supposes the mentioned chemical reactions take place in solid urea aerosols after the evaporation of water [34].

Urea thermolysis is usually considered a solely thermal reaction, whereas the intermediate HNCO is stable in the gas phase but hydrolyzes on the SCR catalyst or on a dedicated hydrolysis catalyst [14].

[A] This chapter is based on the book section:

D. Peitz, A. Bernhard, O. Kröcher „Ammonia storage and release" in *SCR systems for mobile applications in Urea-SCR technology for deNO$_x$ aftertreatment of Diesel exhausts* (Springer, accepted).

Back in 1966, Schmidt described a process to thermolyze urea into NH_3 and HNCO gas on an industrial scale [35]. In this process, solid urea was blown into a fluidized bed of inert material, which was heated above 300°C. The produced HNCO gas was used for melamine synthesis.

The need for carrying out the urea thermolysis above 300°C in the process described in [35] was because of both kinetic and thermodynamic reasons. At low temperature of e.g. 150°C, the thermolysis of pure urea gas is endothermic and endergonic with $\Delta H^0 = 87.9$ kJ/mol and $\Delta G^0 = 18.5$ kJ/mol [36]. Only above 260°C, the ΔG^0 becomes negative [36]. The hypothetical thermolysis of solid urea into gaseous NH_3 and HNCO is even more endergonic with $\Delta G^0 = 54.7$ kJ/mol at 130°C [36]. Notably, these ΔG^0 values do not represent the situation in the urea-SCR application, because the compounds involved in the SCR reaction are strongly diluted. The dilution corresponds to a low gas partial pressure, which shifts the equilibrium of the urea thermolysis reaction to the product side. Therefore, the urea thermolysis reaction is not limited by the thermodynamic equilibrium under urea-SCR conditions [37]. The thermodynamic equilibrium curve for the actual concentrations in our experiments is included into Fig. 6-6a on page 161. In contrast to urea thermolysis, HNCO hydrolysis is significantly exothermic and exergonic over a broad temperature range even at high partial pressures [36].[A]

[A] This paragraph is partly based on the publication:

A. M. Bernhard, D. Peitz, M. Elsener, T. Schildhauer, O. Kröcher "Catalytic urea hydrolysis in the selective catalytic reduction of NO_x: Catalyst screening and kinetics on anatase TiO_2 and ZrO_2" *Catal. Sci. Technol.* DOI: 10.1039/C2CY20668D.

HNCO is kinetically stable in the gas phase at conditions relevant for SCR [14], but is highly reactive with respect to byproduct formation in the condensed state [38]. Fig. 1-3 shows a reaction scheme for urea decomposition, including the two byproducts biuret and CYA that form first.
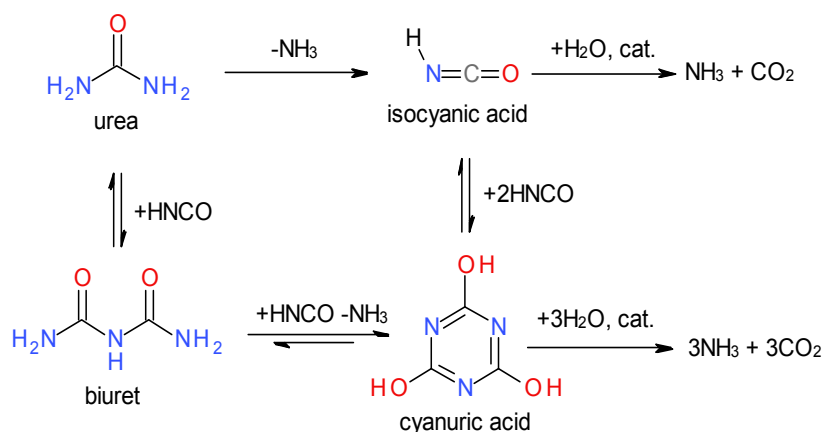
Fig. 1-3. Reaction scheme for urea decomposition, including the two byproducts biuret and CYA that form first.

Basic investigations of urea thermolysis, including the formation and decomposition of byproducts, have been performed using thermogravimetric analysis (TGA) and/or differential scanning calorimetry (DSC) [1, 38-40]. The DSC data consistently show a sharp feature at the melting point of urea at 133°C. Further features strongly depend on experimental conditions, like the type of sample administration [1, 40].

Typically, solid urea was administrated in a crucible. Inside a crucible, volatile compounds produced within the urea melt have to reach the surface of the liquid, desorb to the gas phase and finally leave the crucible by gas diffusion and convection. The slow mass transport of gaseous compounds to leave the crucible leads to long residence times of e.g. the

reactive HNCO inside the crucible, resulting in extensive byproduct formation [1]. Since HNCO is consumed during byproduct formation, the observed HNCO concentration in the gas phase is largely reduced compared to the NH_3 concentration below 300°C [1, 40]. On the other hand, mainly HNCO is observed in the gas phase above 300°C because off CYA decomposition [1, 40]. In addition to experiments using a crucible, Lundström et al. (2009) performed DSC experiments with inert cordierite monoliths, impregnated with urea [40]. Due to the large monolith surface, HNCO desorption was faster than CYA formation, resulting in virtually similar curves for the gas phase concentration of NH_3 and HNCO [40]. An even faster removal of gaseous compounds than in [40] may allow urea sublimation to be predominate over thermolysis [33, 41, 42]. Experiments with a very fast removal of gaseous compounds over a urea film will be reported in chapter 3.

Although urea sublimation under vacuum has been known for decades [33, 41, 42], urea evaporation in the SCR process is usually neglected and urea evaporation under atmospheric pressure has been reported only rarely [38]. However, comparing the saturation vapor pressure of urea [41, 43] with raw NO_x emissions of 200-300 ppm of a modern diesel engine [25] reveals that a temperature of only about 120°C is sufficient for complete sublimation of the required urea (assuming quantitative urea decomposition and quantitative NO_x reduction). Of course, urea-SCR at just 120°C is not feasible due to kinetics of both the urea decomposition and the SCR reaction; however, one should keep in mind that a significant fraction of the dosed urea may reach the catalyst as urea vapor in addition to NH_3, HNCO and urea aerosols.

More realistic experiments on urea decomposition than TGA experiments with urea placed in a crucible were performed with single urea solution droplets on a quartz fiber [8]. Even contact-free experiments are possible with droplets in an acoustical levitator [44]. Experiments with single urea solution droplets also provide information about water evaporation from the droplets as shown in ref. [8, 44]. These data are a valuable input for modeling work, but real urea solution aerosols are much smaller than the droplets used in these studies [8, 44]. It is plausible that, in analogy to the TGA, DSC and TPD experiments mentioned above [1, 38, 40], smaller aerosols with faster mass transport to the surrounding gas favor the desorption of HNCO or even urea vapor over byproduct formation inside the aerosols.

1.5. Urea decomposition byproducts and catalyst deactivation[A]

The byproducts biuret and CYA are observed in the largest quantity at low and moderate temperatures up to about 300°C [38]; however, additional byproducts form in smaller amounts as shown in Fig. 1-4. Substitution of the OH groups of CYA by NH_3 yields the more stable triazines ammelide, ammeline and melamine [38]. Ammelide may also be formed by the reaction of biuret with HNCO, if water is eliminated instead of NH_3 [1]. Melamine may also be produced by trimerization of cyanamide [38] since cyanamide is an intermediate in melamine synthesis [35]. Cyanamide was

---

[A] This chapter is based on the book section:

D. Peitz, A. Bernhard, O. Kröcher „Ammonia storage and release" in *SCR systems for mobile applications in Urea-SCR technology for deNOₓ aftertreatment of Diesel exhausts* (Springer, accepted).

not observed in a previous study on urea decomposition [38], but cyanamide was observed on TiO_2 catalysts, where it may have been formed by disproportionation of HNCO, see [45] and chapter 5. Melamine is more stable than CYA; it slowly sublimes rather than decomposes at temperatures around 300°C [38, 46]. At higher temperatures around 500°C, melamine polymerizes to form melem and melon [1]. Polymeric melamine is water-insoluble and decomposes only above 625°C [1, 39].
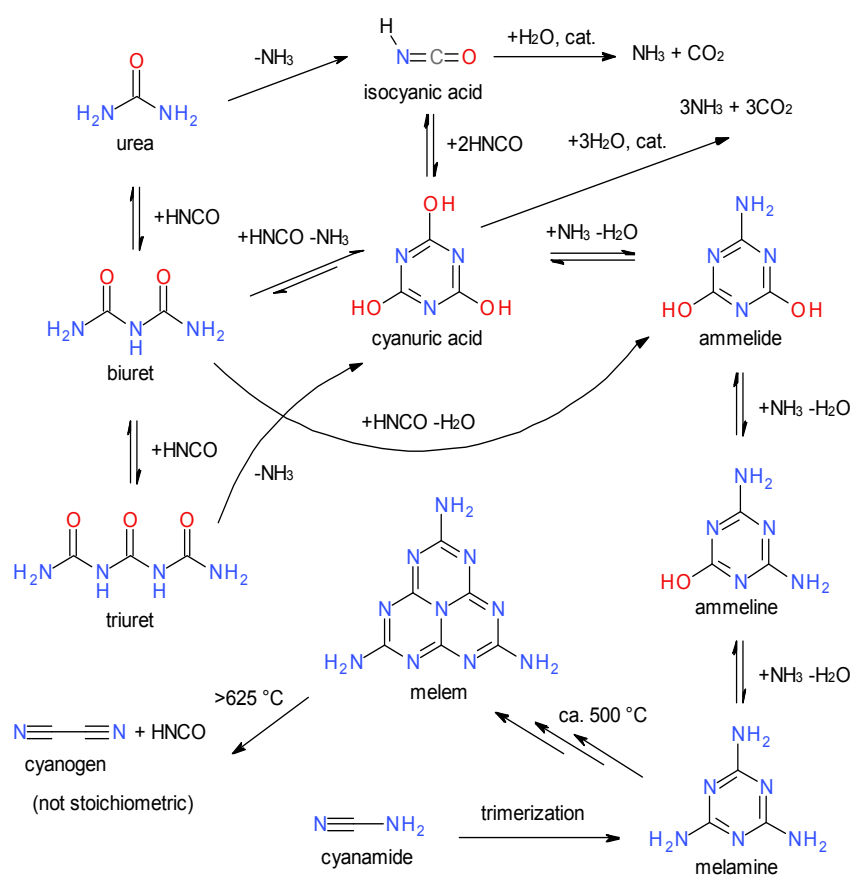
Fig. 1-4. Reaction scheme adapted from chapter 4 and [1, 38].

Of course, byproduct formation is unwanted in the urea-SCR application. One crucial measure to limit byproduct formation is realizing a high spray quality [39, 47]. In addition, the presence of a catalyst is favorable. Since

HNCO, originating from urea thermolysis, plays a key role in byproduct formation, a catalyst can largely reduce byproduct formation by hydrolyzing HNCO [1, 46, 48]. The best hydrolysis catalyst known for the urea-SCR application is anatase TiO_2 [45, 46, 48-50]. Also, V_2O_5/WO_3-TiO_2 [39, 51] and zeolite-based [1, 48, 52] SCR catalysts provide high hydrolysis activities.

If byproducts form on the catalyst in spite of its hydrolysis activity, or if byproduct-containing aerosols are deposited on the catalyst, even these byproducts can be hydrolyzed catalytically. Eichelbaum et al. (2010) found that urea induces a reversible deactivation of an Fe-Beta catalyst [53]. The SCR reaction at 250°C was strongly inhibited by CYA and ammelide, but the activity could be largely restored at 300°C or completely at 500°C [53]. CYA, melamine and even melem can be hydrolyzed on Al_2O_3 [54]. Hydrolysis experiments with biuret, CYA, and melamine on anatase TiO_2 will be reported in chapter 4. In a urea-SCR application, self-regeneration of the SCR-catalyst by its own hydrolysis activity may often be sufficient. If the urea-induced catalyst deactivation is too fast, this deactivation may be avoided by a dedicated hydrolysis catalyst upstream of the SCR catalyst.

1.6. Catalytic urea decomposition[A]

As mentioned in chapter 1.4, urea thermolysis into NH_3 and HNCO is usually considered a solely thermal reaction. If urea thermolyzed completely upstream of the catalyst or if urea thermolysis on the catalyst was very fast, catalytic HNCO hydrolysis would be the rate-determining step in the

---

[A] This chapter is based on the book section:

D. Peitz, A. Bernhard, O. Kröcher „Ammonia storage and release" in *SCR systems for mobile applications in Urea-SCR technology for deNO$_x$ aftertreatment of Diesel exhausts* (Springer, accepted).

overall urea hydrolysis reaction. Catalytic HNCO hydrolysis has been investigated by both experimental and theoretical studies [45, 49-52, 55-57] and is, therefore, well understood. Pure anatase TiO_2 is the best hydrolysis catalyst for urea-SCR applications. ZrO_2 shows even higher activity than TiO_2, but ZrO_2 is sensitive to sulfur poisoning and consequently not used in urea-SCR applications [57]. The addition of V_2O_5 and/or WO_3 to TiO_2 decreases its hydrolysis activity [51, 57]. Also, zeolite catalysts show lower hydrolysis activity than pure TiO_2 [52, 57]. Still, HNCO hydrolysis on SCR catalysts is faster than the actual SCR reaction, indicating that increasing the size of the SCR catalyst is better than placing a hydrolysis catalyst in front of it [51]. When HNCO hydrolysis rates are compared with NO_x reduction rates, one should not forget about urea thermolysis, since a large fraction of the dosed urea remains intact before it enters the SCR catalyst in a real application [14]. Therefore, interaction of molecular urea with catalysts deserves a closer look. Back in 2000, Larrubia et al. carried out a transmission/absorption Fourier transform infrared spectroscopy study on the urea adsorption on a V_2O_5/MoO_3-TiO_2 SCR catalyst [58]. They found that HNCO formed on the catalyst surface from adsorbed urea, which was likely to be explained by catalytic urea thermolysis. Fang et al. (2003) reported that mixing solid urea with a V_2O_5/WO_3-TiO_2 SCR catalyst accelerated the mass loss compared to pure urea in a TGA experiment [39]. Eichelbaum et al. (2010) found an Fe-Beta SCR catalyst and other zeolite catalysts to accelerate the mass loss from urea in analogue TGA experiments [1]. Moreover, the simultaneous presence of a catalyst and water accelerated the mass loss much more strongly [1]. Lundström et al. (2011) found TiO_2, Fe-Beta and γ-Al_2O_3 to catalyze urea hydrolysis, with TiO_2 being most active [48]. In the presented thesis, adsorption of gaseous

urea on TiO_2 was investigated using diffuse reflectance infrared Fourier transform (DRIFT) spectroscopy and high performance liquid chromatography (HPLC) analysis, see chapter 5. Moreover, catalytic urea decomposition was investigated under stationary conditions, see chapter 6.

1.6.1. Anatase TiO_2

Anatase TiO_2 is applied as a highly active, dedicated hydrolysis catalyst in some commercial urea-SCR systems. Therefore, TiO_2 received most attention in the presented thesis and deserves to be introduced in this paragraph. TiO_2 is a white powder, which has been used for a long time in a wide range of common and high technique applications because of its moderate price, chemical stability and nontoxicity [59]. Most often, TiO_2 is used as white pigment in polymers [60], paint and paper. Further, TiO_2 is used as a photocatalyst [59], as a UV-blocker in suncream, as a catalyst support [15] and as a hydrolysis catalyst [57]. TiO_2 exists in three crystalline modifications: rutile, anatase, and brookite [59]. The rutile modification is favored for pigment applications due to its superior light scattering ability and stability [60], whereas the anatase modification is more active as a hydrolysis catalyst [57] and was therefore investigated in the presented thesis.

1.7. Scope of the presented Thesis

The main aim of the presented thesis is to provide information about catalytic urea decomposition in the context of the urea-SCR process. The project was initiated by a research cooperation agreement between TOTAL (France) and Paul Scherrer Institut (PSI), with the objective to reliably avoid deposits during SCR with AdBlue®, by a better understanding of the thermal decomposition of urea and by the development of applicable urea

additives and/or substitutes [61]. The PhD thesis was carried out in the former Exhaust Gas Aftertreatment group (today: Catalysis for Energy group) led by Dr. Oliver Kröcher.

In a first step, the thermal decomposition of urea was re-investigated by TPD experiments. Before the presented thesis stared, TPD experiments with urea placed in a crucible were carried out in our group. These TPD experiments showed poor reproducibility, which was attributed to the ill-defined shape of the molten urea inside the crucible during gas evolution. To improve the reproducibility, inert cordierite monoliths were impregnated with urea and used instead of a crucible. The obtained results were published in "The Journal of Physical Chemistry A" [43]. Chapter 3 of the presented thesis is based on this publication.

The laboratory test reactor for the injection of liquid reducing agents, which was developed by Daniel Peitz in his PhD thesis [26], was adapted to high space velocities and used extensively for urea decomposition experiments. The method development and testing is reported in chapter 2.1 and the results are presented in chapter 6. Chapter 6 is based on the publication in "Catalysis, Science & Technology" [62]. It includes results on catalytic urea thermolysis, which was only supposed to exist when the project was started [61].

Catalytic coatings were also investigated using TPD experiments, with the main focus on byproduct formation and decomposition. These results are presented in chapter 4, which is based on the first publication in "Applied Catalysis B" (published in 2012) [46]. Additionally, urea adsorption and decomposition was investigated using DRIFT spectroscopy; these results

are reported in chapter 5, which is based on the second publication in "Applied Catalysis B" (to be published in 2013) [63].

Catalytic and non-catalytic decomposition of urea additives from TOTAL was investigated by TPD experiments. Also, simultaneous catalytic decomposition of urea and additives, deactivation of an SCR catalyst with the additive and its subsequent regeneration, the influence of the additive on urea-SCR and the influence of the additive on deposit formation was investigated. **All the AdBlue®-additive-related results are presented in a separate, confidential report for TOTAL.**

2. Experimental

2.1. Setup for investigations on NH_3-precursors

Steady-state experiments with urea solutions were carried out using the lab-scale setup developed by Daniel Peitz and described in the publication [64]. Below, this setup is called "spray reactor" in short. The spray reactor marks an important novelty, because common lab-scale setups for testing SCR catalysts do not allow for dosing liquid reducing agents. Instead, NH_3 is used as the reducing agent and compatibility of the catalyst with real liquid reducing agents is only tested at a later stage on a diesel test stand. In this context, the new setup can be seen as a bridging device. For the thesis of Daniel Peitz [26], as well as for the presented thesis, the new setup opened the possibility to investigate the decomposition of liquid SCR reducing agents in a model exhaust gas at steady-state conditions.

2.1.1. Process scheme and heating

Fig. 2-1 shows a scheme of the complete setup.
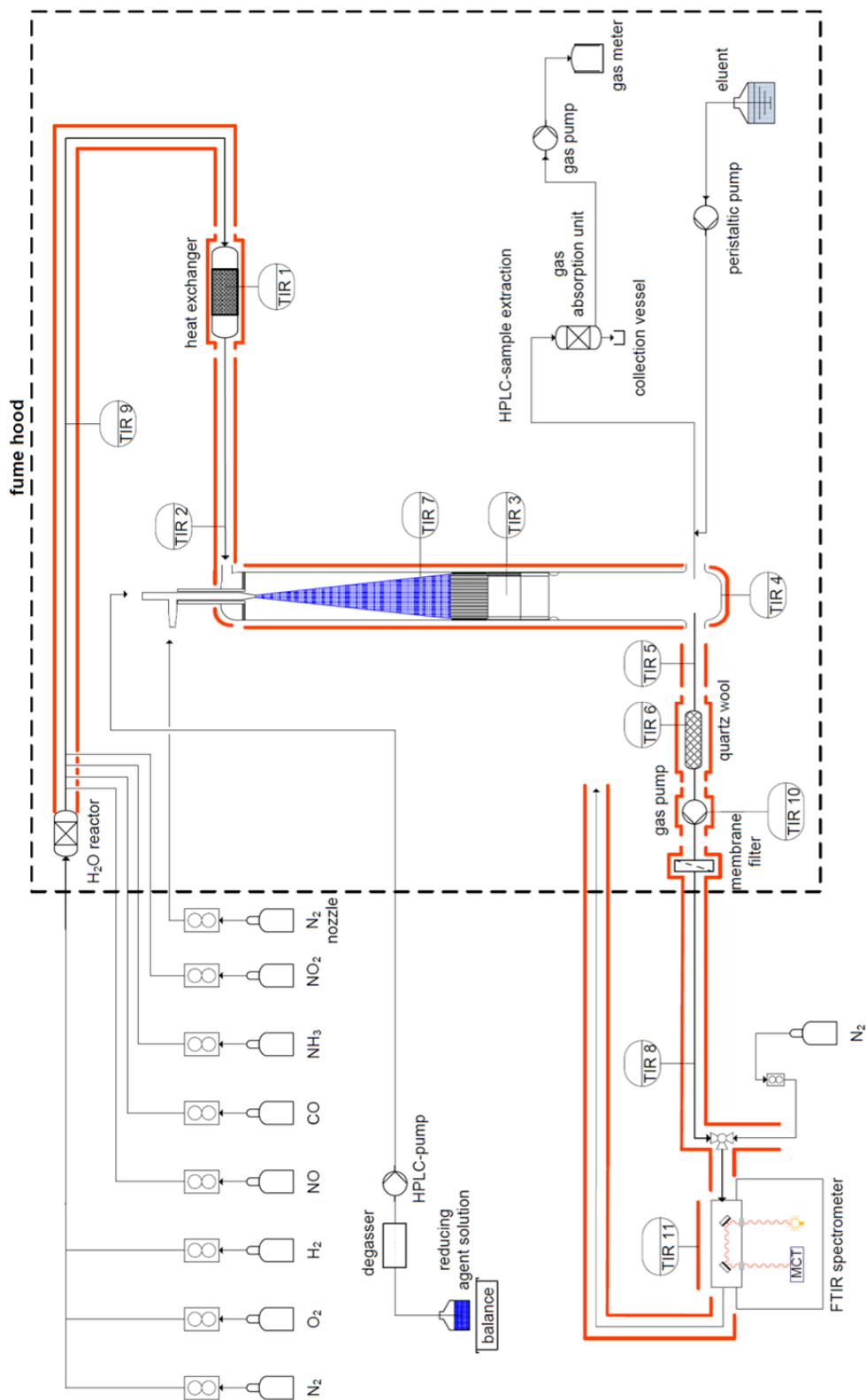
Fig. 2-1. Scheme of the setup for investigations on NH₃-precursors, taken from [64].

The reactor exit and the exit of the FTIR gas cell were open to atmospheric pressure. All parts of the setup that were in contact with the humid model gas were electrically heated to avoid water condensation. Table 2-1 shows the temperature settings; the numbers in brackets (TIR #) indicate the position of the thermocouples shown in Fig. 2-1. The temperature of the top part of the reactor was adjusted so that the cooling effect of the liquid spray was compensated and the temperature upstream of the catalyst (TIR 7) became equal to the reactor temperature (TIR 3).

The glass wool condenser shown in Fig. 2-1 was implemented to protect the FTIR gas cell from condensable compounds like gaseous urea. At a later stage, the glass wool condenser was removed again and gaseous urea was quantified by an extended FTIR spectroscopy method (see chapter 2.1.8).

Table 2-1. Temperature setting.

Heating zone	Final setting	First setting
All tubes unless indicated differently	170°C	170°C
Gas preheating (TIR 1)	as top part	as top part
Top part of the reactor (TIR 2)	adjusted	adjusted
Reactor (TIR 3)	as desired	as desired
Reactor exit (TIR 4)	170°C	220°C
Gas extraction capillary (TIR 5)	150°C	190°C
Glass wool condenser (TIR 6)	removed	120°C
Gas pump (TIR 10)	180°C	180°C
FTIR gas cell (TIR 11)	180°C	180°C

2.1.2. Gas mixing

A model exhaust gas was mixed from pure gases or binary mixtures of a gas with nitrogen, using electronic mass flow controllers (MFC) (Brooks 5850S). The typical model gas composition was 10% O_2, 5% H_2O and balance N_2, at a flow rate of 500 L/h at standard temperature and pressure

(STP: 0°C, 1013 mbar). H_2O was dosed as H_2, which was oxidized on a Pt-catalyst. O_2 was always present in excess and allowed for quantitative H_2 oxidation. The advantages of catalytic H_2 oxidation compared to a water saturator, which is often used to humidify model gases, are pulsation-free operation, a wider concentration range and a faster response. Gases apart from N_2, O_2 and H_2 were added to the main gas flow downstream of the Pt-catalyst. Before entering the reactor, the model gas was preheated to a desired temperature over ceramic beads ("heat exchanger" in Fig. 2-1).

2.1.3. Dosing of the liquid reducing agent

A small and almost pulsation-free liquid flow in the range of 10-200 µL/min was provided by a Shimadzu LC-20AD HPLC pump, equipped with two pistons (one main piston for pumping and a second piston for canceling out pulsation). Eventual gases in the liquid were removed by a Shimadzu DGU-20A3 degasser. To generate the backpressure required for a reliable operation of the HPLC pump, the liquid was passed through a stainless steel capillary. Typically, the liquid flow was set to 14.5 µL/min of 15% urea solution, which resulted in a urea concentration of 100 ppm in the total gas flow of 500 L/h at STP. The exact liquid dosing rate was calculated after an experiment from the weight loss of the reducing agent flask placed on the balance (Fig. 2-1).

The stainless steel capillary that provided the liquid reducing agent was connected with a spray nozzle via a Teflon tube. Additionally, the spray nozzle was supplied with 50 L/h at STP of N_2 as the spraying gas. The spray nozzle is a key component of the setup. It provides a very fine and well-distributed spray at very low liquid dosing rates and at elevated temperatures. A gas-assisted spray nozzle, originally designed for inductivity

coupled plasma mass spectroscopy (ICP-MS), proved to fit this application. We obtained this spray nozzle from e-pond in Lausanne, Switzerland. The design of the nozzle was derived from their "Typhoon nebulizer", but to allow the tip of the nozzle to reach the laminar gas flow while its circuit points are well outside the heated zones of the reactor, the nozzle was lengthened according to our request.

Fig. 2-2 shows the spray nozzle in detail. The liquid (picture: blue ink for evaluating the spray pattern) is fed from the top through a small inner capillary, while the spraying gas passes through the round concentric body of the nozzle. The complete nozzle is made of borosilicate glass so it can withstand elevated temperatures and corrosive liquids. The gas flow insulates the inner capillary from the hot environment of the nozzle, avoiding boiling of the liquid. At the tip, the liquid is sprayed into fine droplets by a convergent-divergent-type nozzle[A] [64].

[A] The convergent-divergent nozzle of our spray nozzle can be called Venturi tube, where the gas flow speed peaks in the neck, while the pressure is at its minimum. A Venturi tube is not to be confused with a de Laval nozzle. A de Laval nozzle exhibits a convergent-divergent shape, too, but the gas flow chokes, i.e. reaches sonic speed, in its neck. Expansion of the gas flow downstream of the neck accelerates the gas flow further at supersonic speed – this is how the high exhaust velocities of rocket engines are achieved.
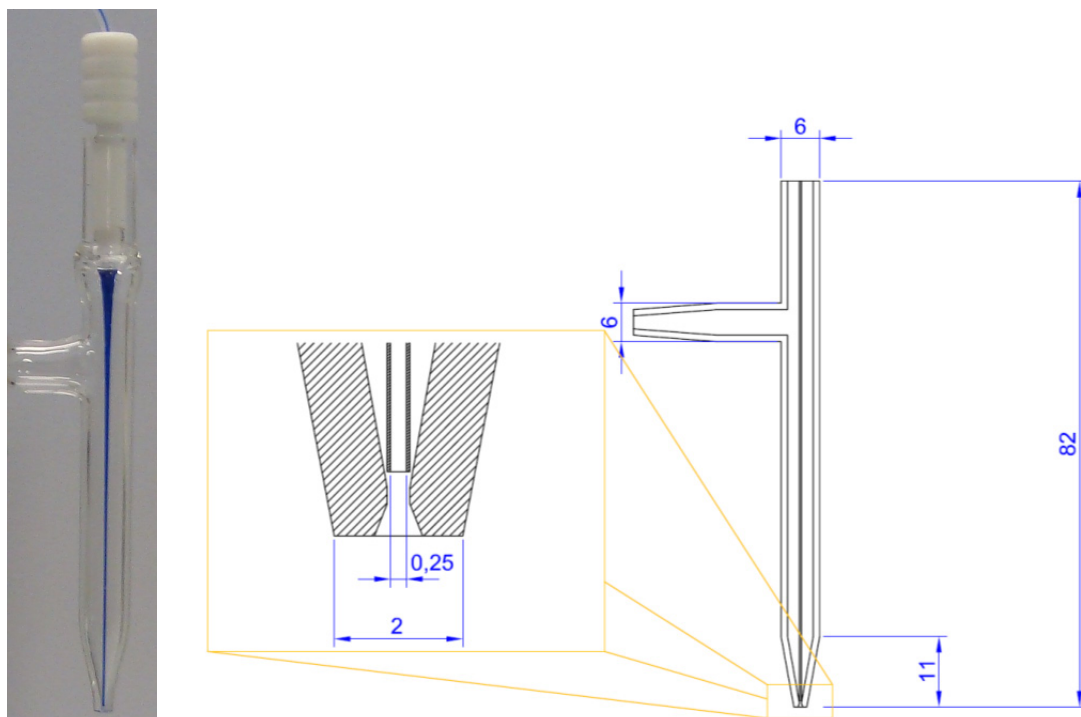
Fig. 2-2. The spray nozzle tested for spraying ink during method development and technical drawing of the spray nozzle. Figure taken from [64].

Fig. 2-3 on page 39 shows how the nozzle is introduced into the top part of the reactor.

2.1.4. HNCO generation for HNCO hydrolysis experiments

Urea was the reactant in most of the experiments. Additionally, experiments with HNCO as the reactant were carried out for comparison. HNCO was generated by thermolysis of CYA in a separate reactor as described in [51]. CYA was sublimed at about 280°C and thermolyzed downstream over stainless steel nuts at 380°C. The carrier gas flow (dry N_2) through the HNCO generator was set to 20 L/h at STP. After leaving the HNCO generator, its product gas was immediately mixed with the main gas stream (total gas flow = 500 L/h at STP). The typical composition of the resulting gas mixture was 100 ppm HNCO, ≈15 ppm NH_3, ≈20 ppm CO_2 and ≈3 ppm CO. Before starting an experiment, the HNCO generator was

allowed to stabilize for about 1 h, while its output was monitored by FTIR spectroscopy (bypassing the reactor containing the catalyst-coated monolith). After an experiment, the HNCO generator output was measured again. Typically, the HNCO concentration was stable within a few percent. From the HNCO generator output before and after the experiment, the values at any time during the experiment were calculated by linear interpolation.

2.1.5. Reactor

Urea decomposition, urea-SCR and NH_3-SCR experiments were carried out in the tubular borosilicate glass reactor with an inner diameter of 20.4 mm, shown in Fig. 2-3. The preheated model gas (coming from the right side in Fig. 2-3) entered the top part of the reactor, in which it was directed downwards and laminarized by a fritted glass filter. In the middle of the fritted glass filter, a duct for introducing the spray nozzle was located.
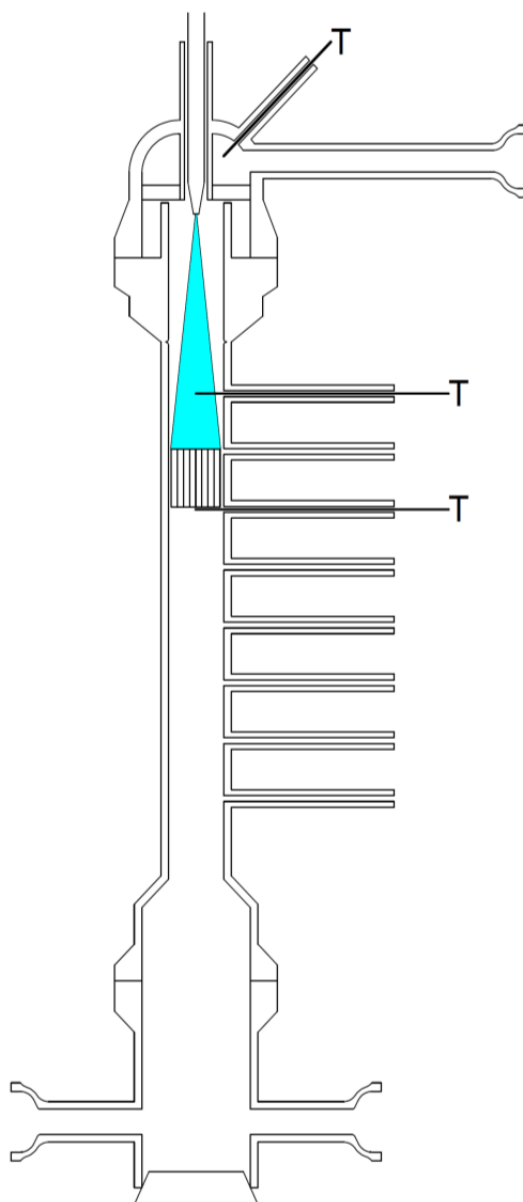
Fig. 2-3. Drawing of the reactor with 20.4 mm inner diameter, including the top part, the nozzle with an estimated spray cone and the exit. The drawing is true to scale.

Since the major part of the fritted glass filter was outside the projected area of the reactor, a significant fraction of the gas flow must have passed the filter in the outer region and then streamed horizontally inwards in between of the fritted glass filter and the upper end of the reactor, thereby causing some turbulence in the gas flow. This turbulence, however, did not induce

an uneven distribution of the spray. The spray was well mixed with the model exhaust gas; see chapter 2.1.9.

The left arm of the reactor exit shown in Fig. 2-3 provided access for the gas extraction capillary for FTIR spectroscopy (see chapters 2.1.7 and 2.1.8). The right arm was used to introduce the liquid-quench probe (see chapter 2.2) to obtain samples for HPLC analysis (see chapter 2.3). The lower end of the reactor exit was closed with a Teflon-lined glass stopper.

2.1.6. Monoliths

Catalyst-coated cordierite monoliths with a cylindrical shape, 18 mm diameter, 20 mm length, 600 cells per square inch (cpsi) and 216 channels were cut out of square shaped monoliths with 256 channels. Additionally, cylindrical monoliths with 400 cpsi cell density and 137 channels were cut out of square shaped monoliths with 169 channels. The monoliths, wrapped in ceramic-fiber mats to avoid a bypass of the carrier gas, were directly fitted into the tubular reactor. At 500 L/h gas flow rate at STP and 20 mm monolith length, the resulting space velocity was 91'000 h^{-1} for the 600 cpsi monoliths and 96'000 h^{-1} for the 400 cpsi monoliths. The space velocity of the 600 cpsi monoliths was somewhat lower because they exhibited a larger cross section, which increased the volume and decreased the space velocity. Catalyst preparation and characterization will be described in chapter 2.6 on page 69.

2.1.7. FTIR spectroscopy: existing method[A]

Gaseous reaction products of low molecular weight were analyzed by FTIR spectroscopy. FTIR spectroscopy is a widespread online method for gas analysis in exhaust gas aftertreatment [25, 65]. Provided that the spectrometer is carefully calibrated, a wide range of compounds can be quantified simultaneously. We used an Antaris IGS FTIR spectrometer from ThermoFisher equipped with a 2 m multi-path gas cell (V = 240 mL) and a liquid nitrogen-cooled mercury cadmium telluride (MCT) detector. The spectral resolution was 0.5 cm^{-1}. The FTIR gas cell was always heated at 180°C and its exhaust was released into the fume hood at atmospheric pressure.

The Quantpad-software (Version 6.1, ThermoNicolet), which is designed for the development of multi-component gas analysis methods and allows for correction of cross-sensitivities between the gas components, was used for quantification of the compounds shown in Table 2-2.

[A] This chapter is partly based on the publication:

A. M. Bernhard, D. Peitz, M. Elsener, O. Kröcher "Quantification of gaseous urea by FTIR spectroscopy and its application in catalytic urea thermolysis" Submitted to *Top. Catal.*

Table 2-2. Calibration ranges and detection limits of the FTIR spectroscopy method. The table was taken from [64] and extended by entries for urea, EtOH and MeOH. Further, the rightmost column was added to give an indication of the matrix effects in the actual product gas from a urea hydrolysis experiment.

Component	Calibration range, ppm	Detection limit in N_2,[A] ppm	Detection limit in product gas,[B] ppm
CO	40-1600	0.4	0.1
CO_2	63-2500	0.9	1.6
NO	25-1000	1.1	0.5
NO_2	16-1000	0.2	0.3
N_2O	10-200	0.1	0.1
H_2O	4000-160000	241	844
NH_3	40-6300	1.3	4.4
HNO_3	300	0.2	0.5
HNCO	10-800	0.1	1.7
HCN	50-400	0.5	0.6
Formic acid	100-2000	0.1	0.1
Formaldehyde	120	0.8	0.2
Methanamide	35	1.8	0.6
Urea	14-100	0.3	4.2
EtOH	451-4730	0.7	0.2
MeOH	3920	1.2	n.a.

A: Pure N_2, 8 scans, detection limit = average + 3 × standard deviation
B: Product gas from hydrolysis of 100 ppm urea on 45 mg TiO_2 at 170°C, 5% H_2O, 64 scans; detection limit = 3 × standard deviation. The standard deviation includes fluctuations in the dosing rate of the urea solution.

For this thesis, the method was extended by the components urea, ethanol (EtOH) and methanol (MeOH); see chapter 2.1.8. The instrument was calibrated using certified reference gas standards and gas mixtures dosed by the MFCs. 32 scans were averaged to obtain the reference spectra. For the experiments, 8-64 scans were averaged. The detection limits shown in the third column in Table 2-2 were calculated from N_2 background measurements with averaging 8 scans; three times the standard deviation plus the average of the measured values gives the detection limit [64]. These detection limits give only a rough estimation for the detections limits in the actual experiments. Matrix effects and cross-sensitivities will worsen the

detection limits; on the other hand, 64 scans were often averaged instead of 8, which improved the detection limits by the factor $\sqrt{8} \approx 2.8$. The rightmost column in Table 2-2 gives an indication of these effects; it is based on the analysis of the actual product gas from a urea hydrolysis experiment. Recording 64 scans resulted in a time resolution of 75 seconds.

At the reactor exit, part of the total gas flow was extracted for gas analysis by FTIR spectroscopy by a narrow stainless steel capillary with 3 mm outer diameter. A constant flow of 180 L/h at STP (total gas flow = 500 L/h) was provided by a heated membrane gas pump (KNF Neuberger N 012 ST.26 E). The excess gas at the reactor exit was released into the fume hood. A PTFE membrane filter with 5 μm pore diameter (Sartorius) was located downstream of the pump to remove aerosols. The membrane filter was heated at 170°C like the tubes.

2.1.8. Extension of the FTIR spectroscopy method by urea, EtOH and MeOH[A]

The existing FTIR spectroscopy method was extended to include gaseous urea, EtOH and MeOH. To the extent of our knowledge, no FITR spectroscopy method was available for the quantification of urea in the gas phase. To measure urea, we have previously applied a liquid-quench of the exhaust gas mixture to absorb urea, followed by HPLC analysis of the quenching solution, see chapter 2.2 and 2.3 and [66]. The HPLC method also allows for quantifying urea decomposition byproducts with high

---

[A] This chapter is partly based on the publication:

A. M. Bernhard, D. Peitz, M. Elsener, O. Kröcher "Quantification of gaseous urea by FTIR spectroscopy and its application in catalytic urea thermolysis" Submitted to *Top. Catal*.

molecular weight like CYA [43, 66]. On the other hand, HPLC is not an online method.

An FTIR spectrum of gaseous urea, recorded under vacuum, has been reported in [42]. Since urea has a rather low vapor pressure [33, 41, 43] and a limited thermal stability [67-69], its quantification in the gas phase is a challenging task. However, previous results in our group on urea evaporation show that gaseous urea is more stable than expected and that an FTIR spectrum of urea can be recorded at atmospheric pressure, see chapter 3 and [43], which motivated us to develop an FTIR spectroscopy method for the quantification of urea.

To avoid both, urea condensation and decomposition, some changes were made to the setup. First of all, the glass wool condenser was removed. Also, the reactor exit was heated to 170°C instead of 220°C and the extraction capillary was heated to 150°C instead of 190°C (see also Table 2-1). The temperature of the gas cell was kept at 180°C in order to not compromise the validity of the existing quantification method. Removing the glass wool condenser increased the gas flow for gas analysis. To maintain the flow of 180 L/h at STP, a narrower stainless steel capillary was used to extract the gas from the reactor exit and to provide the necessary pressure drop.

Reference spectra of urea were recorded when spraying a solution of 4 wt% urea in EtOH into the empty reactor. Dosing 70.4 µL/min of urea solution into a gas flow of 500 L/h (at STP, 10% O_2 in N_2) resulted in a gas mixture containing 100 ppm of gaseous urea. 64 spectrometer scans were always averaged to obtain one spectrum during both method calibration and measurements using a quantification method for urea. EtOH was chosen as the solvent instead of water, because water exhibits very strong and broad

absorption bands, which interfere much more with the urea infrared signals than EtOH (Fig. 2-4). Still, urea could be quantified in the presence of water, as shown in Fig. 2-7. The reactor was heated to 170°C, which induced complete evaporation of the urea solution. According to the saturation vapor pressure of urea [41, 43], a temperature of only 116°C should have been sufficient to achieve evaporation of 100 ppm urea. The need for higher temperatures may have been due to heat transfer limitations in the spray. At the moderate temperatures applied (≤180°C), most of the dosed urea remained intact till the exit of the FTIR gas cell. We did not test urea concentrations higher than 100 ppm to limit the risk of deposits of urea decomposition byproducts on the windows or on the mirrors of the gas cell.

Reference spectra of urea were recorded at six logarithmically equidistant concentrations in the range of 14-100 ppm by varying the dosing rate of the urea solution, while keeping constant the gas flow and the reactor temperature. The measured spectra were corrected by subtracting the spectra of EtOH, NH_3 and H_2O. To allow the best possible subtraction of the EtOH signals, spectra of pure EtOH at the same concentrations as in the raw urea spectra were used. HNCO and CO_2 spectra were not subtracted because their absorption bands do not interfere with those of urea. Fig. 2-4 shows the corrected reference spectrum of 100 ppm urea and two raw spectra for comparison.
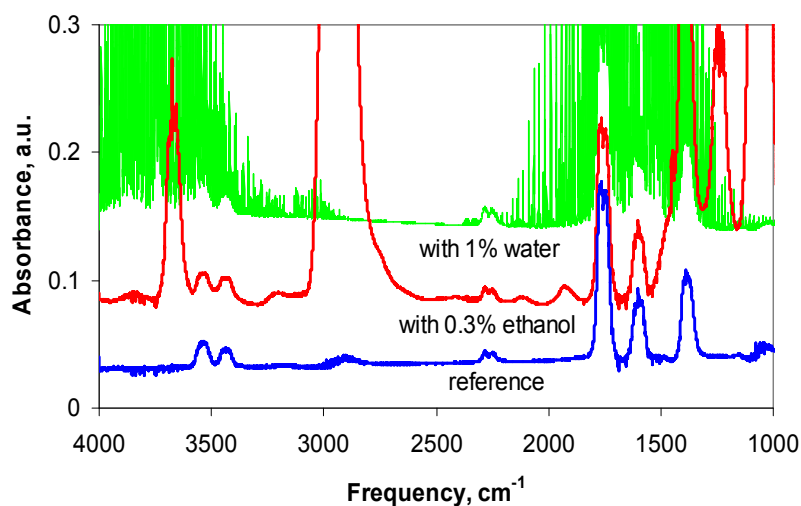
Fig. 2-4. FTIR spectra of 100 ppm urea (1st from bottom to top) after subtraction of EtOH, NH₃ and H₂O; (2nd from bottom to top) raw spectrum with 0.3% EtOH before any subtraction; (3rd from bottom to top) raw spectrum with 1% water.

The urea reference spectrum shows five significant peaks: two around 3500 cm^{-1} and three in the region 1300-1800 cm^{-1}. The most intense peak, corresponding to the C=O stretching vibration [42, 43], was chosen for quantification (region: 1700-1840 cm^{-1}). A calibration curve was calculated using a 3rd order polynom, forced through the intercept. The calibration curve (Fig. 2-5) was close to linear and the average error was 1.4%. EtOH was also included into the method; it was quantified at 2550-3100 cm^{-1}.
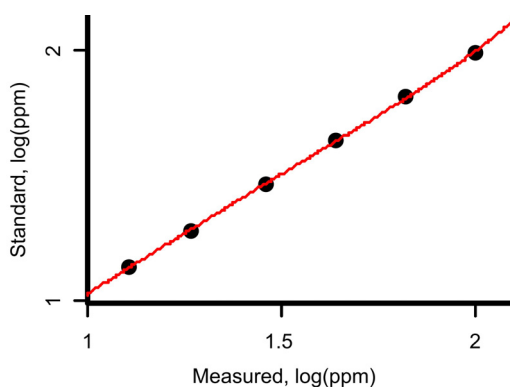
Fig. 2-5. Calibration curve for urea, plotted at a double logarithmic scale.

EtOH was not only used for the urea calibration, it was also used for water-free urea thermolysis experiments. In addition to EtOH, MeOH was used as a water-free solvent to check if changing the solvent influences the thermolysis reaction. Therefore, another method had to be created, which included urea and MeOH. MeOH was quantified in the region 2700-3160 cm^{-1}. Even though MeOH was properly included in the method, the existing NH_3 quantification was unusable in the presence of MeOH. Hence, the considered spectral region for NH_3 quantification was shifted from 987-1197 cm^{-1} [A] to 880-944 cm^{-1}. Besides, the NH_3 calibration range was reduced from 40-6300 ppm to 40-1000 ppm (3rd order polynom, forced through the intercept). The method was not used to measure urea concentrations higher than 100 ppm. Fig. 2-6 shows the spectra of NH_3 and of the organic solvents.
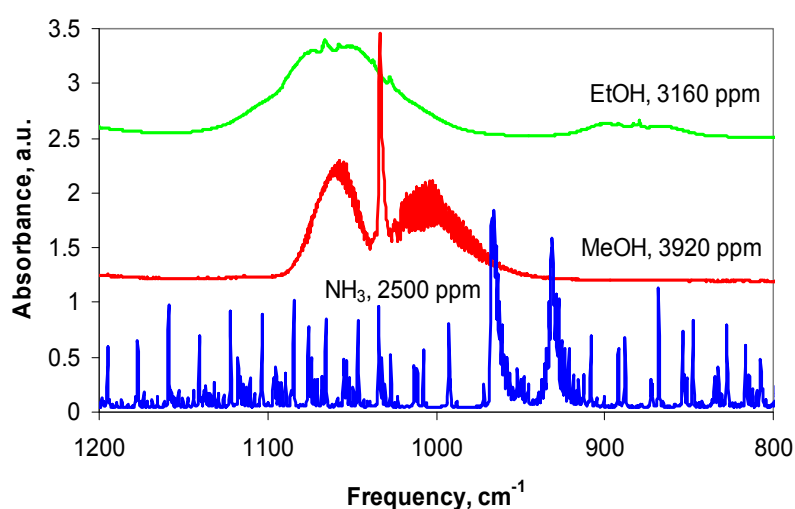
Fig. 2-6. FTIR spectra of NH_3, MeOH and EtOH (from bottom to top).

[A] Several small windows within the region 987-1197 cm^{-1}. The region 987-1197 cm^{-1} was originally chosen, because the absorption in the region remains linear up to higher NH_3-concentrations than the absorption in the region 880-944 cm^{-1}.

A significant drawback of the new methods was the cross-sensitivity of water on urea, which could not be eliminated by the multi-component correction of the Quantpad-software, causing too low urea concentrations. Therefore, we calculated corrections for water concentrations of 3%, 5% and 8% using well-defined linear regression lines. At 5% water concentration, which we used in most experiments, the correction formula was $y = 1.13x + 3.65$, where $x =$ measured urea concentration (ppm).
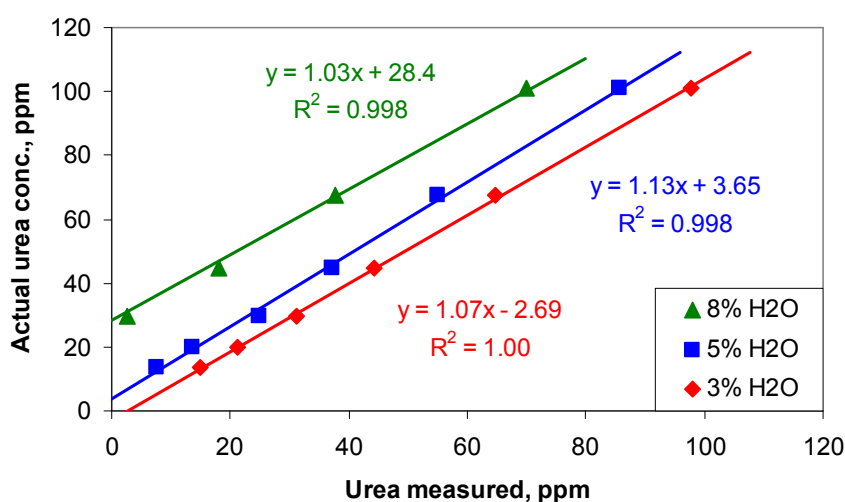
Fig. 2-7. Cross-sensitivity correction for H₂O on urea.

The presence of water did not only change the measured urea concentration but also induced scattering. At 5% water concentration, the detection limit for urea was roughly 10 ppm (estimate, based on comparison with HPLC results).

2.1.9. Method testing: urea-SCR in the laboratory

Comparing NH_3-SCR performance with urea-SCR performance is a sensible method for testing the spray quality. NH_3-SCR sets the reference, because NH_3 is completely mixed with the model exhaust gas inside the gas preheater. The urea-SCR performance comes close to the NH_3-SCR

performance, if the spray is well distributed on the catalyst cross-section. On the other hand, a bad spray distribution results in poor SCR performance, because some catalyst channels are oversupplied with NH_3, causing unwanted NH_3-slip, whereas other channels do not have enough NH_3 to achieve good NO_x reduction.

Of course, the spray quality largely depends on the spray nozzle and, in case of the gas-assisted nozzle used in our setup (see Fig. 2-2, page 37), on the spraying gas flow. We always used the same type of spray nozzle and a spraying gas flow of 50 L/h at STP. Another parameter that can be varied is the nozzle-catalyst distance. The influence of the nozzle-catalyst distance on urea-SCR performance was investigated in detail by Peitz et al. (2011), using a reactor with 40 mm inner diameter (instead of 20.4 mm) [64]. Starting at 4.5 cm nozzle-catalyst distance and only about one third of the optimal performance, the performance increased linearly with increasing distance and reached almost optimal performance at 11 cm distance. At higher distances up to 19 cm, the performance remained constant. Based on this distance-performance relation, Peitz et al. (2011) concluded that a symmetric spray cone was formed due to the laminar gas flow at the reactor entrance [64].

The influence of the nozzle-catalyst distance on urea-SCR performance was investigated likewise with the 20.4 mm reactor in the framework of the presented thesis. Fig. 2-8 shows NH_3-slip vs. $DeNO_x$ curves for NH_3-SCR (diamonds, reference) in comparison with urea-SCR at 9 cm (triangles) and at 5 cm (squares) nozzle-catalyst distance. An introduction on NH_3-slip vs. $DeNO_x$ curves is given in chapter 1.2.1 on page 17.
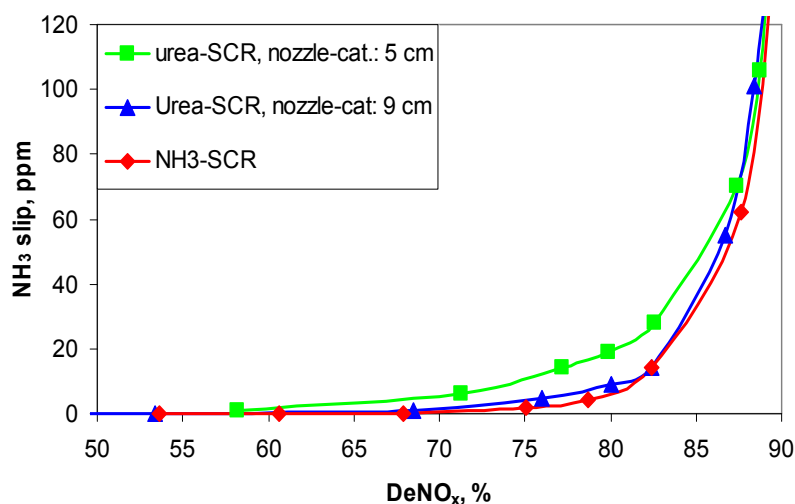
Fig. 2-8. NH₃-slip vs. DeNOₓ curves for NH₃-SCR and urea-SCR. Parameters: T = 300°C; V_2O_5/WO_3-TiO₂-catalyst with 2.2 wt% V_2O_5, coated on a cordierite monolith with 400 cpsi cell density, catalyst load = 131 g/L, catalyst mass = 1.35 g, GHSV = 48,400 h⁻¹; model gas: 1000 ppm NO, 10% O_2, 5% - 5.8%ᴬ H_2O, in N_2, gas flow = 500 L_N/h; 20% urea solution.

At 9 cm nozzle-catalyst distance, the urea-SCR performance was very close to the NH₃-SCR performance. Interestingly, the performance was not much worse at only 5 cm catalyst-nozzle distance. Based on the results obtained with the 40 mm reactor [64], a lower performance was expected. Apparently, combining the original reactor top part for the 40 mm reactor with the 20.4 mm reactor used for this study lead to a turbulent gas flow at the reactor entrance, which improved the mixing of the spray with the model exhaust gas, as mentioned in chapter 2.1.5. The influence of the

---

[A] The H_2O concentration in the base feed gas was kept constant at 5%; hence the effective concentration over the catalyst was increased by dosing the aqueous urea solution. To achieve good comparability, de-ionized water was dosed through the spray nozzle in the NH₃-SCR experiment. 52.9 µL/min of de-ionized water resulted in a total water concentration of 5.76%. In all the other experiments, the water content of the base feed gas was reduced to compensate for the water dosed through the spray nozzle.

50

nozzle-catalyst distance was not investigated further and the distance of 9 cm was chosen for all experiments except where indicated differently.

2.1.10. Method testing: reproducibility

To test the reactor heating and the gas analytics, we performed NH_3-SCR with a catalyst that was previously tested in our group on another setup, which was routinely used for NH_3-SCR experiments. Fig. 2-9 shows the results from (a) the new reactor and from (b) the default setup. We chose a commercial extruded V_2O_5/WO_3-TiO_2-catalyst with 400 cpsi cell density for this comparison. Using an extruded catalyst opened the possibility to match the total gas flow to the catalyst weight. Please note the catalyst weight could be determined more precisely than the catalyst volume. To match the gas flow to the catalyst weight, the gas flow for the experiment shown in Fig. 2-9a was set to 590 L/h (at STP) (instead of 500 L/h as usual). The results from the two different setups showed good agreement.
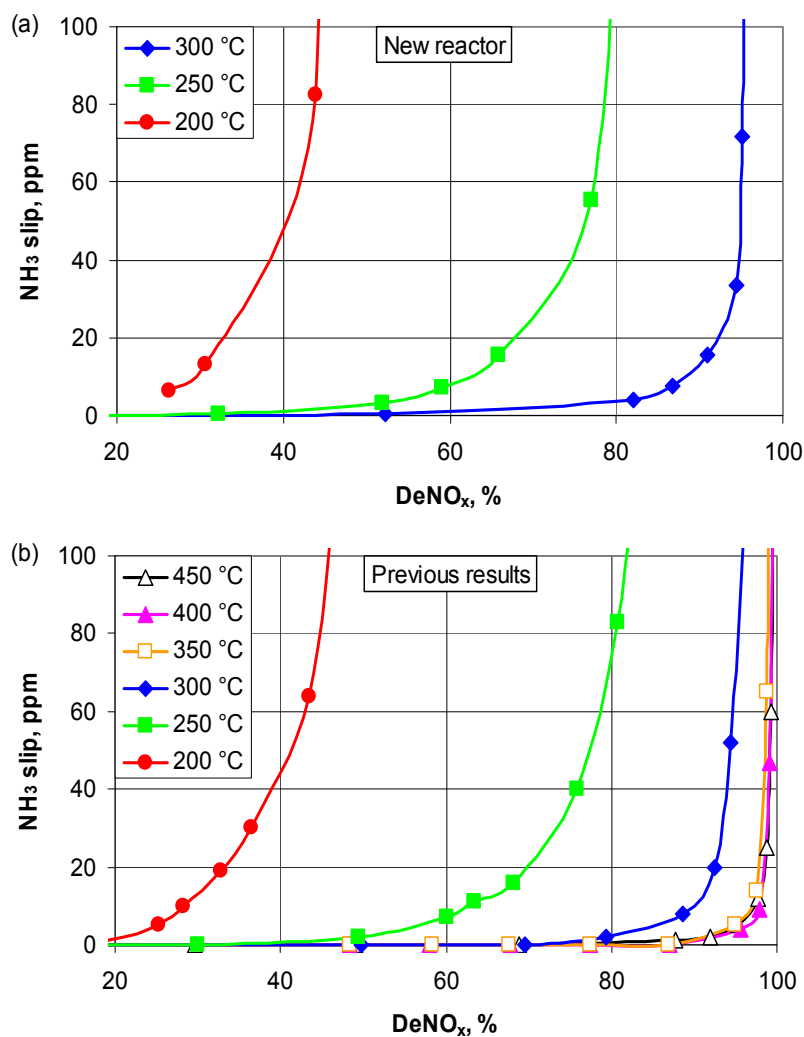
Fig. 2-9. Comparison between (a) the new setup and (b) a setup routinely used for NH$_3$-SCR in our group. Parameters: Commercial extruded V$_2$O$_5$/WO$_3$-TiO$_2$-catalyst, 1.9% V$_2$O$_5$; model gas: 1000 ppm NO, 10% O$_2$, 5% H$_2$O, in N$_2$. (a) New reactor, round monolith, gas flow = 590 L/h (at STP), GHSV = 57,300 h^{-1}, catalyst mass = 8.58 g. (b) Previous results, cuboid-shaped monolith, gas flow = 494 L$_N$/h GHSV = 52'000 h^{-1}, catalyst mass = 7.27 g.

Fig. 2-10 shows repeated urea hydrolysis experiments. The same TiO$_2$-coated monolith was always used, but the experiments were carried out over a time-span of three months during different measuring campaigns. The experiments showed good reproducibility.

(a)

(b)

(c)
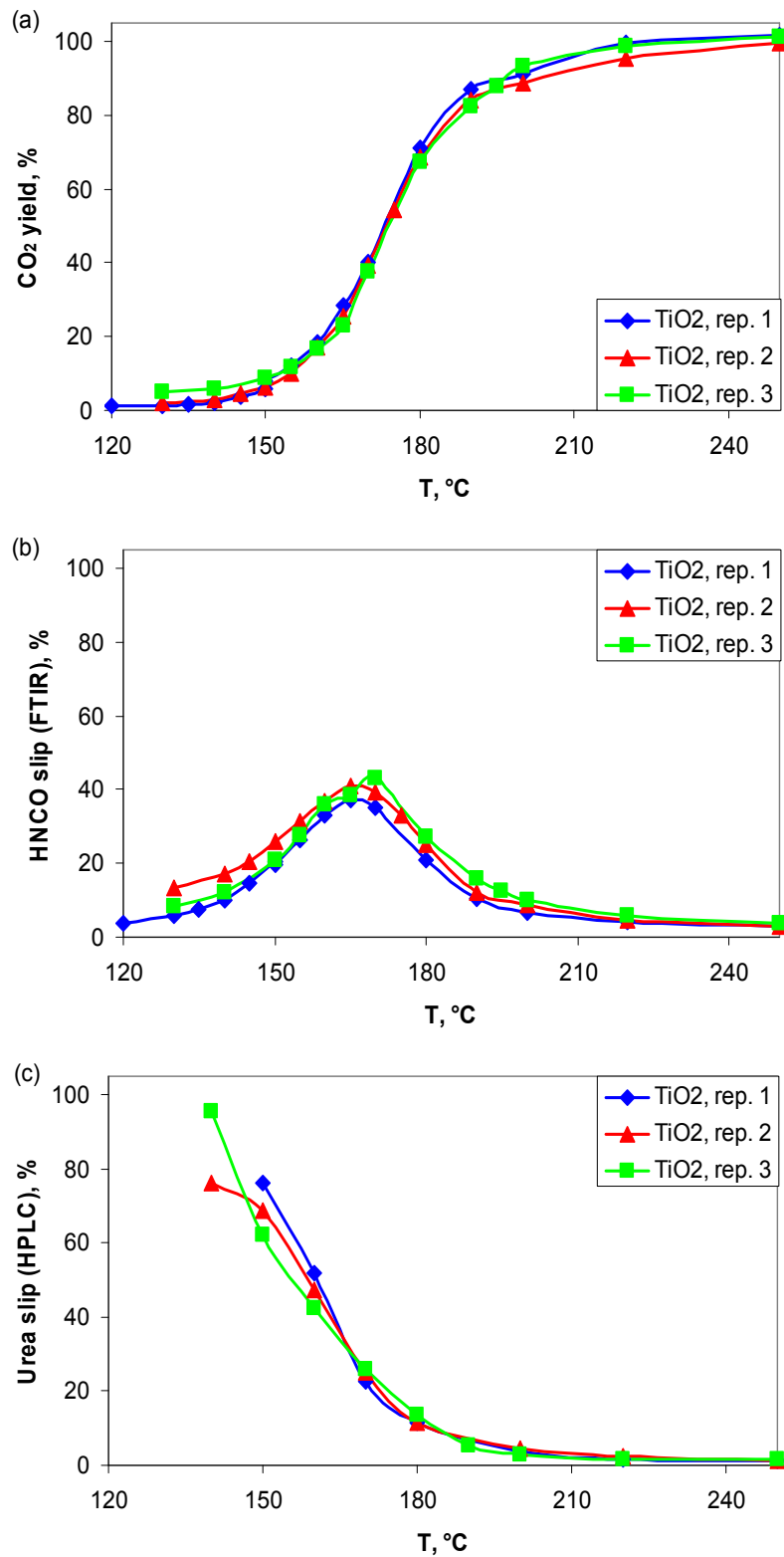
Fig. 2-10. Reproducibility of urea hydrolysis experiments. Parameters: 45 mg anatase TiO_2 coated on a cordierite monolith with 600 cpsi cell density; GHSV = 91'000 h^{-1}; model gas: 100 ppm urea, 10% O_2, 5% H_2O in N_2; total gas flow = 500 L/h (at STP); 15% urea solution.

2.1.11. Method testing: spray evaporation

The NH_3-slip vs. $DeNO_x$ curves with urea-SCR and NH_3-SCR in Fig. 2-8 showed good agreement. However, the urea dosing rate does not directly influence the NH_3-slip; only after its decomposition, the dosed urea is measured as NH_3. If urea aerosols slip through the catalyst and remain intact, they are not accounted for in NH_3-slip vs. $DeNO_x$ curves. To directly account for the urea dosing rate, Fig. 2-11 shows $DeNO_x$ values plotted against α. Again, urea-SCR and NH_3-SCR showed good agreement.
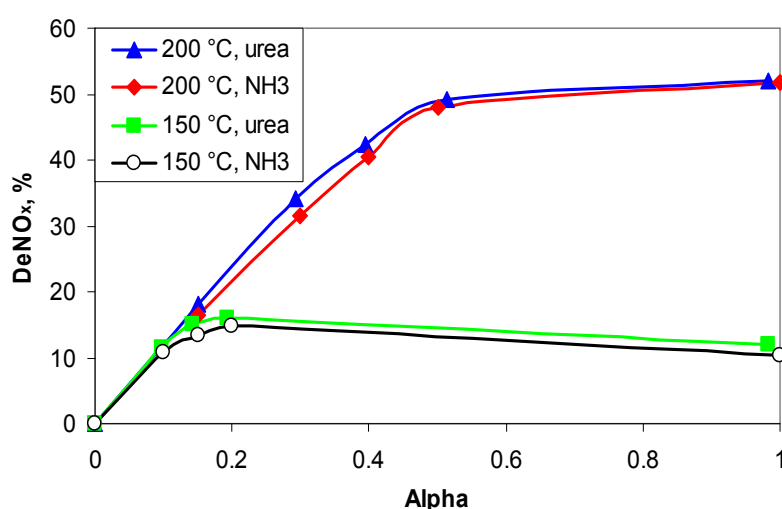
Fig. 2-11. Urea-SCR vs. NH_3-SCR. Parameters: Commercial extruded V_2O_5/WO_3-TiO_2 catalyst, 1.9% V_2O_5; model gas: 1000 ppm NO, 10% O_2, 5% H_2O, in N_2; gas flow = 500 L/h (at STP); GHSV = 48,600 h^{-1}.

Since we used a liquid-quench plus HPLC method (see chapters 2.2 and 2.3) in addition to gas analysis by FTIR spectroscopy, we could also measure urea-slip and HNCO-slip vs. $DeNO_x$ curves (Fig. 2-12).[A] At temperatures allowing for reasonable SCR performance, both, the urea slip and the HNCO slip were small. By contrast, large slips were measured at 150°C.

[A] The FTIR spectroscopy method for the quantification of urea was yet available when the experiments presented in Fig. 2-12 were carried out.
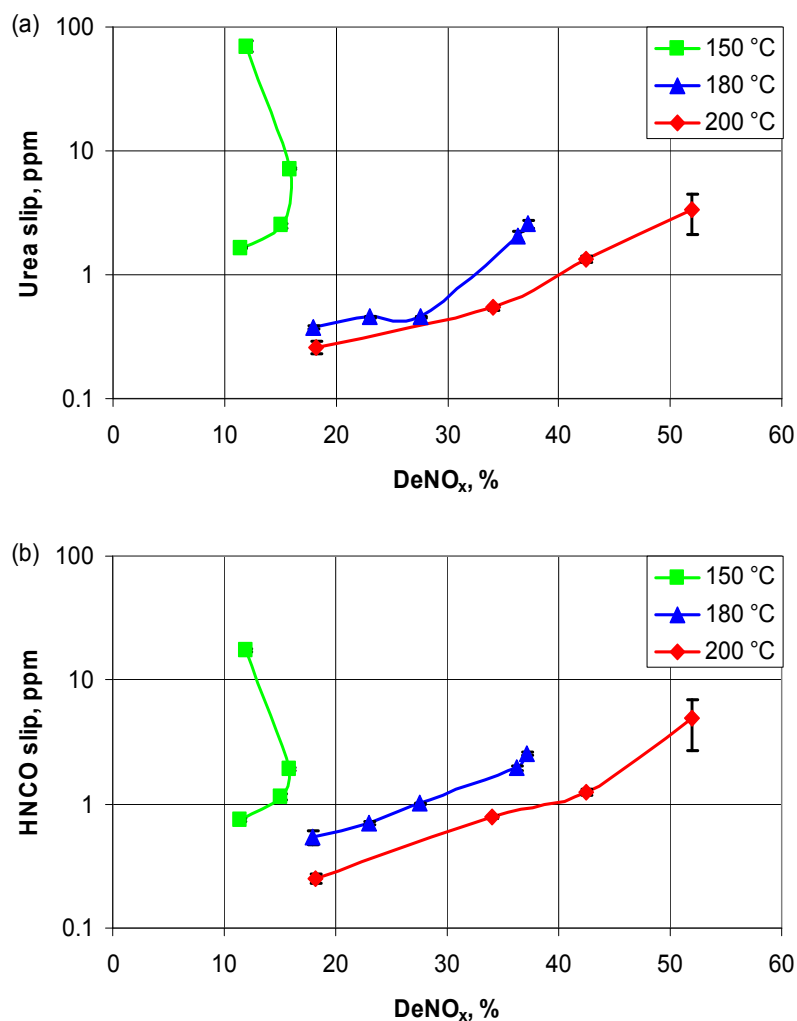
Fig. 2-12. Urea-SCR shown as (a) urea and (b) HNCO vs. DeNO$_x$ curves. Urea and HNCO were measured by HPLC analysis at pH 7. Parameters: Commercial extruded V$_2$O$_5$/WO$_3$-TiO$_2$ catalyst, 1.9% V$_2$O$_5$; model gas: 1000 ppm NO, 10% O$_2$, 5% H$_2$O, in N$_2$; gas flow = 500 L/h (at STP); GHSV = 48,600 h^{-1}; 5% or 20% urea solution (depending on the urea dosing rate).

Unfortunately, we could not directly measure if the urea slip was in the form of urea aerosols or urea vapor. The liquid-quench plus HPLC method (chapters 2.2 and 2.3) does not allow for distinguishing between urea aerosols and urea vapor. On the other hand, FTIR spectroscopy is insensitive to aerosols, but urea aerosols may evaporate downstream of the catalyst in the reactor, in the heated gas tubes or on the PTFE membrane

filter located downstream of the gas pump, which provided the constant gas flow for FTIR spectroscopy (chapter 2.1.7).

To investigate the physical state of the urea that slips through the catalyst, we performed urea hydrolysis experiments with an inert cordierite foam upstream of the catalyst as shown in Fig. 2-13. For comparison, an analogue experiment was performed without the inert foam, but with the catalyst in the same position.
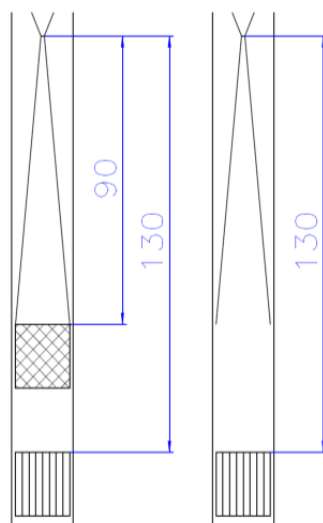
Fig. 2-13. Inert cordierite foam upstream of the TiO$_2$-coated catalyst (left) and TiO$_2$-coated catalyst only in a nozzle-catalyst distance of 13 cm.

If the aerosols evaporated slowly, the inert foam should increase the urea conversion. Part of the urea aerosols would stick to the inert foam and decompose to NH$_3$ and HNCO [40] or evaporate (see chapter 3). The urea vapor would then be transported faster from the bulk gas phase inside the catalyst channels to the active surface than from urea aerosols. In other words, the inert foam would increase the urea conversion by increasing the residence time of the urea in the reactor, improving the heat transfer from the model gas to the urea and improving the mass transport inside the catalyst. Fig. 2-14 shows urea hydrolysis with and without the inert cordierite foam upstream of the catalyst. The inert foam did not increase

the urea conversion, which suggests that the urea evaporated upstream of the inert foam.
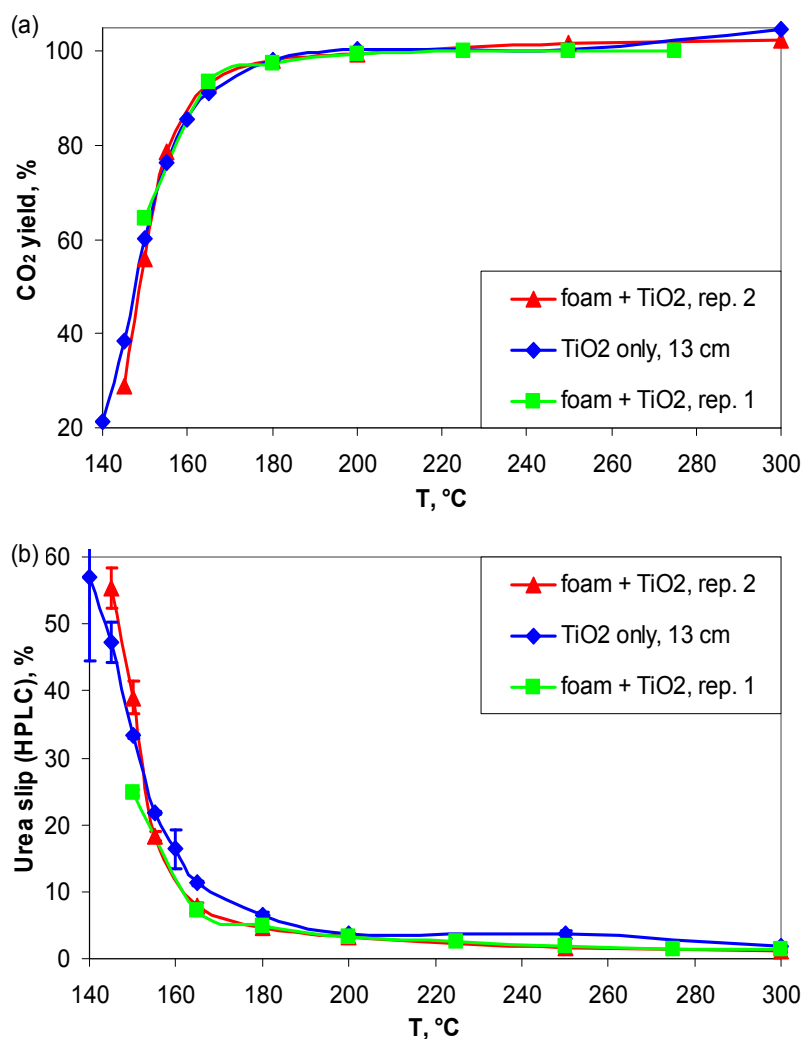
Fig. 2-14. Urea hydrolysis (a) with and (b) without inert foam upstream of the catalyst. Parameters: 710 mg anatase TiO_2 coated on a cordierite monolith with 400 cpsi cell density; GHSV = 98'000 h^{-1}; model gas: 100 ppm urea, 10% O_2, 5% H_2O in N_2; total gas flow = 500 L/h (at STP); 32.5% urea solution.

2.2. Liquid-quench of the product gas[A]

As an independent and rugged quantification method for urea and HNCO, as well as for the quantification of decomposition byproducts, we applied HPLC analysis. Liquid samples for HPLC analysis were obtained by a liquid-quench of the product gas using the apparatus shown in Fig. 2-15. The liquid-quench apparatus also allows for dissolving byproducts with low vapor pressure and the tendency to form aerosols like urea, biuret, triuret CYA, ammelide, ammeline and melamine [43, 66].
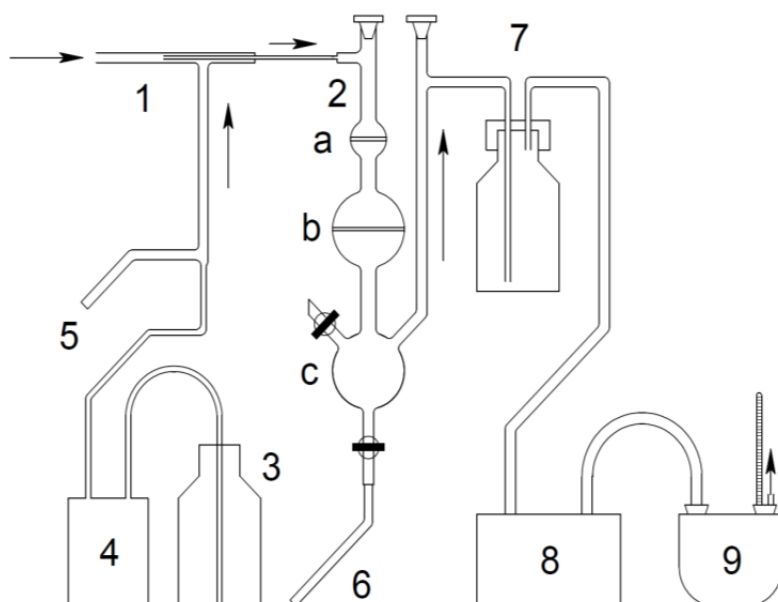
Fig. 2-15. Gas sampling apparatus: (1) liquid-quench probe; (2) fritted glass filters; (a) glass frit P100, 30 mm diameter; (b) glass frit P40, 60 mm diameter; (c) collection vessel; (3) absorbing solution reservoir; (4) peristaltic pump; (5) access for flushing; (6) access to withdraw samples; (7) empty gas wash bottle as a water trap, (8) membrane gas pump, (9) gas clock, equipped with a thermometer.

Experimental

In the liquid-quench apparatus shown in Fig. 2-15, the possibly aerosols-containing product gas was sucked into a liquid-quench probe, made of borosilicate glass, (1 in Fig. 2-15) and quenched by mixing with the absorbing solution, which is supplied by a peristaltic pump (4 in Fig. 2-15). The absorbing solution was the HPLC eluent itself: 5 mM sodium phosphate buffer, set to pH 7 or pH 10.4. The reactive product compound HNCO was quickly absorbed and stabilized in the buffer in the form of NaOCN. The two-phase mixture was then sucked out of the liquid-quench probe through a Teflon tube and through two fritted glass filters (2a-b in Fig. 2-15). Aerosols that dissolve slowly were held back to solubilize on the large wet surface on the fritted glass filters. The solution ready for HPLC analysis, was accumulated in the collection vessel (2c in Fig. 2-15) and periodically withdrawn using a syringe. The gas volume flow was passed through a wash bottle to remove condensed water, and finally sucked out of the gas sampling apparatus by a membrane gas pump (KNF Neuberger HN79 KN.18) (8 in Fig. 2-15). The effective flow through the gas sampling apparatus was measured by a gas clock (Wohlgroth G-4 (C-0)) (9 in Fig. 2-15), equipped with a thermometer. Based on the gas temperature, the saturation vapor pressure of water at the given temperature and the atmospheric pressure, the gas flow at STP through the liquid-quench apparatus was calculated, it typically amounted to 100 L/h. Finally, the analyte concentrations and the weight of the liquid samples were used to calculate the product gas concentration. Please note that the liquid-quench plus HPLC method yields the concentration in mg/m^3 in the gas phase. These concentrations were converted into ppm (volume fraction), assuming monomolecular gas phase species. This assumption was proven

for urea (provided that the aerosols evaporate) (see chapter 3); the other compounds were treated likewise to allow simple comparability.

2.3. HPLC analysis[A]

Urea, HNCO and urea decomposition byproducts were measured by HPLC analysis. In principle, the same HPLC method was applied as described by Koebel et al. (1995) [66], but the method had to be improved for reliable analysis of the urea-decomposition byproducts. Measurements were carried out on a Dionex UltiMate 3000 instrument, equipped with an anion exchange column (Waters WAT026770 IC-PAK ANION HC 4.6X150) and a photodiode-array detector, which was typically set to a measuring wavelength of 197 nm. At a later stage, the chromatograms were recorded at several wavelengths simultaneously to improve both, the sensitivity and the selectivity of the analyses, see Table 2-3. A sample volume of 20 μL was injected for analysis.

The eluent was a 5 mM phosphate buffer set to pH 7 or pH 10.4 by adding NaOH to an aqueous solution of NaH_2PO_4 or Na_2HPO_4, respectively. The separation of urea decomposition byproducts was significantly improved by increasing the pH from 7 in [66] to pH 10.4. Increasing the pH to 10.4 allows for separating of ammelide from CYA. On the other hand, the separation of urea from NH_3 is better at pH 7, a crucial aspect in urea hydrolysis experiments. Fig. 2-16 shows a chromatogram of a standard solution containing the typical urea decomposition byproducts, measured at pH 10.4. Table 2-3 also lists additional compounds with their retention

---

times and response factors. The slight deviations in the retention times between Fig. 2-16 and Table 2-3 result from the fact that the two independent analyses were carried out at different days with a new eluent and a different column.
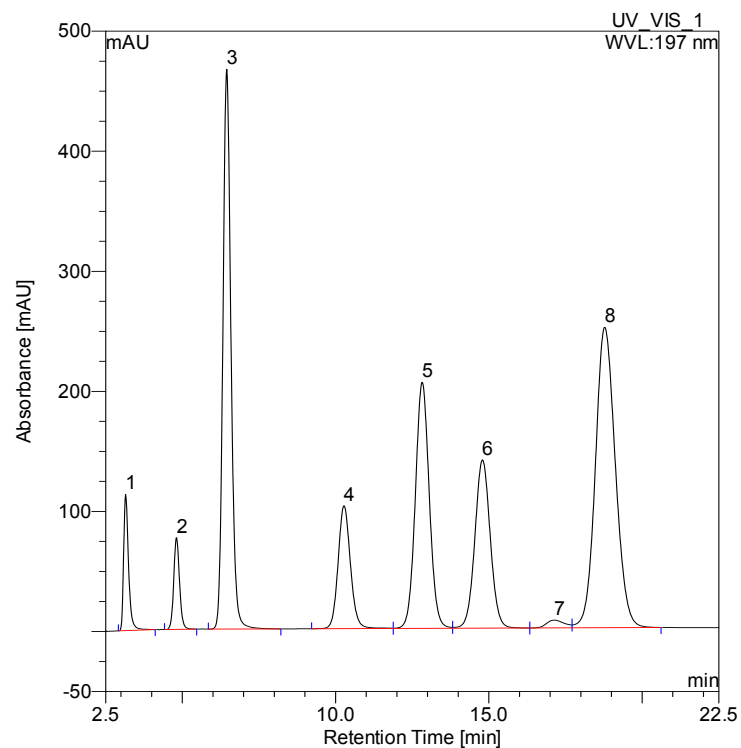
Fig. 2-16. Chromatogram of a standard solution containing the main urea-decomposition byproducts. Eluent pH = 10.4, detector wavelength = 197 nm. (1) Solvent peak, (2) 10 ppm biuret, (3) 10 ppm melamine, (4) 10 ppm triuret, (5) 10 ppm ammeline, (6) 10 ppm ammelide, (7) carbonate impurity, (8) 100 ppm CYA.

Table 2-3. Retention times and response factors for the HPLC method at pH 10.4.

Compound	Retention time, min	Response factor at 197 nm, ppm/area	Preferred wavelength, nm	Response factor at preferred nm, ppm/area
Solvent	3.1			
NH₃	3.6 [43]			
Urea	3.8	9.4	192	3.0
Unknown	4.6			blank impurity
Biuret	4.7	0.49	197	
Guanylurea	4.9	0.32	214	0.15
Formoguanamine	5.7 [43]			qualitative
1-Formylguanidine	5.9	0.065	204	0.054
Melamine	6.3	0.064	204	0.061
Dicyandiamide	6.8	0.25	214	0.13
Cyanamide	8.6	1.2	197	
Oxamic acid	8.8	0.29	197	
Formate	9.4	15.7 [43]	250	
Triuret	10.3	0.17	197	
Ammeline	13.2	0.086	197	
Ammelide	15.4	0.12	230	0.34
Carbonate	18.1			impurity
CYA	19.7	0.47	214	0.28
Nitrite	20.9 [43]	0.246 [43]	214	
HNCO	25.7		197	1.79

For comparison with the standard solution, Fig. 2-17 shows an example chromatogram of a real liquid-quench sample. A biuret TPD experiment was chosen for Fig. 2-17 because it produced a maximum number of components, which are also included in the method. The significantly shorter retention times and the decreased separation quality compared to the chromatogram shown in Fig. 2-16 are explained by the age of the column.
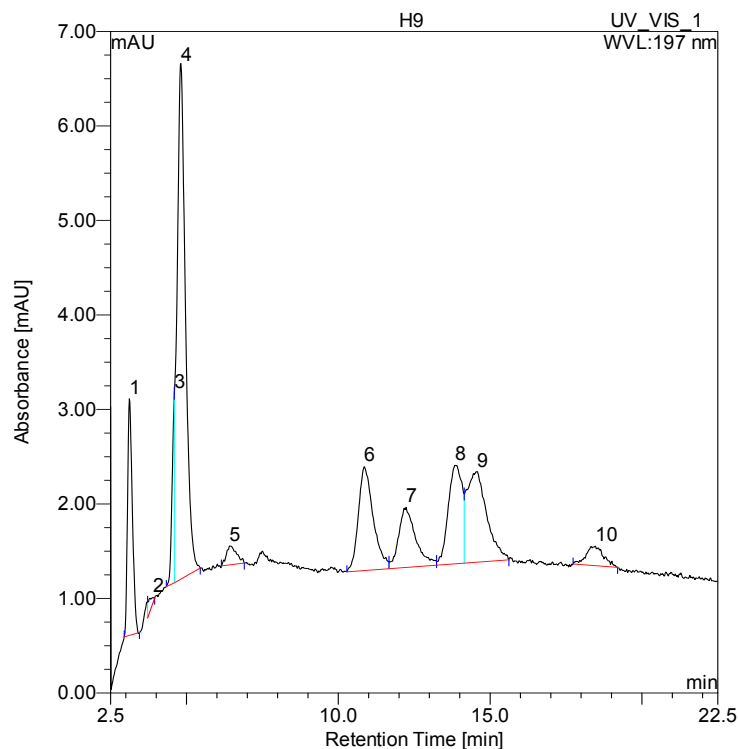
Fig. 2-17. Chromatogram of a liquid-quench sample collected in a TPD experiment of biuret (10.4 mg) in the temperature range of 275-300°C. Eluent pH = 10.4, detector wavelength = 197 nm. (1) Solvent peak, (2) urea, (3) unknown impurity, (4) biuret, (5) melamine, (6) ammeline, (7) ammelide, (8) carbonate impurity, (9) CYA, (10) HNCO.

2.4. TPD experiments[A]

2.4.1. Setup

TPD experiments were carried out using a tubular quartz reactor with an inner diameter of 28 mm (Fig. 2-18). Below, this setup is called "TPD reactor" in short. The gas-mixing unit was quite similar to the one described in chapter 2.1.2: Electronic mass-flow controllers (Brooks 5850S) provided a model gas stream that typically consisted of 5% or 0% H_2O,

---

[A] This chapter is partly based on the publication:

A. M. Bernhard, I. Czekaj, M. Elsener, A. Wokaun, O. Kröcher „Evaporation of Urea at Atmospheric Pressure" *J. Phys. Chem. A* **115**, 2581 (2011).

10% O_2 in N_2. H_2O was added by a water saturator.[A] The total gas flow was 431 L/h at STP in the TPD experiments and 215 L/h at STP in the isothermal experiments except when otherwise stated. The heating rate was always 10 K/min.

The heating of the reactor was divided into three sections (entrance, center and exit), which could be heated individually. The entrance and center temperatures were measured by thermocouples placed in the gas stream; the center-thermocouple was placed downstream of the sample. The mantle temperature in the exit section was measured below the heating wire. Fig. 2-18 shows the placement of the thermocouples in the reactor.
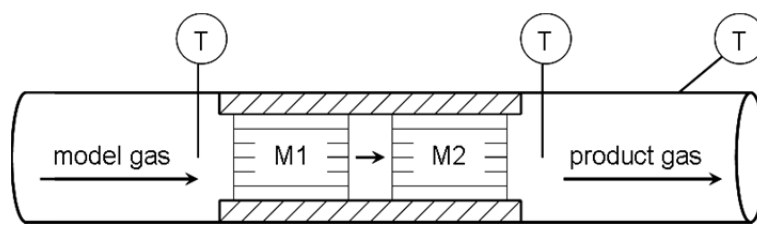
Fig. 2-18. Scheme of the quartz reactor for TPD experiments with two monoliths (M1 and M2) in the metal adaptor.

The temperature of the reactor entrance was always set to the same value as the center, whereas the reactor exit was usually heated 50 K higher to avoid condensation of product gases. Lower exit temperatures resulted in a tailing of the gas-phase components due to re-adsorption. On the other hand, higher exit temperatures did not influence the measured urea nor the HNCO concentrations (Fig. 2-19), indicating that neither urea re-adsorption nor decomposition in the gas phase occurred due to heat transfer from the reactor wall.

[A] The two last biuret decomposition experiments and the preparation of DRIFT samples were performed with catalytic H_2 oxidation for water generation.
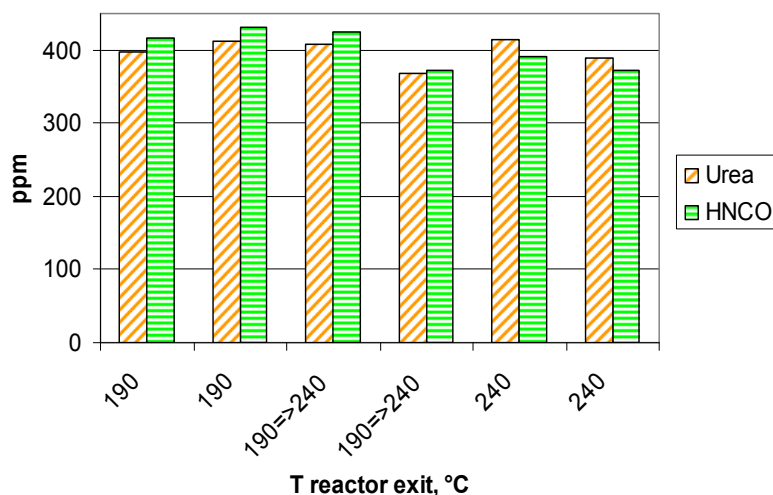
Fig. 2-19. Urea evaporation and decomposition at 140°C with different reactor exit temperatures. Model gas: 10% O_2, 5% H_2O in N_2, gas flow = 215 L/h at STP, GHSV = 9400 h^{-1}.

The gaseous low-molecular-weight compounds NH_3, CO_2, H_2O, NO, NO_2, N_2O, CO, HNCO, formic acid, HCN, formaldehyde, methanamide and HNO_3 were measured with a multi-component analysis method developed in-house [25]. The quantification method was quite similar to the method used at the spray reactor (see chapter 2.1.7), but it was developed on a Nexus FTIR spectrometer from ThermoNicolet. A similar liquid-quench method as for the spray rector (chapter 2.2) was also applied for TPD experiments.

2.4.2. Monoliths

For most TPD experiments, small cuboid monoliths with 20.5 mm length, 17.5 mm width, 12.4 mm height, 400 cpsi and 9 · 13 = 117 channels were used. Besides, cuboid monoliths with doubled length (40 mm) were used as well. The monoliths were inserted into a metal adaptor to fit the round reactor, as shown in Fig. 2-18. In some experiments, a large inert cylindrical monolith with dimensions 27 mm diameter, 42 mm length, 400 cpsi and

293 channels was used. The resulting space velocities were 97'000 h^{-1} for the small monoliths at 431 L/h (at STP) gas flow and 9400 h^{-1} at 215 L/h (at STP) for the large monolith. The catalyst preparation and characterization will be described in chapter 2.6 on page 69.

Before starting an experiment, a monolith was impregnated with the reactant by dipping it into a solution of urea, biuret or CYA. For biuret and CYA, the solutions had to be heated to solubilize these reactants. Melamine, which is poorly soluble in water, was suspended.[A] Next to dipping, the excess solution was blown out of the monolith channels, the outer monolith surface was cleaned with a tissue and the monolith was weighted in the wet state. Finally, the monolith was gently dried using a blow dryer.

2.4.3. Experiment types

In Fig. 2-18, two small cuboid monoliths are shown in the metal adaptor. In fact, different arrangements were made for different types of experiments:

- Evaporation and non-catalytic decomposition with one inert cordierite monolith only, impregnated with the reactant. All the three monolith sizes mentioned above were used, namely: small cuboid, long cuboid and large cylindrical. These experiments were either performed at a temperature ramp of 10 K/min or isothermally [43].
- Catalytic decomposition with two catalyst-coated monoliths, the first one impregnated with the reactant and the second one clean to complete the

---

[A] For comparison, CYA was suspended as well in selected experiments.

reaction. Theses experiments were performed at a temperature ramp of 10 K/min.

- Catalytic decomposition with one inert monolith, impregnated with the reactant (M1 in Fig. 2-18), followed by a clean, catalyst-coated monolith (M2 in Fig. 2-18) to perform the catalytic reaction. Theses experiments were performed at a temperature ramp of 10 K/min or isothermally. For the isothermal experiments, a long cuboid monolith was preferably used as the first monolith to slow down the depletion of the reactant. In the context of the DRIFT experiments reported in chapter 5, the clean second monolith was loaded with gaseous urea and then washed to check the surface species by HPLC analysis.

- Isothermal catalytic decomposition on one impregnated and catalyst-coated monolith. The reaction was quenched after a certain time by pulling the monolith out of the hot reactor and letting it cool down at ambient conditions. Remained reactant, reaction intermediates and non-volatile reaction products were then washed off the monolith by immersing it into the HPLC eluent and leaving it overnight at room temperature. Finally, the washing solution was analyzed by HPLC (chapter 2.3).

To check the washing efficiency, some catalyst-coated monoliths were washed a second time by boiling in de-ionized water. Additionally, one monolith was washed once and then used for a TPD experiment. In conclusion, the washing efficiency (first washing) was very high if urea or biuret was the reactant, or about 90% (based on the N-balance) if melamine was the reactant. The stability of the byproducts in the eluent was checked by boiling an HPLC standard solution containing 10 ppm of biuret, triuret,

melamine, ammeline, ammelide and 100 ppm of CYA for 15 min. The boiling decreased the triuret concentration significantly, but the other compounds appeared to be stable. Since the predominant share of the reactants and products were washed off from the monolith with eluent already at RT, further decomposition could be neglected.[A]

2.5. Chemicals

Table 2-4 shows the chemicals used.

Table 2-4. Chemicals used.

Material	Producer, product name or details
Urea	Merck, ≥99.5% purity
Biuret	Fluka, puriss p.a.
Triuret	synthesized in our group
CYA	Fluka, purum >98%
Ammeline	≥ 95% purity
Ammelide	≥ 98% purity
Melamine	Fluka, purum >99%
silicate	Ludox, AS-40, commercial inorganic binder
Na_2HPO_4	Merck, p.a. > 99.5% purity
NaH_2PO_4	Fluka, p.a. > 99% purity
EtOH	Merck, ≥ 99.9% purity
MeOH	VWR, <0.05% water
KBr	Fluka, >99% purity
CaF_2	Sigma-Aldrich, puriss.

[A] This paragraph is based on the publication:

A. M. Bernhard, D. Peitz, M. Elsener, A. Wokaun, O. Kröcher „Hydrolysis and thermolysis of urea and its decomposition byproducts biuret, cyanuric acid and melamine over anatase TiO_2" *Appl. Catal., B.* **115-116**, 129 (2012).

2.6. Catalyst preparation and characterization[A]

Cordierite monoliths were coated with catalyst powders. TiO_2 powder was suspended in a diluted aqueous NH_3 solution; the other powders were suspended in de-ionized water. The stability of the coating was improved using a commercial colloidal silica binder (Ludox AS-40, 10% of the catalyst mass). The monoliths were calcined at 550°C for 5 h. The catalytic activity of the silica binder could be neglected, because a silica catalyst with a high surface area of 380 m^2/g showed only little urea decomposition activity, see chapter 6. Moreover, in a previous study on HNCO hydrolysis, silica demonstrated to be not very active for this reaction as well [57].

The BET surface area of the catalysts was measured by nitrogen physisorption on a Quantachrome Autosorb 1-c instrument, considering relative pressures p/p_0 from 0.05-0.3 (0.05-0.15 for Fe-Beta and 0.01-0.1 for H-ZSM-5). The samples for physisorption measurements were either fresh catalyst powders or dried and calcined catalyst coating suspensions.

Fig. 2-20 shows the pore size distribution of the TiO_2 catalyst. The average pore diameter was 18 nm (mesopores) and the total pore volume was 0.41 cm^3/g at $p/p_0 = 0.993$. The crystallinity of the untreated catalyst powder was checked by X-ray diffraction (XRD). The diffraction pattern showed excellent agreement with the theoretical diffraction pattern of anatase TiO_2. The particle size of the untreated catalyst powder was ØD50 = 1.70 µm,

---

measured on a Horiba LA-950 laser diffraction particle analyzer, using the Mie-theory for size determination [26].

Table 2-5. Catalysts used.

Material	Producer, product name or details	BET sample	BET surface, m^2/g
Anatase TiO_2	Crystal Global, DT-51	powder	90
Anatase TiO_2	Crystal Global, DT-51	coating	89
Al_2O_3	Condea, Disperal S,	coating	200
ZrO_2	MEL Chemicals, XZO881	powder	72
ZrO_2[a]	MEL Chemicals, XZO881	coating	67
ZrO_2[b]	MEL Chemicals, XZO1452/01, PRB842	coating	39
SiO_2	Davison Catalysts, Davicat ® SI 1452	coating	380
H-ZSM-5	Süd-Chemie, H-MFI 27	coating	420
V_2O_5-WO_3-TiO_2	Ceram, V2, commercial SCR catalyst, 1.9% V_2O_5	powder	61
V_2O_5-WO_3-TiO_2	Crystal Global, DT-52 plus 2.2% V_2O_5	coating	80
V_2O_5-MoO_3-TiO_2	K141, 2.4% V_2O_5, 6.3% MoO_3, DT51	powder	62
Fe-Beta	Süd-Chemie, Fe-TZB223L SCR catalyst	coating	500
Cu-zeolite[c]	Damiler, commercial coated catalyst	n.a.	n.a.
Crushed cordierite	Corning	powder	very small

a: This catalyst was used to coat 600 cpsi monoliths.
b: This catalyst was used to coat 400 cpsi monoliths.
c: We only received a catalyst-coated monolith without further information. Also, the pure catalyst powder was not available. The SCR activity indicates that the coating is based on Cu-SSZ-13. From a large monolith for a real SCR application, smaller monoliths were cut for our experiments.
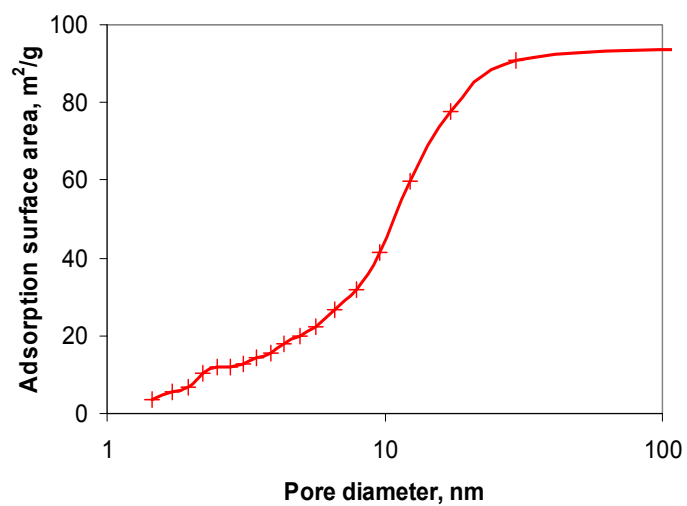
Fig. 2-20. Barrett–Joyner–Halenda (BJH) plot, showing the pore size distribution of the TiO$_2$ catalyst (second sample in Table 2-5).

3. Urea evaporation at atmospheric pressure[A]

3.1. Introduction

Urea is generally considered an unstable molecule in the gas phase at elevated temperatures in the literature referring to urea decomposition [38, 40, 67-70] or the reduction of nitrogen oxides in diesel vehicles with the urea-SCR process [14, 27, 28]. In the SCR process, urea solution is used as a safe NH_3-precursor compound, which is sprayed into the hot exhaust pipe to release the actual NO_x-reducing agent, NH_3. As a consequence of the reported instability of gaseous urea, academic and commercial computational fluid dynamic (CFD) models of the injection, spray formation and decomposition of urea solution in the SCR process usually do not consider gaseous urea but assume that urea decomposes either inside the formed aerosols or instantly after evaporation according to reaction 1 [14, 28].

Urea thermolysis: $\qquad CO(NH_2)_2 \rightarrow NH_3 + HNCO \qquad\qquad$ (1)
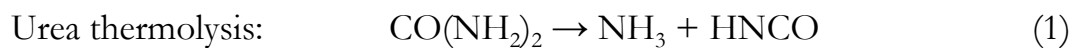
In contrast, Schaber et al. (2004) carried out TGA experiments on urea decomposition and observed a mass loss prior to decomposition (140-152°C), which they tentatively attributed to urea evaporation [38]. The assumption that mass is lost by urea evaporation was tested by identifying some condensate as urea, but the issue was not investigated further. More experimental results on gaseous urea under vacuum conditions are

---

available. The saturation vapor pressure of urea in the temperature range of 81-136°C (without taking into account data above the melting point) was measured by Ferro et al. (1987) using the torsion-effusion method [33]. Analogous measurements in the temperature range of 56-130°C were carried out by Krasulin et al. (1987) using the Knudsen integral effusion method [41]. It is worth noting that the vapor pressure reported in ref. [41] was calculated based on the weight loss of urea due to sublimation and based on the assumption that urea exists in monomolecular form. The assumption that urea is monomolecular was tested by mass spectrometry. Additionally, the assumption that urea is monomolecular fits the thermodynamic evaluation of the stability of urea dimers in the gas phase [41]. Unlike the Knudsen integral effusion method, the torsion-effusion method applied by Ferro et al. (1987) yields the vapor pressure independently of the weight of the gaseous species. The agreement between the vapor pressures determined by these two methods proves that gaseous urea exists in monomolecular form under vacuum conditions. In contrast to these vacuum experiments, we have studied the evaporation of urea at atmospheric pressure as a function of temperature from 80-153°C under flow reactor conditions.

The saturation vapor pressure of urea under atmospheric conditions was estimated by Birkhold et al. (2006) [71] using their CFD model to fit the experimental data on the decomposition of a spray of urea-water solution by Kim et al. (2004) [72]. In their CFD model, Birkhold et al. assumed that urea decomposes instantaneously after evaporation. The different curve fits developed so far for the description of the saturation vapor pressure of urea are summarized in Table 3-1 and Fig. 3-1. Because the fitted curve of Krasulin et al. (1987) [41] best matches the thermodynamic data [36] and

our measurements, it was used as reference in our study. The estimation of Birkhold et al. (2006) [71] largely deviates from the published thermodynamic data in refs. [41] and [33].

Table 3-1. Fitting curves for the saturation vapor pressure of urea and sublimation enthalpies determined by different methods.

Method	Saturation vapor pressure	Units	Sublimation enthalpy, kJ/mol	Source
Torsion-effusion	$\log(p) = 10.3 - 4750 \cdot T$	p in kPa, T in K	93.5	[33]
Knudsen integral effusion	$\ln(p) = -(11755 \pm 268) \cdot T^{-1} + (32.472 \pm 0.716)$	p in Pa, T in K	97.6 ± 1.0 at 93°C	[41]
CFD fit, see text	$p_u = \exp(12.06 - 3992/T_d)$	p_u in Pa, T_d in K		[71]
Thermodynamic software "HSC"			97.38 at 93°C	[36]
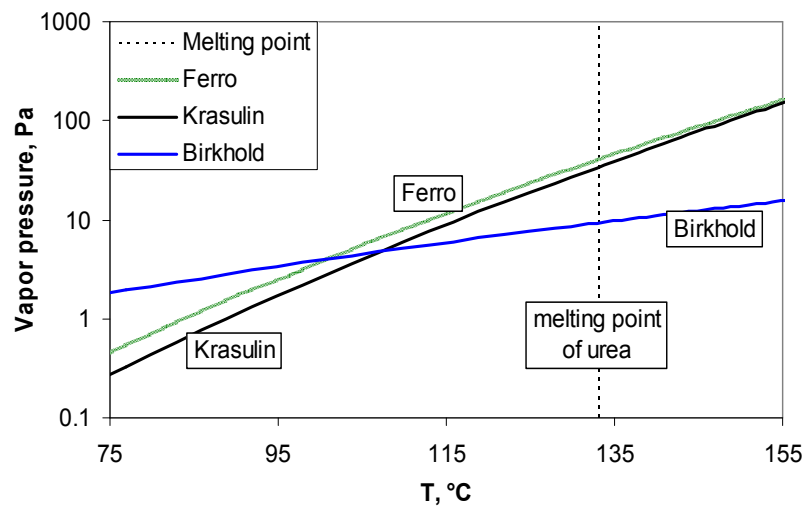
Fig. 3-1. Different fitting curves of the saturation vapor pressure of urea taken from refs. [33, 41, 71]. The fitting curves from Ferro et al. [33] and Krasulin et al. [41] only consider measurements below the melting point. The saturation curve from Birkhold et al. (2006) [71] is developed from a study by Kim et al. (2004) [72].

Recently, Lundström et al. (2009) investigated the decomposition of urea under flow reactor conditions using DSC and FTIR spectroscopy [40]. In

their work, dry urea was placed in a silica cup, or a cordierite monolith was impregnated with urea/water solution. In our work, a cordierite monolith was likewise impregnated with urea/water solution. The conditions applied in their experiments deviate sharply from ours. Most of the urea was decomposed in their experiments due to the experimental conditions. The virtually complete decomposition of urea allowed for closing the mass balance with the urea decomposition products NH_3 and HNCO only. The potential evaporation of small amounts of urea could not be detected by Lundström et al. (2009) because their analysis method did not allow for the measurement of urea. The differences between their experiments and ours will be discussed.

For our purposes, urea quantification using direct gas-phase FTIR spectroscopy is desirable because it allows the concentration of urea to be followed online with an elegant measurement method. Langer et al. (1995) were indeed able to record an FTIR spectrum of urea by evaporating urea, but at 120°C and an absolute pressure of 10^{-3} hPa [42]. In this TPD study, we were able to measure an FTIR spectrum of gaseous urea at 180°C and measure atmospheric pressure for the first time. At a later stage of the presented thesis, a quantification method for gaseous urea by FTIR spectroscopy was developed, see chapter 2.1.8.

3.2. Experimental and theoretical details

3.2.1. Measuring procedure

The TPD reactor described in chapter 2.4 was used for the study on urea evaporation. Inert cordierite monoliths with 400 cpsi were impregnated with urea by dipping them into urea solutions. A small cuboid monolith with 20.5 mm length, 17.5 mm width and 12.4 mm height and $9 \cdot 13 = 117$

channels or a large cylindrical monolith with dimensions L = 42.1 mm, Ø = 27 mm and 293 channels was used. The resulting space velocities (GHSV) were 97'000 h^{-1} for the small monolith (431 L/h at STP) and 9400 h^{-1} for the large monolith (215 L/h at STP). For the dipping solution, a urea concentration of 5.8% by mass was chosen for most TPD experiments, whereas concentrations of 32.5% (exp. 1-4) or 50% (exp. 5) were used for the isothermal experiments. In addition, 2% and 10% solutions were used to investigate the influence of different urea loads in isothermal experiments.

Two types of experiments were carried out: TPD experiments at a temperature ramp of 10 K/min and isothermal experiments. In the TPD experiments, samples for the HPLC analysis were taken at intervals of 25 K (50 K below 100°C and above 250°C), see chapter 2.2 for the liquid-quench method to obtain liquid samples. To avoid carry-over of compounds between analysis intervals due to residues in the fritted-glass filters in the absorption apparatus, the filters were rinsed with 10 mL of absorption solution immediately before sampling. For the isothermal experiments, three samples were taken for HPLC analysis at intervals of 3-6 min at a selected temperature. The HPLC analysis method is described in chapter 2.3. The average gas-phase concentration and the standard deviation are given in the plots as dots with error bars. A missing standard deviation means that only one value was taken into account. Note that systematic errors are not included in this standard deviation. Specifically, the trend of measured vapor pressures being lower than expected, possibly because of too low effective monolith temperatures, is not included. Please note that the thermocouple for regulating the reactor temperature was located downstream of the monolith (see Fig. 2-18, page 64). Hence, the heating

should have compensated for endothermic processes on the monolith. Still, we observed a trend for too low vapor pressures at higher temperatures.

The FTIR spectrum of gaseous urea was measured during the TPD experiment shown in Fig. 3-2b. The model gas consisted of 10% O_2 in N_2, and the humidifier was bypassed to avoid interference with the water spectrum. 25.3 mg of urea were present on the monolith. The 30 spectra with the highest urea concentrations were averaged, and the spectra of NH_3, HNCO and CO_2 were subtracted.

3.2.2. Computational details[A]

The program code StoBe [24] together with the non-local generalized gradient corrected functionals according to Perdew, Burke, and Ernzerhof (RPBE) [73, 74] were used for density functional theory (DFT) calculations. The vibrational frequencies were calculated with an anharmonic approximation, as implemented into the StoBe code [75]. Theoretical vibrational spectra were obtained by convolution of the urea and HNCO vibrations, applying Gaussian line-shapes. The frequencies are reported as obtained from the calculations, without scaling.

3.3. Results

3.3.1. Desorption of urea under TPD conditions

In the first experiments, urea was desorbed/decomposed under TPD conditions at a heating rate of 10 K/min. Fig. 3-2a shows the urea and HNCO concentrations measured by HPLC, whereas Fig. 3-2b shows the NH_3, HNCO and CO_2 concentrations measured by FTIR spectroscopy.

[A] The second author Izabela Czekaj carried out the DFT calculations.
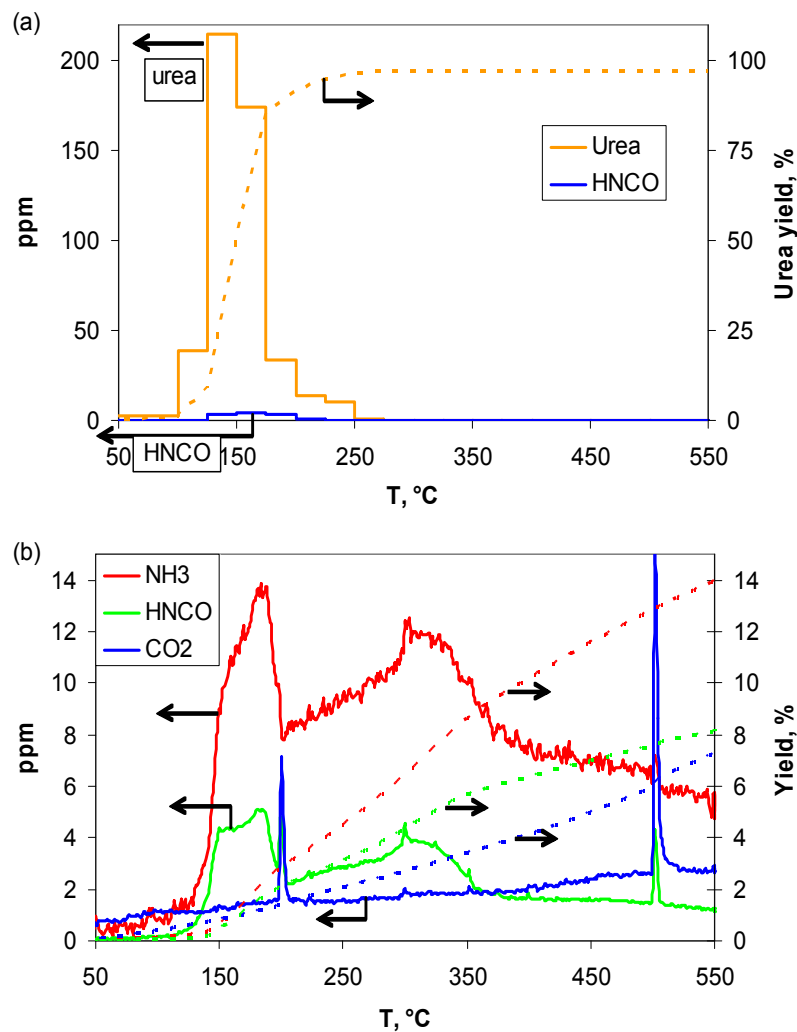
Fig. 3-2. Urea desorption from a small cordierite monolith at a heating rate of 10 K/min. Base feed: 10% O_2 in N_2. Gas flow = 431 L/h at STP, GHSV = 97'000 h^{-1}. (a) 5% H_2O in the base feed. Urea and HNCO desorption measured by HPLC, m(urea) = 24.5 mg. (b) Base feed without water. NH$_3$, HNCO and CO$_2$ emissions measured by FTIR spectroscopy, m(urea) = 25.3 mg.

In contrast to the results reported in the literature [40], urea was the major compound reaching the gas phase, instead of NH_3 and HNCO. Our results are attributed to the high GHSV and the large surface area of the urea film, allowing urea evaporation to be faster than urea decomposition. This

conclusion is supported by the fact that a larger amount of urea led to lower urea and higher HNCO yields (Fig. 3-3).
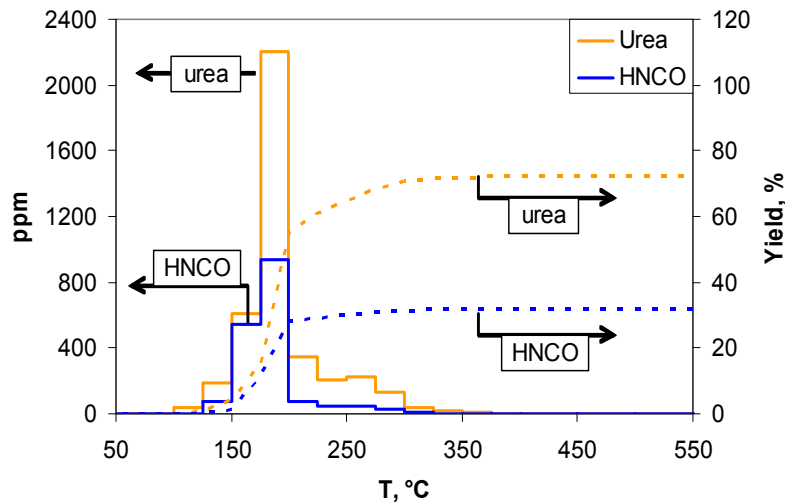
Fig. 3-3. Urea desorption from a large monolith at a heating rate of 10 K/min. Base feed: 10% O_2, 5% H_2O in N_2. Gas flow = 215 L/h at STP, GHSV = 9400 h^{-1}, m(urea) = 127 mg.

A comparison of the experiments with small (Fig. 3-2a) and large (Fig. 3-3) urea amounts revealed that the urea concentration was similar in both experiments up to 150°C. However, in the temperature interval from 150-175°C, the urea concentration decreased again for the small monolith as a result of urea depletion (Fig. 3-2a), whereas the highest urea concentration was observed in the next temperature interval, from 175-200°C, for the large monolith (Fig. 3-3). Therefore, a larger relative amount of urea was left on the larger monolith at higher temperatures, resulting in a higher yield of the thermolysis product HNCO. Besides urea, some biuret and CYA (0.03% per mass each) and a trace of triuret were detected downstream of the large monolith, while no byproduct formation could be observed in the case of the small monolith. The low byproduct yield in our experiments is attributed to fast desorption of the reactive intermediate HNCO [38].

In the DSC experiments performed by Lundström et al. (2009) [40], virtually complete urea thermolysis into NH_3 and HNCO was observed. The reason for this result, which is in contrast to our experiments, must be the different experimental conditions. Urea was also desorbed from a monolith in their experiments, but the monolith was bypassed by a large fraction of the sweep gas, causing a much lower GHSV inside the channels. The urea loading per total gas flow was lower in our small-monolith experiment than in their experiments (450 $\mu g \cdot (L/h)^{-1}$ urea at STP compared to 57 $\mu g \cdot (L/h)^{-1}$ urea at STP) but similar in our large-monolith experiment (591 $\mu g \cdot (L/h)^{-1}$ urea at STP). Thus, the above-mentioned low GHSV inside the channels of the monolith is likely to be the main reason for the high HNCO yields observed in their experiments. Still, some urea vapor may have formed in their experiments, explaining the lack of about 10% NH_3 at 10 K/min heating rate [40]. At 20 K/min heating rate, more urea must have been left on the monolith at high temperatures, which improved urea decomposition and decreased the urea evaporation to an insignificant level.

The FTIR spectroscopy results (Fig. 3-2b) show a broad HNCO peak between 150 and 190°C. A peak between 150 and 190°C fits the HPLC results (Fig. 3-2a), where the maximum HNCO emission was observed between 150 and 175°C and somewhat lower emissions between 175 and 200°C. The NH_3 peak was shifted to higher temperatures (184°C), which could be due to a chromatography effect. The NH_3 and HNCO curves also showed a second peak at 310°C. The yields of roughly 14% NH_3, 8% HNCO and 7% CO_2 seem to disagree with the HPLC results, where 97% urea and 2% HNCO were observed. The disagreement between FTIR and HPLC yields is attributed to urea decomposition inside the tubes from the

reactor to the spectrometer, inside the gas pump and inside the measuring cell. This explanation is supported by Langer et al. (1995), who also observed HNCO formation inside a measuring cell due to urea decomposition at only 120°C [42]. The second peaks in the NH_3 and HNCO curves may be caused by urea that condensed at the entrance of the gas tube, which is a cold spot due to imperfect insulation. The condensed urea was thermolyzed when the tube was sufficiently heated by the temperature ramp, which heated the product gas. CO_2 formation inside the reactor should be negligible because HNCO is stable in the gas phase [14], water was absent in the dry experiment and the quartz reactor and the cordierite monoliths are chemically inert. However, slight CO_2 formation (< 3 ppm) was always observed in both the dry and the wet experiment (wet experiment not shown). Because CO_2 can only be produced from the hydrolysis of HNCO in the investigated reaction network, water must have been present from small impurities in the model gas and in the urea film. Moreover, due to the stability of HNCO in the gas phase even in the presence of water, it is likely that the metal-oxide surface in the stainless-steel tubes to the FTIR spectrometer acted as a catalyst for the hydrolysis of HNCO according to reaction 2. HNCO hydrolysis over different metal-oxide catalysts, including Fe_2O_3, was reported in [57, 76]. The observed CO_2 concentration was always small and did not affect our major findings.

HNCO hydrolysis: $\qquad HNCO + H_2O \rightarrow NH_3 + CO_2 \qquad$ (2)
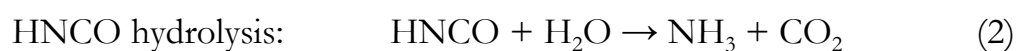
3.3.2. FTIR spectrum of monomolecular urea

In the TPD experiment under dry model gas, presented in Fig. 3-2b, urea was detected by FTIR spectroscopy. Analysis of the gas-phase FTIR spectra showed that urea was present in the gas phase in monomolecular

form. Fig. 3-4a shows a comparison between the raw spectrum and a corrected spectrum that was calculated by subtracting the FTIR spectra of NH_3, HNCO and CO_2; thereby almost completely removing the large HNCO signal at 2300 cm^{-1}. Fig. 3-4b and Table 3-2 show a comparison between our corrected spectrum, the spectrum reported by Langer et al. (1995) that was measured at 120°C and 10^{-3} hPa [42] and the theoretical spectra. Because Langer et al. (1995) did not subtract the interfering spectra, the HNCO signal at 2300 cm^{-1} was still prominent, but smaller than in our uncorrected spectrum, which must be due to their use of a lower temperature.
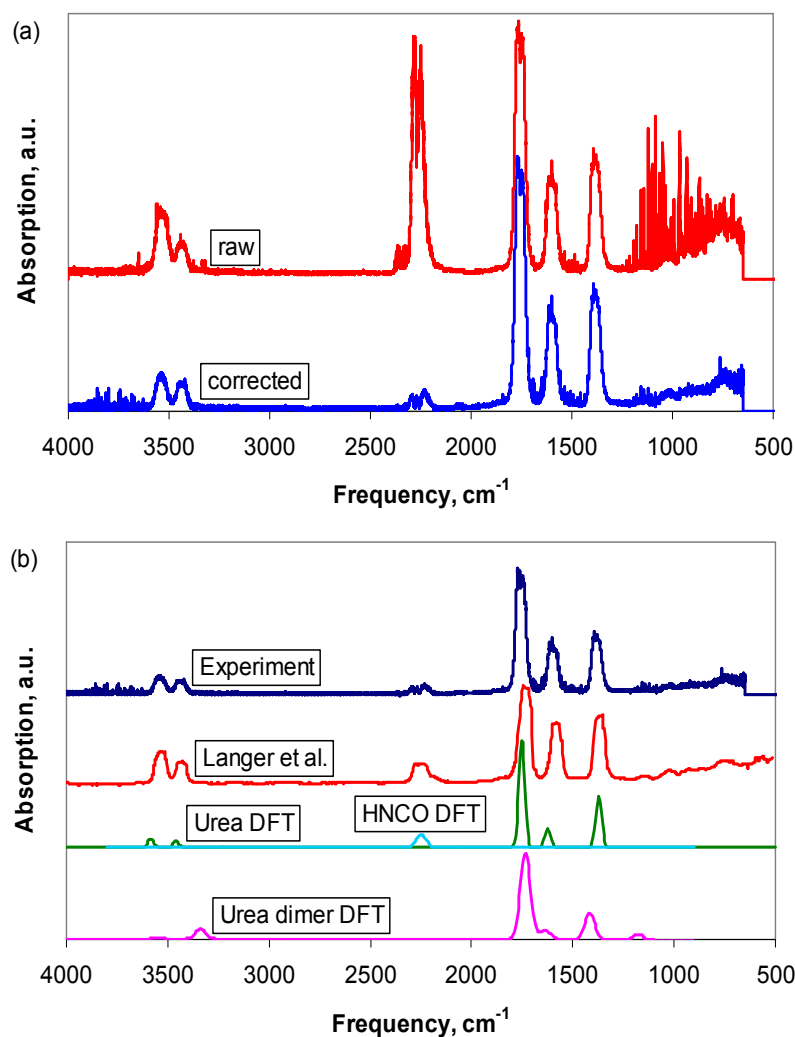
Fig. 3-4. (a) Raw infrared spectrum of urea at 180°C and atmospheric pressure and corrected spectrum after subtracting the spectra of NH_3, HNCO and CO_2. Model gas feed: 10% O_2 in N_2. (b) Comparison between (1st row) the corrected measured urea spectrum, (2nd row) the spectrum reported by Langer et al. (1995) measured at 120°C and 10^{-3} hPa [42], (3rd row) the theoretical spectra of urea and HNCO as single molecules in the gas phase and (4th row) the spectrum of the urea dimer shown in Fig. 3-5.
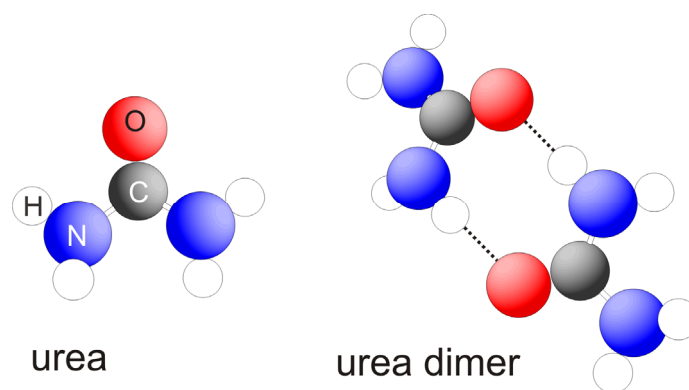
Fig. 3-5. Schemes of a single urea molecule and of the considered urea dimer.

Table 3-2. Comparison of the measured infrared frequencies of urea in the gas phase with DFT calculations of a single urea molecule in the gas phase, dimeric urea in the gas phase and literature data from ref. [42].

Measured, cm^{-1}	Assignment	DFT calculation, cm^{-1}	Lit. experiment, cm^{-1}	Lit. calculated, cm^{-1}	Urea dimer DFT calculation, cm^{-1}
1392	A1 ν_s (CN)	1372	1394	1406	1416
1600	A1 δ_s (NH$_2$)	1624	1604	1676	1621 1645, 1649
1773	A1 ν (C=O)	1752	1776	1769	1734
2233 2270 2295	HNCO	2259 [21]	2237 (2269)		
≈ 3437	B1 ν_s (NH)	3455	3434	3439	3460
≈ 3437	A1 ν_s (NH)	3459	3460	3442	3462
≈ 3540	B1 ν_{as} (NH)	3584	3533	3553	3552
≈ 3540	A1 ν_{as} (NH)	3584	3559	3557	3586

The strongest bands at 1773 cm^{-1} and 1392 cm^{-1} in the measured spectrum are assigned to C=O and C-N vibrations and are in good agreement with the theoretical vibrations of monomolecular urea at 1752 cm^{-1} and 1372 cm^{-1}, respectively (20 cm^{-1} below the experimental values). A slightly higher deviation of 24 cm^{-1} between experiment and theory was observed for the NH$_2$ vibrations (1624 cm^{-1} versus 1600 cm^{-1}). The peaks above 3400 cm^{-1} in the calculated spectrum correspond to the N-H stretching vibrations; they are also shifted to higher frequencies compared with the experimental

values. A similar shift between measurement and DFT calculations has been observed for the NH vibrations in another study [55]. The satisfying agreement between the theoretical and experimental spectra supports our assumption that urea was present in the gas phase in monomolecular form. To exclude the presence of dimeric urea, an additional spectrum was calculated for the urea ribbon dimer. This dimer conformation, shown in Fig. 3-5, is most stable according to a study by Masunov et al. (1998) [77]. The strongest bands of the dimer should appear at 1734 cm^{-1} and 1416 cm^{-1}. These bands clearly deviate more strongly from the measured spectrum than do the theoretical bands for monomolecular urea (-39 and +24 cm^{-1} instead of -21 and -20 cm^{-1}). Moreover, the calculated spectrum for the urea dimer shows significant peaks at 3338 cm^{-1} (coming from the O-H vibration in the dimer) and at 1178 cm^{-1}, which were not observed in our experimental spectrum.

3.3.3. Desorption of urea at constant temperature

To quantify the urea evaporation as a function of temperature, experiments were carried out under quasi-stationary conditions. Saturation of the model gas with urea vapor at a constant temperature and delayed depletion of the urea-coated monolith were achieved by decreasing the gas flow, using a larger monolith and increasing the urea concentration of the dipping solution compared to the previous TPD experiments. Table 3-3 (rows 1-6) shows a comparison between low and high GHSV. For both low and high GHSV at 80 and 110°C, the measured urea evaporation rates were similar within the error margins (rows 1-4). At 130°C, the urea concentration was 30% lower in the case of high GHSV (rows 5-6). However, the decrease of 30% is still moderate compared to the increase of GHSV by a factor of 10.

Therefore, we assume that the low GHSV allowed for the saturation of the model gas.

Another issue that must be addressed is urea decomposition. HNCO formation (urea thermolysis) was observed not only in the TPD experiments (Fig. 3-2 and Fig. 3-3) but also in isothermal experiments at T ≥ 100°C. As shown in Fig. 2-19 on page 65, urea decomposition was negligible between the impregnated monolith and the probe for the gas-liquid-quench in our experiments. Thus, the observed urea decomposition must have taken place on the impregnated monolith. Table 3-3 (rows 7-9) shows the dependence of urea and HNCO desorption from the urea load at 120°C. Urea evaporation was quite constant, whereas the HNCO desorption strongly increased with increasing load. It is therefore reasonable to assume that urea thermolysis took place on the monolith in parallel with urea evaporation, but that the two processes did not directly affect each other. In addition to urea thermolysis, byproduct formation was also observed. Traces of biuret were observed in exp. 3 and exp. 4 at 150 and 153°C, respectively. In exp. 5, traces of biuret and triuret were observed at 140°C, which is attributed to the high urea load, and at 153°C, significant amounts of biuret, triuret and CYA were measured (0.22 Pa biuret, 0.082 Pa triuret, 0.12 Pa CYA). Also in this experiment, byproduct formation must have taken place on the monolith, and byproduct formation is considered to take place independently of urea evaporation.

Table 3-3. Desorption of urea under quasi-stationary conditions. Comparison between low and high GHSV (rows 1-6) and different urea loads (rows 7-9). Model gas: 10% O$_2$, 5% H$_2$O in N$_2$.

Row	T, °C	Urea on monolith, mg	Interval, min	Gas flow at STP, L/h	GHSV, h^{-1}	p(urea), Pa	Stdev p(urea), Pa	p(HNCO), Pa	Stdev p(HNCO), Pa
1	80	704	6	215	9400	0.46	0.18	0.00	0.00
2	80	199	6	431	97'000	0.43	0.05	0.00	0.00
3	110	704	4	215	9400	3.65	0.04	0.13	0.01
4	110	124	3	431	97'000	4.00	0.21	0.00	0.00
5	130	755	3	215	9400	19.8	0.90	11.1	6.73
6	130	124	3	431	97'000	13.9	0.15	0.22	0.03
7	120	37.7	3	215	9400	8.84	0.24	0.14	0.06
8	120	206	3	215	9400	10.2	0.25	0.47	0.44
9	120	704	3	215	9400	10.9	0.16	0.97	0.08

In Fig. 3-6, the urea concentrations measured in the gas phase at low GHSV are compared to the saturation vapor pressure of urea according to the equation that was given by Krasulin et al. (1987): $\ln(p) = -(11755 \pm 268) T^{-1} + (32.472 \pm 0.716)$, where p is the pressure in Pa and T is the temperature in K [41]. The curve is only plotted as a solid line below 130°C because the investigation by Krasulin et al. (1987) did not cover higher temperatures. Above 130°C, the curve is extrapolated without taking into account the phase change from solid to liquid. Table 3-4 provides additional information about the performed experiments.
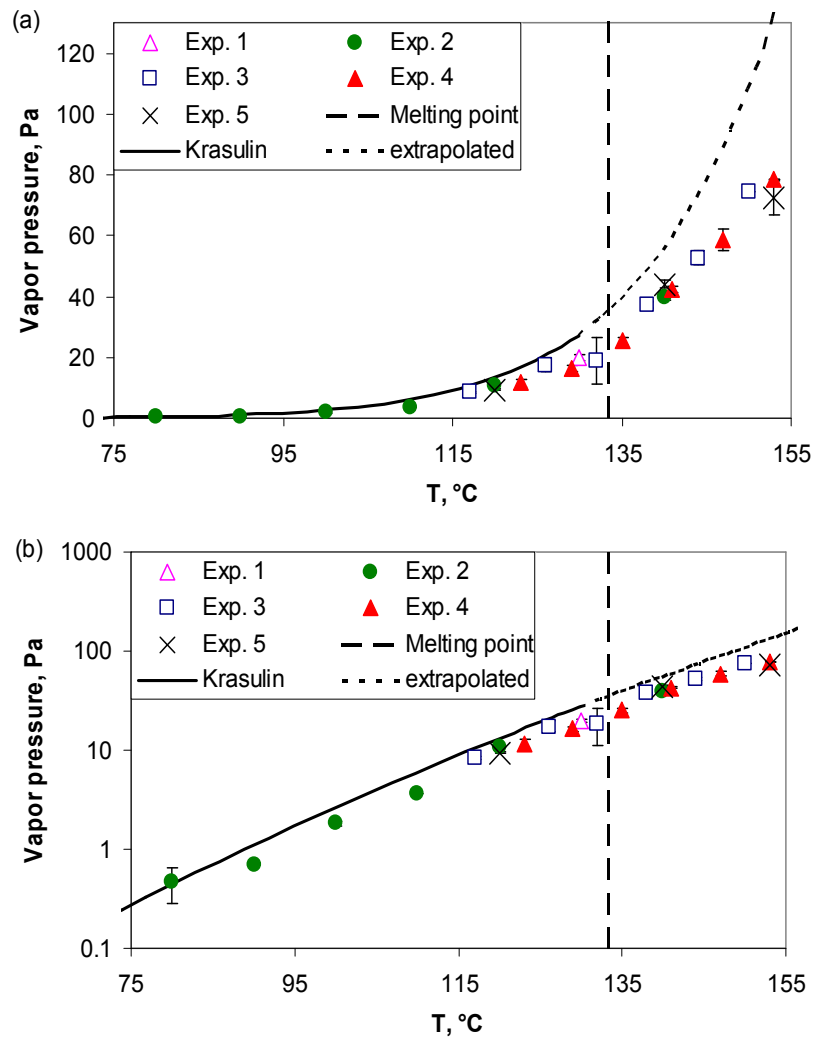
Fig. 3-6. Urea desorption from an inert urea-coated monolith. Model gas: 10% O₂, 5% H₂O in N₂, gas flow = 215 L/h at STP, GHSV = 9400 h⁻¹. Curve calculated according to ref. [41]. (a) Linear scale, (b) logarithmic scale.

Table 3-4. Details of the experimental results presented in Fig. 3-6.

Exp.	Urea on monolith, mg	Sampling interval, min	T_{set}, °C	p(urea), Pa	Stdev p(urea), Pa	Measured/ literature, %	p(HNCO), Pa	Stdev p(HNCO), Pa
1	755	3	130	19.8	0.90	72.0	11.06	6.73
2	704	6	80	0.46	0.18	104	0.00	0.00
		5	90	0.71	0.02	63.7	0.00	0.00
		4	100	1.82	0.11	69.1	0.03	0.02
		4	110	3.65	0.04	60.9	0.13	0.01
		3	120	10.9	0.16	83.0	0.97	0.08
		3	140	39.7	0.72	71.2	5.10	n.d.
3	715	3	117	8.43	0.38	81.0	0.67	0.03
		3	126	17.4	2.31	84.9	3.24	0.54
		3	132	18.8	7.77	59.1	4.88	2.04
		3	138	37.3	1.20	76.9	26.9	1.16
		3	144	52.6	2.26	71.9	53.7	2.60
		3	150	74.3	0.00	68.1	72.4	n.d.
4	640	3	123	11.5	1.18	70.0	1.69	0.73
		3	129	16.4	0.88	64.1	2.92	0.13
		3	135	25.3	1.30	64.3	7.69	0.45
		3	141	42.4	0.99	71.1	39.4	0.94
		3	147	58.7	3.41	65.6	59.6	3.63
		3	153	78.4	0.00	59.1	68.5	n.d.
5	1105	3	120	9.42	0.14	69.9	0.17	0.04
		3	140	43.9	1.24	77.4	77.5	1.98
		3	153	72.2	5.59	52.2	229	17.2

Table 3-5 shows a comparison between the fitting constants given by ref. [41] and our corresponding values. The calculation was not based on the average values given in Table 3-4 but on the single values for T ≤ 130°C or for the single values over the whole temperature range. Our values are outside the limits given in ref. [41]. As mentioned in chapter 3.2.1, this deviation is attributed to the endothermic nature of urea evaporation and urea decomposition causing an overly low effective monolith temperature. As expected, the deviation of our fitting constants from the reference is much larger when the considered temperature range is extended up to 153°C. Due to the extensive endothermic HNCO formation, the decrease

of the effective monolith temperature compared to the set temperature will be larger at higher temperatures. In addition, the melting point of urea is surpassed at 133°C, which falsifies the extrapolation of the reference curve. Incomplete saturation of the gas flow might also contribute to the observed overly low values. Different space velocities were only tested up to 130°C, see Table 3-3. Still, our values are not very different from the reference values. Taking into account the evidence of monomolecular urea presented in chapter 3.3.2, our results indicate that the saturation vapor pressure measured under vacuum is also valid for atmospheric pressure conditions.

Table 3-5. Fitting constants for the saturation vapor pressure of urea using the general equation ln(p) = A − B/T.

Used data	Value(A)	± (95%)	Value(B)	± (95%)
Krasulin	32.472	0.716	11755	268
T = 80-130°C	29.525	1.951	10765	752
T = 80-153°C	23.744	2.797	8588	1115

To estimate the impact of urea evaporation in the SCR process, a modern diesel engine with raw NO_x emissions of 200-300 ppm [25] was considered. Assuming a stoichiometric SCR reaction, this emission level requires 100-150 ppm urea. According to the saturation vapor pressure curve given by Krasulin et al. (1987) [41], a temperature of 116-122°C (calculated for p(atm) = 980 hPa) is thermodynamically sufficient to provide 100-150 ppm of gaseous urea. Given that the lower temperature limit for significant SCR performance is 150°C [14], the vapor pressure of urea poses no principle limitation for complete urea evaporation. However, due to the limited space in diesel vehicles, SCR systems usually have very short distances between the point of urea injection and the catalyst entrance, and thus the kinetics of urea evaporation becomes dominant at low temperatures.

3.3.4. Conclusions

It was shown that urea can be evaporated under flow reactor conditions at atmospheric pressure. In contrast to previous studies reported in the literature, urea was the main compound reaching the gas phase in our TPD experiments. We succeeded in evaporating up to 97% of the original urea without byproduct formation. The large surface of the urea film coated on an inert cordierite monolith and the applied high GHSV allowed the urea evaporation to be much faster than urea decomposition.

Product gas analysis was carried out both by FTIR spectroscopy and by a liquid-quench method followed by HPLC. HPLC was used to quantify urea and HNCO, whereas FTIR spectroscopy was used to record a spectrum of gaseous urea at atmospheric pressure for the first time. The obtained urea spectrum is in agreement with a spectrum recorded under vacuum in literature and a theoretical gas-phase spectrum of monomolecular urea, which we calculated using DFT. The existence of urea dimers in the gas phase could be excluded due to the clear mismatch of the measured spectrum and a DFT-calculated infrared spectrum of dimeric urea in the gas phase.

Urea evaporation experiments at atmospheric pressure substantially agreed with thermodynamic data obtained under vacuum and reported in literature. The deviation towards lower vapor pressures compared with the reference data was attributed to a temperature effect due to endothermic processes. Taking into account the evidence found for monomolecular urea, our results indicate that the saturation vapor pressure measured under vacuum is also valid for atmospheric pressure conditions.

4. Urea hydrolysis and side-reactions on titanium dioxide[A]

4.1. Introduction

Aqueous urea solution is widely used as NH_3-precursor in the SCR process. Urea is inexpensive, non-toxic and decomposes according to reactions 1 and 2 to yield the actual reducing agent NH_3.

Urea thermolysis: $\quad\quad CO(NH_2)_2 \rightarrow NH_3$ (g) + HNCO (g) $\quad\quad$ (1)

HNCO hydrolysis: $\quad\quad HNCO + H_2O \rightarrow NH_3 + CO_2$ $\quad\quad$ (2)

Direct urea hydrolysis: $\quad CO(NH_2)_2 + H_2O \rightarrow 2\ NH_3 + CO_2$ $\quad\quad$ (3)
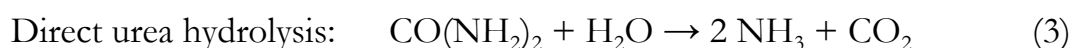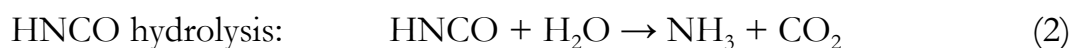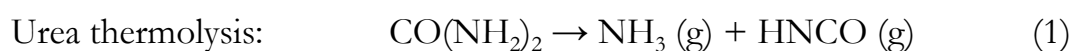
According to Todorova et al. (2011), there may also be an direct reaction pathway without intermediate HNCO formation (reaction 3) [78]. Direct urea hydrolysis will be discussed in chapter 6.

Unfortunately, the use of urea solution is associated with disadvantages including possible formation of solid deposits consisting of condensed urea and decomposition byproducts. The formation of byproducts is basically a consequence of the highly reactive intermediate HNCO participating in reactions other than hydrolysis [1, 48]. Starting above the melting point of urea at 133°C [79], biuret is formed in the reaction of HNCO with urea (reaction 4) [80].

[A] This chapter is based on the publication:

A. M. Bernhard, D. Peitz, M. Elsener, A. Wokaun, O. Kröcher „Hydrolysis and thermolysis of urea and its decomposition byproducts biuret, cyanuric acid and melamine over anatase TiO_2" *Appl. Catal., B.* **115-116**, 129 (2012).

$$CO(NH_2)_2 \text{ (m)} + HNCO \text{ (g)} \rightarrow NH_2\text{-}CO\text{-}NH\text{-}CO\text{-}NH_2 \qquad\qquad (4)$$
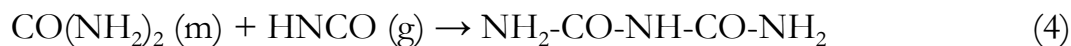
The often observed byproduct CYA is mainly formed between 190 to 250°C according to reaction 5 [38].

$$\text{biuret (m)} + HNCO \text{ (g)} \rightarrow CYA \text{ (s)} + NH_3 \text{ (g) [80]} \qquad\qquad (5)$$
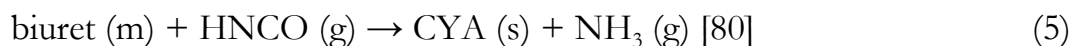
Further possible byproducts, which are sometimes observed in minor quantities, include the triazines ammelide, ammeline, melamine and the heptazines melam and melem [1, 66, 81, 82].

In general, the formation of byproducts is reversible. Different thermal and catalytic decomposition reactions of the byproducts are reported in the literature. For instance, biuret decomposes again into urea and HNCO above 193°C [38]. CYA was found to be stable up to a temperature of 250°C, where sublimation starts, but significant thermal decomposition into HNCO was only observed between 320 to 330°C [38]. Depolymerization of CYA over Al_2O_3 in the absence of water is known as a convenient method to generate HNCO in the laboratory [56]. Zahn et al. (1996) reported catalytic hydrolysis of CYA, melamine and derivatives over Al_2O_3 [54]. Mixing of urea with SCR catalyst powders was reported to improve the decomposition of urea and also the decomposition of byproducts [1, 39]. In most of the studies on urea and byproduct formation and decomposition, TGA and DSC were applied and the starting material was administrated in a crucible [1, 38, 39, 80], which induced a slow mass transport from the starting material to the gas phase. In reality, mass transport is much faster, as urea solution is nebulized to fine droplets when injected into the exhaust gas. When these droplets hit the walls of the exhaust pipe or the catalyst, they may rebounce to the gas phase, splatter to

smaller droplets or form a thin film [28, 71, 83]. In any of these cases, urea evaporation and decomposition to the gas phase should be easier than in experiments using solid urea in a crucible. In our study, monoliths were impregnated with a thin layer of the starting materials as described in chapter 2.4.2 in order to better represent the actual conditions in the exhaust pipe than did the previous TGA studies.

4.2. Experimental

The TPD reactor described in chapter 2.4.1 was used for the study on urea decomposition byproducts. The experimental parameters were as follows, unless indicated differently: Model gas: 10% O_2, 5% H_2O in N_2, gas flow rate = 431 L/h at STP, GHSV ≈ 100'000 h^{-1}. For the water-free experiments, the water saturator was bypassed and water traces were removed by a P_4O_{10} cartridge.

Inert or TiO_2-coated monoliths were impregnated by dipping them into aqueous solutions of urea, biuret CYA or melamine. The catalyst preparation and characterization is described in chapter 2.6. For biuret and CYA, which show limited solubility in water, the solutions had to be heated. Melamine was suspended in water at room temperature. TiO_2-coated cordierite sheets were impregnated with urea, CYA and melamine likewise and investigated by optical microscopy. CYA and melamine were found to be present as small particles (roughly 100 μm) on the TiO_2 surface. CYA crystals must have grown in the supersaturated solution due to cooling and evaporation of the solvent after dipping. In the case of urea, no particles were visible. Assuming that urea was present as a smooth film on the geometric monolith surface area of 120 cm^2, impregnation with 50 mg urea resulted in a film thickness of 3 μm. The amount of urea, biuret or

CYA coated on the monoliths was measured by weighing the wet monoliths immediately after dipping. Alternatively, the amount of starting material was calculated after the experiments, based on the C-balance or the reaction equations, which explain the formation of the observed product compounds (see chapter 4.3.2). For biuret and CYA, the calculated amount of starting material may be more accurate than the value obtained by weighing, since evaporation of the hot solution from the monolith led to underestimation of the wet weight. For melamine, only the calculated value was available, because the effective concentration of the suspension was not known. The conversion was always based on the calculated amount of starting material.

Liquid samples for HPLC analysis (see chapter 2.2 for the liquid-quench method and chapter 2.3 for the HPLC method) were collected at intervals of 2.5-6 min. The sampling intervals correspond to the concentration steps plotted in Fig. 4-7 and Fig. 4-8. In addition to TPD experiments at a temperature ramp of 10 K/min, experiments at constant temperature were carried out. The reactor was heated to a selected temperature, kept at this temperature for a certain time and then the reaction was quenched by pulling the monolith out of the hot reactor and letting it cool down under ambient conditions. The solid compounds on the monolith were washed off and analyzed by HPLC, see chapter 2.4.3. In some isothermal experiments, three liquid-quench samples were taken sequentially while the temperature was stable.

4.3. Results and Discussion

4.3.1. Overview

A summary of the observed urea decomposition reactions, including byproduct formation and decomposition, is shown in Fig. 4-1 and will be used as a reference point in the discussion of the resulting reaction network. Unlike analogous schemes reported in the literature [1, 38], our scheme was not derived from TGA/DSC experiments with samples placed in a crucible, but from flow reactor experiments with impregnated monoliths, which should better simulate the conditions in actual urea-SCR applications. Moreover, the main focus of our study was reactions occurring over anatase TiO_2 as a hydrolysis or thermolysis catalyst. Based on these experiments, we were able to significantly clarify urea decomposition chemistry.
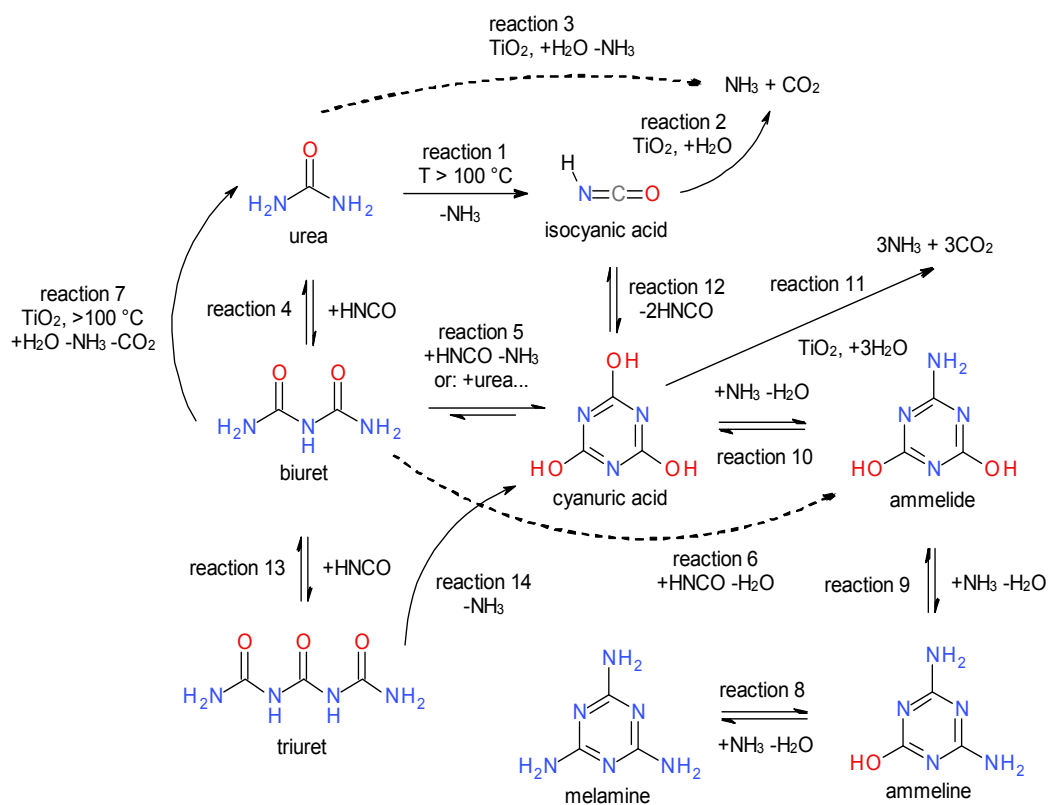
Fig. 4-1. Reaction network for urea decomposition with byproduct formation and decomposition.

The following list of reaction equations incudes all the reactions shown in Fig. 4-1:

$$CO(NH_2)_2 \text{ (urea)} \rightarrow NH_3 + HNCO \tag{1}$$

$$HNCO + H_2O \rightarrow NH_3 + CO_2 \tag{2}$$

$$\text{urea} + H_2O \rightarrow 2\,NH_3 + CO_2 \tag{3}$$

$$\text{urea} + HNCO \rightarrow NH_2\text{-CO-NH-CO-NH}_2 \text{ (biuret)} \tag{4}$$

$$\text{biuret} + HNCO \rightarrow C_3N_3(OH)_3 \text{ (CYA)} + NH_3 \tag{5a}$$

$$\text{biuret} + \text{urea} \rightarrow CYA + 2\,NH_3 \tag{5b}$$

$$2\,\text{biuret} \rightarrow CYA + HNCO + 2\,NH_3 \tag{5c}$$

$$\text{biuret} + HNCO \rightarrow \text{ammelide} + H_2O \tag{6}$$

$$\text{biuret} + H_2O \rightarrow \text{urea} + NH_3 + CO_2 \tag{7}$$

$$\text{melamine} + H_2O \rightarrow \text{ammeline} + NH_3 \tag{8}$$

$$\text{ammeline} + H_2O \rightarrow \text{ammelide} + NH_3 \tag{9}$$

$$\text{ammelide} + H_2O \rightarrow CYA + NH_3 \tag{10}$$

$$CYA + 3\,H_2O \rightarrow 3\,NH_3 + 3\,CO_2 \tag{11}$$

$$CYA \rightarrow 3\,HNCO \tag{12}$$

$$\text{biuret} + HNCO \rightarrow \text{triuret} \tag{13}$$

$$\text{triuret} \rightarrow CYA + NH_3 \tag{14}$$
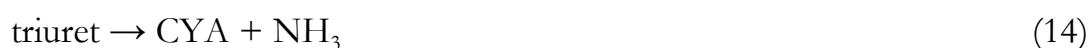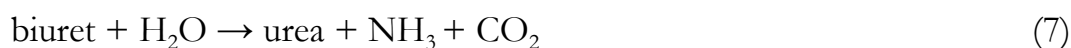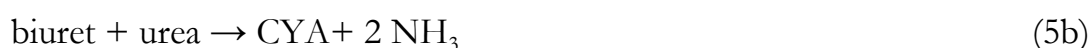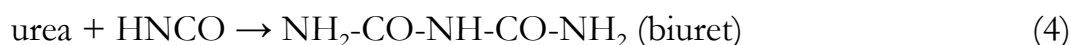
4.3.2. Urea hydrolysis[A]

Fig. 4-2 shows urea hydrolysis on (a) TiO_2 and (b) Fe-Beta. An inert cordierite monolith, impregnated with urea, was used as the source of gaseous urea (see Fig. 3-2a, page 78). A clean catalyst-coated monolith was placed downstream of the impregnated inert monolith to perform urea hydrolysis. In accordance with the literature, urea was efficiently hydrolyzed

---

[A] This chapter is based on results that were not used for a peer-reviewed publication.

into NH_3 and CO_2 [25, 48, 49, 56] and no byproduct formation was observed. Notably, one TiO_2-coated monolith did not achieve complete hydrolysis: 20% urea slip and 1.7% HNCO slip were observed. By contrast, two TiO_2-coated monoliths allowed for complete hydrolysis, see Fig. 4-3a.
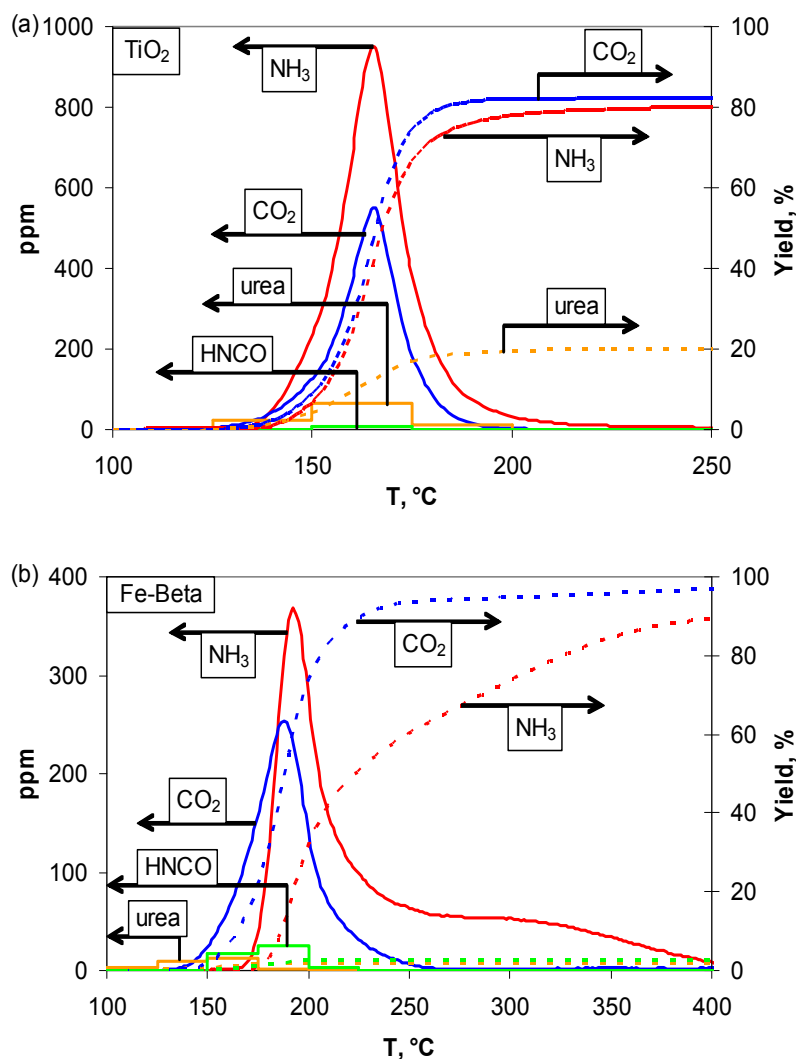
Fig. 4-2. Urea hydrolysis on one clean (a) TiO_2-coated or (b) Fe-Beta-coated monolith with an impregnated inert monolith as the urea source placed upstream; gas flow = 431 L_N/h with 5% H_2O, GHSV = 98'000 h^{-1} per monolith, heating rate = 10 K/min.

Other catalysts were tested likewise; Table 4-1 summarizes the results.

Table 4-1. Summary of TPD experiments on urea hydrolysis. NH$_3$ and CO$_2$ was measured by FTIR spectroscopy, urea and HNCO was measured by HPLC unless indicated differently.

Catalyst	Curve features, °C					Urea slip %	HNCO slip %	Urea mg
	NH$_3$ peak	CO$_2$ peak	HNCO peak	c(NH$_3$) >5 pm	c(CO$_2$) >5 ppm			
TiO$_2$	165	165	160	133-257	127-197	20	1.7	24.9
V$_2$O$_5$/WO$_3$-TiO$_2$	163	162	158	129-197	142-191	24[a]	11[b]	7.8
Cu-ZSM-5	180	177	170	152-340	137-240	15[a]	2.3[b]	7.8
Fe-Beta	193	189	180	196-417	140-254	7.2	2.8	19.7
Al$_2$O$_3$	178	180	173	144-239	141-234	18	1.3	18.6
ZrO$_2$	166	168	158	120-206	126-250	28	0.23	20
SiO$_2$	176	176	170	140-331	140-206	72	6.7	21.1

a: Not measured by HPLC but calculated form the NH$_3$ and HNCO yield
b: Measured by FTIR spectroscopy

The Fe-Beta SCR catalyst showed the highest urea conversion (Fig. 4-2b and Table 4-1). In contrast to the stationary experiments that will be shown in chapter 6, a high conversion in the TPD experiments does not necessarily indicate a high catalyst activity. In fact, Fe-Beta showed the NH$_3$, CO$_2$ and HNCO peaks at the highest temperature of all the tested catalysts, which indicates low hydrolysis activity. As expected, the strong acidity of the Fe-Beta catalyst induced a pronounced tailing of the NH$_3$ peak. However, CO$_2$, which is not strongly adsorbed, also showed its peak at the highest temperature, which further indicates low hydrolysis activity. Hence, the high urea conversion on Fe-Beta must be attributed to strong urea adsorption, resulting in an increased residence time of the urea on the catalyst. According to literature, the moderate strength Lewis acid sites of TiO$_2$ are favorable for HNCO hydrolysis, whereas strong acidity has an adverse effect [51, 52]. Apparently, TiO$_2$ is also favorable for urea hydrolysis, whereas the acidity of Fe-Beta [84] was too strong to provide high hydrolysis activity, but allowed for strong urea adsorption.

ZrO_2 showed the smallest HNCO slip, which can be explained by its very high HNCO hydrolysis activity [57]. Please note that this ZrO_2 catalyst exhibited a BET surface of 39 m^2/g. In chapter 6, results from a different ZrO_2 catalyst with higher BET surface of 67 m^2/g, coated on a 600 cpsi monolith, will be shown.

SiO_2 showed only little urea conversion and it also shows little HNCO hydrolysis activity [57]. In conclusion, urea and HNCO hydrolysis activities seem to be correlated. Catalytic urea hydrolysis and urea thermolysis will be further discussed in chapter 6.

4.3.3. Biuret decomposition

Fig. 4-3 shows the hydrolysis of (a) urea and (b) biuret over TiO_2. A catalyst-coated monolith was impregnated with urea or biuret and a second catalyst-coated monolith was placed downstream (see Fig. 2-18, page 64 for the placement of the monoliths in the reactor). Since two TiO_2-coated monoliths were used instead of one as for the experiment shown in Fig. 4-2a, urea was completely hydrolyzed. Biuret was also completely hydrolyzed (Fig. 4-3b), which suggests that this reaction was catalyzed, too. In order to facilitate comparing the emissions from urea and biuret, the CO_2-emission curve for urea hydrolysis from Fig. 4-3a was added to Fig. 4-3b. Comparison of the CO_2-emission curves reveals that biuret hydrolysis started at a lower temperature than urea hydrolysis. Since biuret is more stable against thermal decomposition than urea [38], the low temperature offset of biuret hydrolysis strongly indicates catalytic biuret hydrolysis. Another feature of the experiment with biuret was a broader shape of the NH_3 and CO_2 emission curves, which is attributed to slower mass transport of biuret to the catalytically active centers. CYA production from biuret

cannot explain the broader curves, because hydrolysis of pure CYA showed an NH_3 emission peak at a higher temperature of 240°C, see Fig. 4-8.
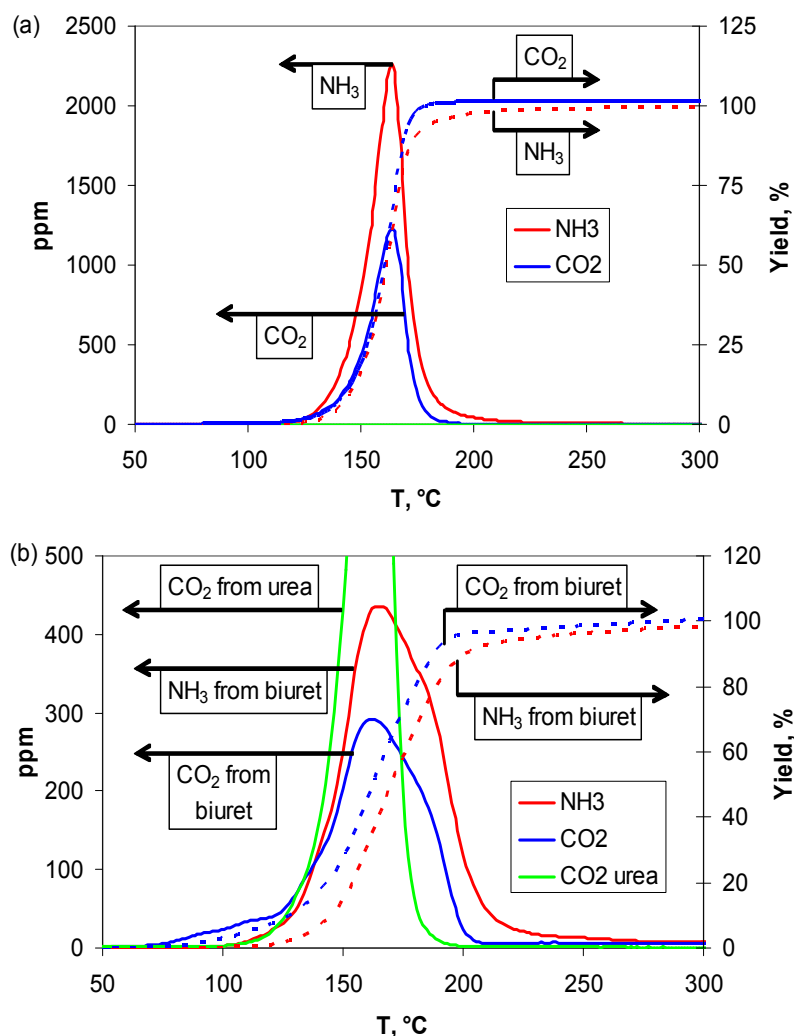
Fig. 4-3. Hydrolysis of (a) urea and (b) biuret over TiO_2. Two TiO_2-coated monoliths were placed in the reactor; the first monolith was additionally impregnated with urea or biuret; the second TiO_2-coated monolith was clean. Parameters: Heating rate = 10 K/min, model gas: 10% O_2, 5% H_2O in N_2, gas flow = 431 L/h at STP, GHSV = 98'000 h^{-1} per monolith, active masses ≈ 0.6 g per monolith, m(biuret) = 24.8 mg, m(urea) = 47.9 mg.

The CO_2 emission from biuret over TiO_2 at low temperature (Fig. 4-3) indicated catalytic biuret decomposition, but did not indicate whether

HNCO was eliminated and then hydrolyzed (reaction 4' plus reaction 2) or if biuret was directly hydrolyzed (reaction 7). Hence, biuret thermolysis according to reaction 4', without subsequent HNCO hydrolysis, was investigated under dry model gas conditions. An impregnated, TiO_2-coated monolith was placed in the reactor. The reactor was first heated to 130°C and then to 150°C, as shown in Fig. 4-4a. In spite of the dry model gas, CO_2 was still formed, which can only be explained by hydrolysis reactions with residual water in the system. Most likely, this water was adsorbed on the catalyst surface because the monolith had been impregnated with an aqueous biuret solution. Heating the reactor to 130°C induced a prominent CO_2 peak, but the CO_2 emission dropped to a very low level within roughly 10 min (Fig. 4-4a). The absence of an HNCO peak when heating the reactor to 130°C suggests that the observed CO_2 and NH_3 peaks were caused by direct biuret hydrolysis (reaction 7). When the reactor was heated to 150°C, only little water was left on the catalyst. Fig. 4-4b shows the averaged quasi-stationary emissions from the impregnated catalyst at 130°C and 150°C. The time ranges considered for averaging the gaseous emissions were 26.5 to 42.5 min at 130°C and 52.5 to 61.5 min at 150°C. For the purpose of comparison, emissions from an impregnated, inert monolith and from a urea thermolysis experiment are included in Fig. 4-4b. After heating to 150°C, the biuret thermolysis reaction was quenched, the monolith was washed and the washing solution was analyzed by HPLC (Table 4-2).
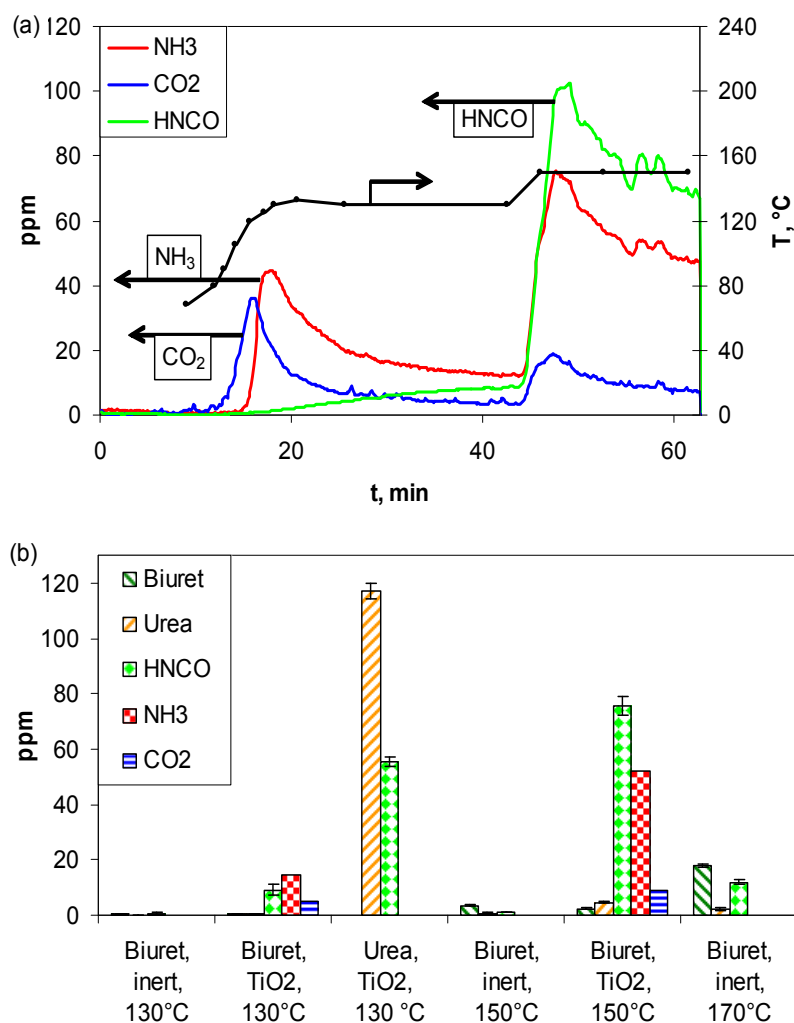
Fig. 4-4. Dry biuret and urea thermolysis over TiO_2. One impregnated, TiO_2-coated monolith was placed in the reactor. (a) Gaseous emissions from biuret thermolysis during heat up at 130°C and 150°C measured by FTIR spectroscopy. (b, columns 1, 4 and 6) Non-catalytic, quasi-stationary biuret thermolysis at 130°C, 150°C and 170°C compared to (columns 2 and 5) catalytic biuret thermolysis and (column 3) catalytic urea thermolysis. For the catalytic urea thermolysis, urea was desorbed from an inert monolith and then passed through a clean, TiO_2-coated monolith. Parameters: Model gas: 10% O_2 in N_2 (dry), gas flow = 431 L/h at STP, GHSV = 98'000 h^{-1}, active mass ≈ 0.6 g, m(biuret on catalyst) = 130 mg (calc. from C-balance) or 84 mg (weight), conversion = 36%, m(biuret on inert monolith) = 78 mg (weight).

The comparison shown in Fig. 4-4b reveals that biuret was quite stable in the absence of the catalyst (columns 1, 4 and 6). Even at 170°C, the main compound detected in the gas phase was intact biuret (rightmost column in Fig. 4-4b). In the presence of the catalyst, the HNCO emission was dramatically increased (columns 2, and 5), indicating catalytic biuret thermolysis (reaction 4'). Catalytic biuret thermolysis followed by HNCO hydrolysis (reaction 4' plus reaction 2) cannot explain the low temperature CO_2 emission from biuret shown in Fig. 4-3b, because urea thermolysis (reaction 1, column 3 in Fig. 4-4b) over TiO_2 was even faster than biuret thermolysis (reaction 4', column 2). Hence, the low temperature CO_2 emission in the biuret hydrolysis experiment shown in Fig. 4-3b must be due to catalytic, direct biuret hydrolysis over TiO_2 according to reaction 7.

Table 4-2 shows the selectivity of the biuret thermolysis reaction based on the analysis of the catalyst washing solutions and the gaseous emissions integrated over the complete duration of the experiment shown in Fig. 4-4a.

Table 4-2. Detailed results on the catalytic biuret thermolysis experiment at T ≤ 150°C shown in Fig. 4-4a.

Compound	Amount, µmol	Yield, mmol/mol-biuret	Selectivity, mmol/mol-biuret	Selectivity, C-%	Selectivity, N-%
Starting material	1290	-	-		
Intact biuret (s+g)	820	640	-		
NH_3	510	400	1100	0	36
CO_2	160	130	340	17	0
HNCO (s+g)	500	390	1100	53	35
CYA	43	33	91	14	9.1
Urea (s+g)	68	52	140	7.2	9.6
Triuret	17	13	36	5.5	4.8
Ammelide	8.9	6.9	19	2.8	2.5
Ammeline	2.6	2.0	5.4	0.8	0.9
Sum				100	98

To estimate the importance of the different reactions shown in Fig. 4-1, we considered a set of reactions that is able to explain the formation of the observed compounds. Hydrolysis reactions were neglected, because hydrolysis was mainly caused by undesired, residual water adsorbed on the catalyst. Also, we assumed that CYA was produced by the reaction of biuret with HNCO (reaction 5a). CYA production may also proceed via ring closure of triuret (reaction 14), but since reaction 5a is the sum of triuret formation (reaction 13) plus reaction 14, the experiment does not allow for distinguishing between these two pathways. Hence, reactions 4', 1, 5a, 13, 10' and 9' were considered. From the stoichiometries of the reactions and all the measured reaction products, except NH_3 and CO_2, the contributions of the considered reactions were calculated (Fig. 4-5). Biuret thermolysis (reaction 4') appeared to be the predominant reaction. Reaction 4' produces equimolar amounts of urea and HNCO. HNCO was observed during the experiment with high yield, but the urea yield was much lower, because most of the produced urea was further thermolyzed (reaction 1). The small yield of urea is in agreement with the low stability of urea against catalytic thermolysis at 130°C concluded from Fig. 4-4b.
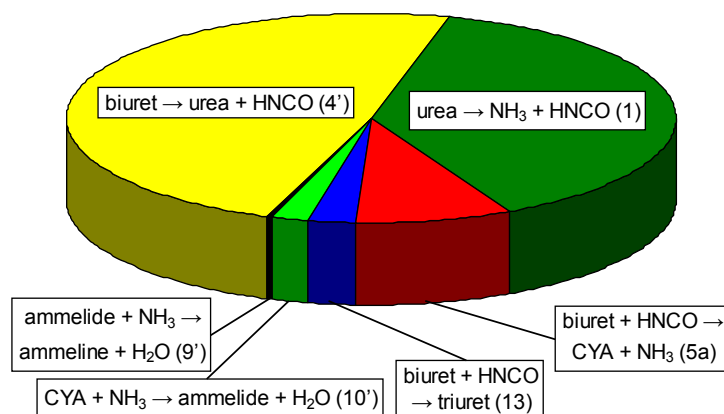
Fig. 4-5. Calculated proportions of the different reactions observed during the biuret thermolysis experiment presented in Fig. 4-4a.

To increase the urea yield, biuret decomposition experiments were performed at only 100°C. An impregnated, TiO_2-coated monolith was placed in the reactor and the water concentration in the model gas was set to 5%. The reactor was heated to 100°C and the temperature was kept constant for about 2 h. Then, the reaction was quenched and the solid compounds were washed off the monolith and measured by HPLC. For comparison, a similar experiment was performed under dry model gas conditions. Before starting the water-free experiment, the impregnated monolith was dried inside the reactor at 70°C for 1 h. Table 4-3 shows the selectivities measured by HPLC. The conversions and the selectivities towards NH_3, CO_2 and H_2O were calculated according to Fig. 4-6. The amounts of gaseous compounds measured by FTIR spectroscopy could not be evaluated because the concentrations were too low.

Table 4-3. Selectivities in the biuret decomposition experiments. Parameters: T = 100°C, model gas: 10% O_2, 5% or 0% H_2O in N_2, gas flow = 431 L/h at STP, GHSV = 98'000 h^{-1}, active mass ≈ 0.6. Experiment with 5% H_2O: m(biuret) = 25 mg, conversion = 33%. Experiment with 0% H_2O m(biuret) = 22 mg, conversion = 20%. The amounts of starting material and the conversions were calculated according to Fig. 4-6.

Selectivities	5% H_2O in the model gas			0% H_2O in the model gas		
Compound	mmol/mol-biuret	C-%	N-%	mmol/mol-biuret	C-%	N-%
Urea	760	38	51	470	23	31
CYA	74	11	7.4	160	23	16
Ammelide	25	3.7	3.3	56	8.4	7.5
Triuret	15	2.2	2.0	34	5.2	4.6
Ammeline	8	1.2	1.3	20	3.0	3.4
NH_3 (calc.)	1100	0.0	36	1100	0.0	38
CO_2 (calc.)	880	44	0.0	730	37	0.0
H_2O (calc.)	-840			-640		
Sum		100	100		100	100

The main solid reaction product was urea. The high selectivity for urea formation is in agreement with the apparently lower activation energy for the hydrolysis of biuret to urea (reaction 7) compared to urea hydrolysis, indicated by Fig. 4-3. On the other hand, if urea hydrolyzed faster than biuret, most of the produced urea would have been hydrolyzed. Under dry model gas conditions, water was still sufficiently abundant on the catalyst surface to allow for significant biuret hydrolysis. Of course, it had to be expected that drying the catalyst at 70°C would remove only part of the adsorbed water. Piazzesi et al. (2006) found, by DRIFT experiments, that some residual OH groups are present on TiO_2 even when treated at 450°C [49]. However, in the experiment with dry model gas, the biuret conversion and the selectivity towards urea were lower, whereas the byproduct yields were higher.

Fig. 4-6 shows the proportions of a set of considered reactions to explain the solid products reported in Table 4-3. Fig. 4-5 was calculated likewise.

As concluded from Fig. 4-3b and Fig. 4-4b, direct biuret hydrolysis was assumed (reaction 7). Urea thermolysis (reaction 1) was considered as the source of HNCO, which is required to explain the byproduct formation, because urea thermolysis was found to be much faster than biuret thermolysis (reaction 4') (Fig. 4-4b). Biuret thermolysis (reaction 4') was neglected because of the low temperature applied (100°C). Also, we assumed that, in spite of the presence of water, most of the intermediately produced HNCO formed CYA and triuret (reaction 5a and 13) instead of being hydrolyzed (reaction 2). Further, the HNCO yield was set to zero. For the experiment with dry model gas, HNCO hydrolysis (reaction 2) was neglected. For the experiment with wet model gas, we assumed that HNCO hydrolysis caused the decreased byproduct yield. The decrease in the absolute yields of CYA, ammelide, ammeline and triuret corresponded to a decrease in the consumption of HNCO by 9.3 µmol. The proportion of reaction 2 in the experiment with water in the model gas was chosen so that 9.3 µmol HNCO were hydrolyzed. Hence, reactions 7, 1, 5a, 10', 13, 9' and 2 were considered.

(a)

biuret + $H_2O \rightarrow$ urea + NH_3 + CO_2 (7)

urea $\rightarrow NH_3$ + HNCO (1)

biuret + HNCO $\rightarrow$ CYA + NH_3 (5a)

CYA + $NH_3 \rightarrow$ ammelide + H_2O (10')

biuret + HNCO $\rightarrow$ triuret (13)

ammelide + NH_3 $\rightarrow$ ammeline + H_2O (9')

(b)

biuret + $H_2O \rightarrow$ urea + NH_3 + CO_2 (7)

urea $\rightarrow NH_3$ + HNCO (1)

biuret + HNCO $\rightarrow$ CYA + NH_3 (5a)

ammelide + $NH_3 \rightarrow$ ammeline + H_2O (9')

biuret + HNCO $\rightarrow$ triuret (13)

CYA + $NH_3 \rightarrow$ ammelide + H_2O (10')
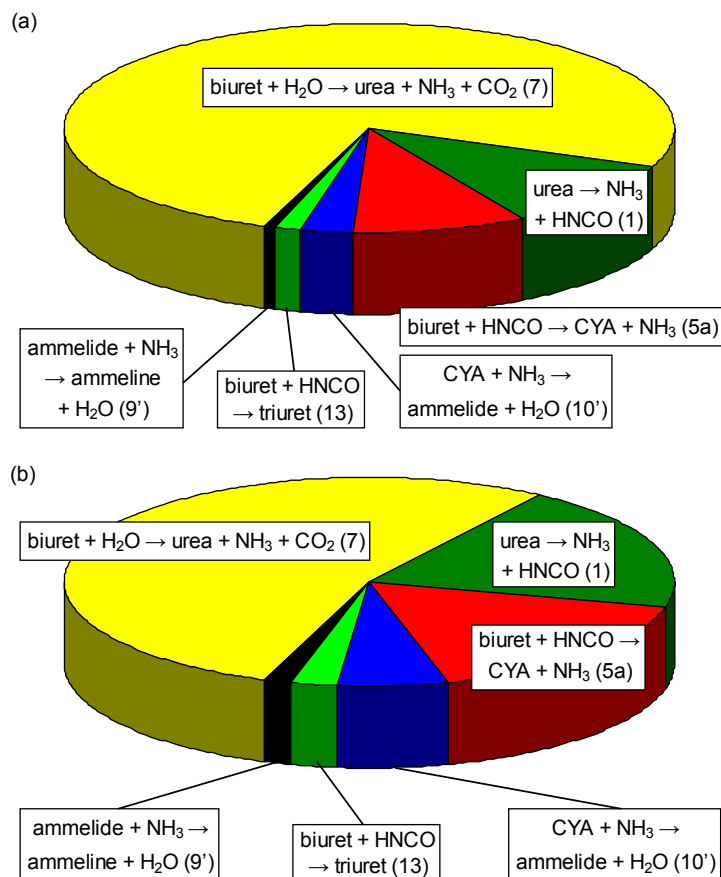
Fig. 4-6. Calculated proportions of the different reactions observed during the biuret decomposition experiments at 100°C, presented in Table 4-3. (a) 5% H_2O in the model gas, (b) without H_2O in the model gas.

According to Fig. 4-6, direct biuret hydrolysis (reaction 7) was the predominant reaction. Also, a significant amount of the urea produced seemed to have been thermolyzed (reaction 1) to provide the HNCO required for CYA and triuret production. Still, urea remained the main solid reaction product, which supports our conclusion that the direct hydrolysis of biuret to yield urea (reaction 7) caused the low temperature CO_2 emission shown in Fig. 4-3b. The following order of reaction rates was concluded from the biuret hydrolysis experiments: reaction 7 (biuret + $H_2O \rightarrow$ urea + NH_3 + CO_2) > reaction 1 (urea $\rightarrow NH_3$ + HNCO) $\approx$

reaction 5a (biuret + HNCO → CYA + NH_3) > reaction 2 (HNCO + H_2O → NH_3 + CO_2)

4.3.4. Melamine hydrolysis

It is known that melamine hydrolysis in boiling alkaline solution is a multi-step reaction yielding CYA [81]. Zhan et al. (1996) reported catalytic melamine hydrolysis over Al_2O_3 yielding NH_3 and CO_2 [54]. The reaction proceeded apparently in one step under their experimental conditions.

Fig. 4-7 shows melamine sublimation from (a) an inert monolith and (b) melamine hydrolysis over TiO_2. The steps in the concentration curves are due to the intervals for collecting the liquid samples for HPLC analysis. The first sampling interval in Fig. 4-7a was started when the reactor reached 150°C and ended at 175°C.
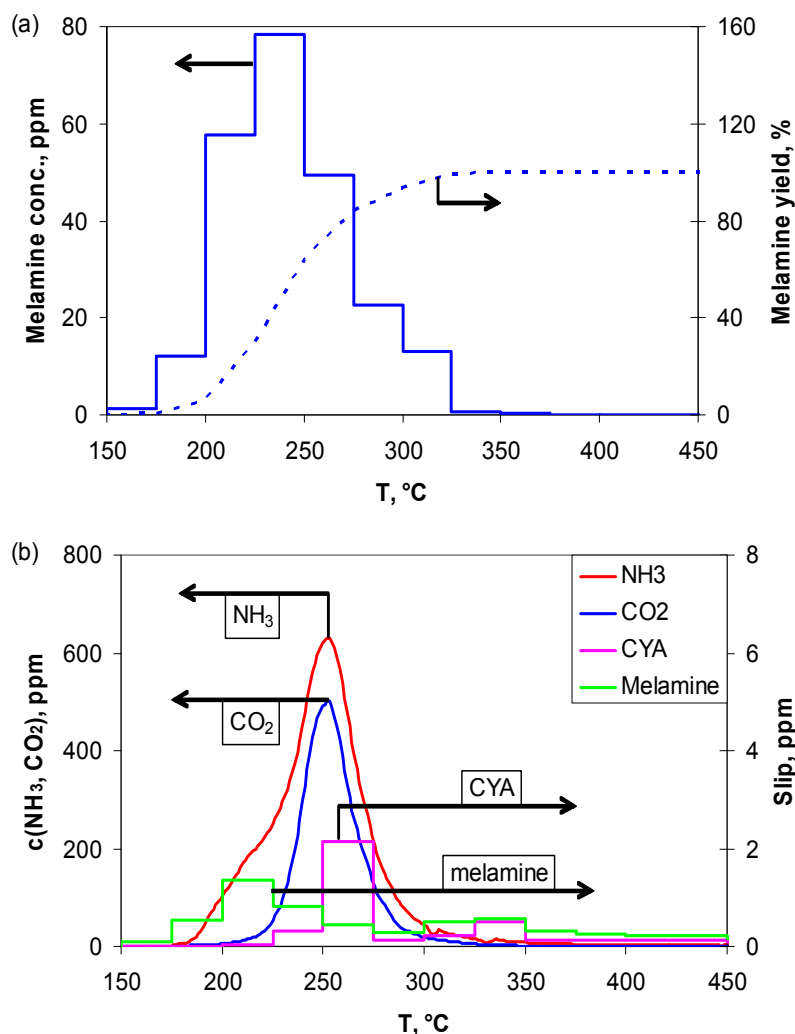
Fig. 4-7. (a) Melamine sublimation from an impregnated inert monolith. Parameters: Model gas: 10% O_2 in N_2 (dry), $GHSV_{inert}$ = 97'000 h^{-1}, m(melamine) = 23.8 mg (calc. from C-balance). Only HPLC analysis. (b) Melamine hydrolysis over TiO_2. Two TiO_2-coated monoliths were placed in the reactor, the first monolith was impregnated with melamine, and the second TiO_2-coated monolith was clean. Parameters: Model gas: 10% O_2, 5% H_2O in N_2, $GHSV_{cat}$ = 98'000 h^{-1}, active mass ≈ 0.6 g per catalyst-coated monolith, m(melamine) = 22.1 mg (calc. from C-balance). Gas flow = 431 L/h at STP.

When a melamine-impregnated inert monolith was heated, melamine sublimed without detectable byproduct formation (Fig. 4-7a). In the presence of TiO_2, melamine was efficiently hydrolyzed (Fig. 4-7b). Interestingly, the NH_3 emission started at a lower temperature than did the

CO_2 emission. In all the experiments starting with a material other than melamine, the CO_2 emission started at a lower temperature than the NH_3 emission, which is attributed to the pronounced adsorption properties of NH_3. Compared to CYA hydrolysis, the NH_3 emission from melamine started 27 K below (rows 1 and 2 in Table 4-4).

Table 4-4. Summary of melamine and CYA hydrolysis TPD experiments (row 1: Fig. 4-7b, row 2: Fig. 4-8, row 3: not plotted).

Row	Monoliths	Starting material	Con-version, %	NH₃ curve features, °C		CO₂	Selectivity, mmol/mol		
				c > 5 ppm	Peak		Ammeline	Ammelide	CYA
1	2x TiO₂	melamine	97	178-369	253	2900	0.1	-	18
2	2x TiO₂	CYA	98	205-342	243	3000	-	-	-
3	inert + 1x TiO₂	melamine	68	184-338	268	2300	35	6.3	200

The early NH_3 emission observed during melamine hydrolysis indicates a multi-step reaction pathway, where the amine groups were hydrolyzed first according to reactions 8, 9, 10 and CYA was produced as an intermediate. Only cleavage of the triazine ring (reaction 11) at higher temperature resulted in CO_2 emission. In agreement with the assumption of intermediate CYA formation, a small CYA slip could be detected (Fig. 4-7b). If only one instead of two TiO_2-coated monoliths was used, the intermediates ammeline and ammelide were detected as well (row 3 in Table 4-4).

The formation of intermediates in the multi-step hydrolysis of melamine was further investigated by an isothermal experiment at 160°C. An impregnated, TiO_2-coated monolith was heated to 160°C for approximately 1 h. The reaction was then quenched, the monolith was washed and the washing solution was analyzed by HPLC. The melamine desorption was measured in the time interval of 28 to 43 min and linearly extrapolated to

the whole time range for calculating the conversion. Table 4-5 shows the yields and selectivities of the reaction. In an analogous experiment at 165°C, more CYA and less ammeline was formed (rightmost column).

Table 4-5. Melamine hydrolysis over TiO$_2$ at 160°C. Parameters: Model gas: 10% O$_2$, 5% H$_2$O in N$_2$, gas flow = 431 L/h at STP, GHSV$_{cat}$ = 98'000 h^{-1}, active mass ≈ 0.6 g, m(melamine) = 8.3 mg (calc. from C-balance, neglecting CO$_2$), conversion = 75.4%. Additionally, selectivities from an analogous experiment at 165°C are shown.

Compound	Yield at 160°C, mmol/mol-melamine	Selectivity at 160°C			Selectivity at 165°C		
		mmol/mol	C-%	N-%	mmol/mol	C-%	N-%
Ammeline	400	530	53	44	130	13	11
CYA	340	450	45	22	750	75	37
Ammelide	15	20	2.0	1.3	70	6.5	4.3
Biuret	3.4	4.5	0.3	0.2	30	1.8	1.4
NH$_3$	1100	1500	-	24	2500	-	42
CO$_2$	neglected				110	3.8	
HNCO						0.8	0.4
Sum			100	92		100	96

The observed selectivities indicate the following order of reaction rates: reaction 8 (melamine + H$_2$O → ammeline + NH$_3$) ≈ reaction 10 (ammelide + H$_2$O → CYA + NH$_3$) > reaction 9 (ammeline + H$_2$O → ammelide + NH$_3$) > reaction 11 (CYA → 3 NH$_3$ + 3 CO$_2$)

4.3.5. Hydrolysis and de-polymerization of CYA

It is known that the hydrolysis (reaction 11) [54] and the de-polymerization (reaction 12) of CYA are catalyzed over Al$_2$O$_3$ [56]. Our results show that TiO$_2$ catalyzes these reactions as well. Fig. 4-8a shows CYA desorption from an inert monolith, Fig. 4-8b shows CYA thermolysis and Fig. 4-8c shows CYA hydrolysis over TiO$_2$.
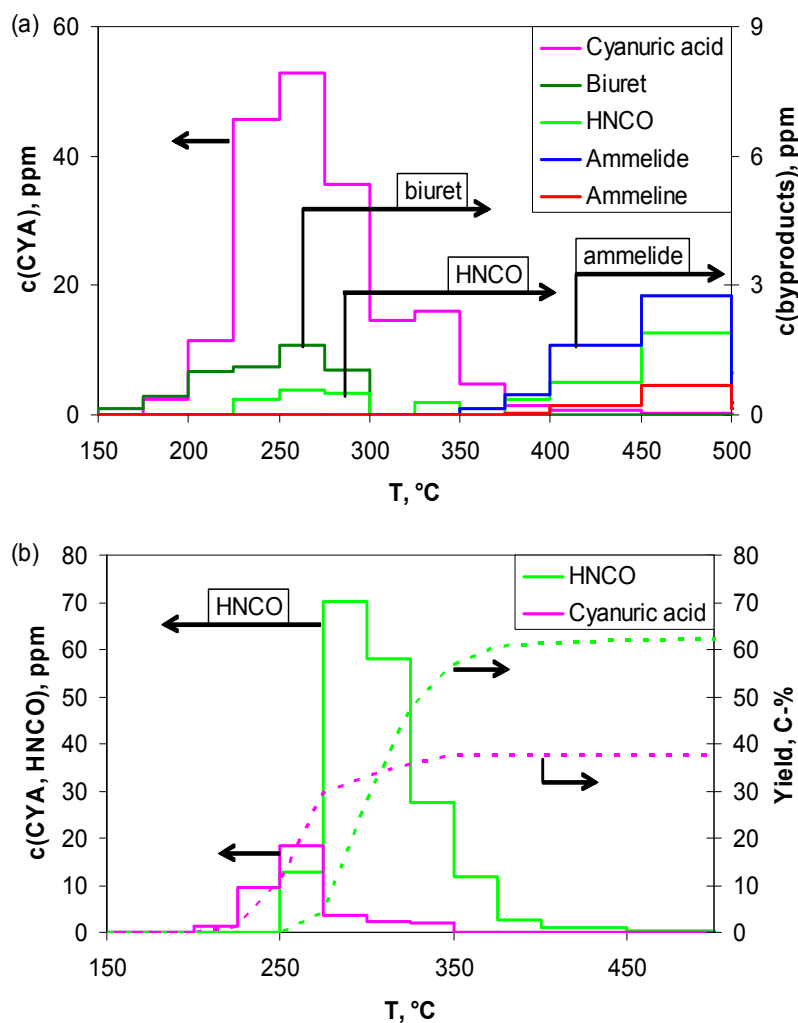
Fig. 4-8 (a-b). (a) CYA desorption from an inert monolith, m(CYA) = 20.4 mg (calc. from C-balance). (b) CYA thermolysis on TiO$_2$: CYA was desorbed from an inert monolith and then passed through a TiO$_2$-coated monolith, m(CYA) = 10.5 mg (calc. from C-balance) or 10.3 mg (weight). Model gas: 10% O$_2$, 0% H$_2$O in N$_2$; gas flow = 431 L/h at STP; GHSV$_{inert}$ = 97'000 h^{-1}, GHSV$_{cat}$ = 98'000 h^{-1}; active mass ≈ 0.6 g; only HPLC analysis.
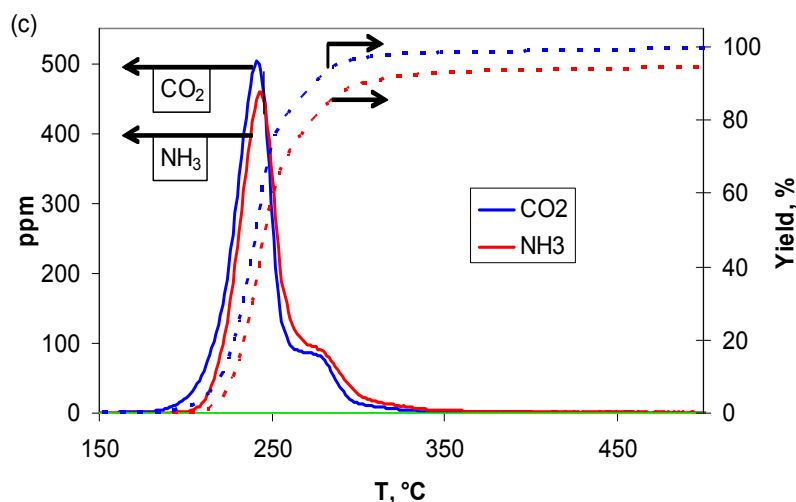
Fig. 4-8 (c). CYA hydrolysis over TiO$_2$: two TiO$_2$-coated monoliths were placed in the reactor, the first monolith was impregnated, and the second monolith was clean, m(CYA) = 23.4 mg (weight). Model gas: 10% O$_2$, 5% H$_2$O in N$_2$; gas flow = 431 L/h at STP; GHSV = 98'000 h^{-1} per monolith; active mass ≈ 0.6 g per monolith.

CYA sublimed from an impregnated inert monolith (Fig. 4-8a) with lower vapor pressure than melamine (Fig. 4-7a). In addition to CYA, small amounts of biuret, HNCO, ammelide and ammeline were detected; the total yield of these byproducts was 6 wt%. For the dry CYA depolymerization over TiO$_2$ shown in Fig. 4-8b, a clean, catalyst-coated monolith was placed downstream of a CYA-impregnated inert monolith. Due to the catalyst, 63% of the CYA was depolymerized into HNCO. The reaction was highly selective; no byproducts could be detected. It is important to mention that NH$_3$ and CO$_2$ could not be measured, since FTIR spectroscopy was not applied in the experiments presented in Fig. 4-8a and Fig. 4-8b. Fig. 4-8c shows CYA hydrolysis over TiO$_2$, followed by FTIR spectroscopy. Two TiO$_2$-coated monoliths were placed in the reactor, the first was impregnated and the second was clean. CYA was almost completely hydrolyzed due to the catalyst. Only 1.4% of the CYA was emitted unconverted and no byproducts were detected by HPLC

analysis. The shoulders in the emission curves in Fig. 4-8c are attributed to a mass transport limitation from CYA grains to the active catalyst centers. Indeed, CYA grains in the size of roughly 30-200 μm were observed on the TiO_2 surface by optical microscopy.

4.3.6. CYA formation

CYA formation could, in principle, proceed via reactions 5a, 5b, 5c, 10, 12' and 14. The present results do not allow for definite evaluation of the contribution of each of these or to elucidate further reactions. Yet, some conclusions can be made. Table 4-6 and Fig. 4-9 summarize our results relating to CYA production from urea or biuret.

Table 4-6. Summarized results for CYA formation from urea and biuret. TiO_2-coated monoliths were impregnated with urea or biuret and exposed to selected temperatures.

Row	Comp.	T,°C	Gas	CYA	Ammelide	Ammeline	HNCO	Urea	Biuret	Triuret	CO₂	NH₃
1	urea	125	dry	0.4			310		170	2.7	230	1300
2	urea	145+	dry	7.2	1.6	0.1	890		30	6.7	no FTIR	
3	urea	150+	dry	12	1.5	0.2	890		23	6.8	no FTIR	
4	biuret	100	dry	160	56	20	0	470		34	FTIR ignored	
5	biuret	125	dry	170	46	26	710	450		38	no FTIR	
6	biuret	≤150	dry	91	19	5.4	1100	140		36	340	1100
7	urea	100	wet	0.9	2.8	4.6	40		2.4	0	930	2000
8	biuret	100	wet	74	25	8	0	760		15	FTIR ignored	
9	biuret	114	wet	34	6.2	2.8	26	240		2.3	1600	2100
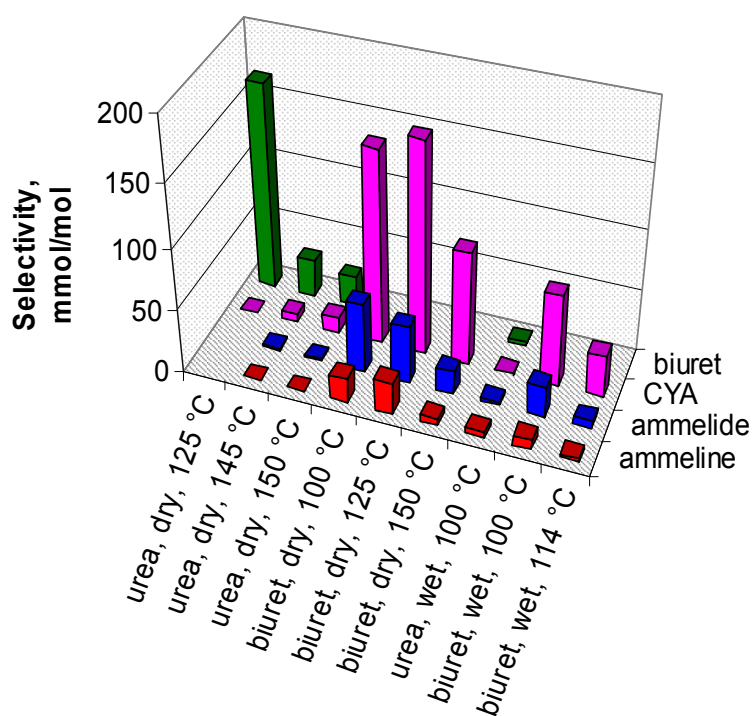
Fig. 4-9. Formation of solid byproducts in the experiments presented in Table 4-6.

A significant amount of CYA was produced during biuret thermolysis at 125°C (row 5 in Table 4-6). By contrast, from urea under similar conditions, very little CYA but significant biuret production was observed (row 1). The small CYA production from urea indicates that HNCO preferentially reacted to form biuret (reaction 4) rather than CYA (reaction 5a or reaction 12). Combination of HNCO and biuret to form ammelide (reaction 6) did not seem to be important, as less ammelide than CYA was formed. Since a large amount of NH_3 relative to water was present on the catalyst surface, it is plausible that ammelide and ammeline were formed in reactions with NH_3 (reactions 10', 9',). The combination of biuret with urea (reaction 5b) appeared to be unimportant, as the biuret produced during urea thermolysis (row 1 in Table 4-6) did not react further to produce CYA.

Interestingly, CYA was also produced from biuret under wet model gas conditions at only 100°C (row 8 in Table 4-6), indicating that HNCO preferentially formed CYA (reaction 5a) instead of being hydrolyzed (reaction 2). The stability of HNCO on the TiO_2 surface required for reaction 5a is plausible, because Piazzesi et al. (2006) reported a steep drop of the HNCO hydrolysis activity when the temperature was decreased from 150°C to 100°C [49]. Also, the results presented in chapter 6 show that the urea thermolysis activity of TiO_2 does not drop as steeply as the hydrolysis activity, which should allow a significant surface concentration of HNCO to be built up at low temperature. Biuret hydrolysis at 100°C was discussed in chapter 4.3.3. In contrast to biuret hydrolysis, urea hydrolysis at 100°C did not yield significant amounts of byproducts (row 7 in Table 4-6). It is possible that a large fraction of the intermediately produced HNCO reacted with urea to form biuret as another intermediate (reaction 4) and the biuret was then directly hydrolyzed (reaction 7).

Alternatively, HNCO hydrolysis (reaction 2) at 100°C might still be too fast to allow for CYA formation by the reaction of biuret with HNCO (reaction 5a). In this case, biuret dimerization (reaction 5c) might be the reason for the CYA formation observed during biuret hydrolysis at 100°C (row 8 in Table 4-6). However, the difference in the temperature dependence of CYA formation under either dry or wet model gas conditions supports the assumption that HNCO is needed for CYA formation. When the temperature for biuret decomposition under dry model gas was increased from 100°C to 125°C, the CYA yield remained quite constant (row 4 and row 5 in Table 4-6). At 150°C, CYA formation was moderately decreased, which was most probably caused by HNCO desorption (row 6 in Table 4-6). By contrast, wet model gas induced a decreased CYA formation at

100°C, with a further decrease at 114°C (row 8 and row 9 in Table 4-6). HNCO hydrolysis (reaction 2) is likely to explain the decreased CYA formation by reducing the amount of HNCO available for reaction 5a. If biuret dimerization (reaction 5c) was the main reaction pathway for CYA formation, more CYA should have been produced from biuret under wet model gas conditions. Further, the combination of biuret with urea (reaction 5b), which is an analogous reaction, seemed to be unimportant as well (row 1 in Table 4-6) and simultaneous elimination of two NH_3 molecules plus one HNCO molecule seems unlikely. Hence, the following order of reaction rates at 100°C is a plausible conclusion from Table 4-6: reaction 4 (urea + HNCO → biuret) > reaction 5a (biuret + HNCO → CYA + NH_3) > reaction 2 (HNCO + H_2O → NH_3 + CO_2)

4.4. Conclusions

Thermolysis and hydrolysis of urea decomposition byproducts was investigated with and without as anatase TiO_2 catalyst under flow reactor conditions. TiO_2 was found to catalyze the hydrolysis of all the investigated compounds including urea, biuret, melamine and CYA. It was shown that biuret is directly hydrolyzed in one step to urea, whereas melamine is hydrolyzed in a multi-step reaction. First, the amine groups are substituted to yield CYA, which is then completely hydrolyzed.

As expected, byproduct formation was favored in the absence of water. If urea was the starting material, significant amounts of biuret and only small amounts of CYA were formed, indicating that the reaction of HNCO with urea to form biuret is faster than the reaction with biuret. Using biuret as the starting material largely increased CYA formation. Interestingly, CYA was also produced during biuret hydrolysis at only 100°C, indicating that

the combination of HNCO with biuret was even faster than HNCO hydrolysis at the low temperature applied.

Regarding urea-SCR, our results emphasize the suitability of anatase TiO_2 as a dedicated catalyst for urea hydrolysis. Also, TiO_2 appears to be suitable for use as an anti-deposit-coating for exhaust pipes, since condensed urea, as well as the eventually formed byproducts, will be hydrolyzed efficiently in the presence of TiO_2. However, there may still be the need for operating intervals at elevated engine loads to increase the exhaust gas temperature above 200°C, where CYA can be hydrolyzed on the heated TiO_2 surface.

5. Urea adsorption on titanium dioxide[A]

5.1. Introduction

In mobile SCR applications, urea solution is dosed into the hot exhaust to produce the actual reducing agent, NH_3 [14]. According to the established mechanism, urea first thermolyzes to yield NH_3 and HNCO in a non-catalytic reaction, and the intermediately formed HNCO is subsequently hydrolyzed on the SCR catalyst or on a dedicated hydrolysis catalyst [51]. However, a large fraction of the dosed urea remains intact before it enters the catalyst [14]. Therefore, the possibility that urea thermolysis is a catalytic reaction should also be considered.

Urea thermolysis: $\qquad CO(NH_2)_2 \rightarrow NH_3 + HNCO \qquad$ (1)

HNCO hydrolysis: $\qquad HNCO + H_2O \rightarrow NH_3 + CO_2 \qquad$ (2)
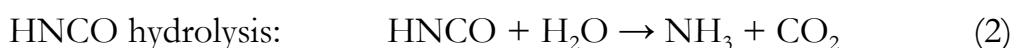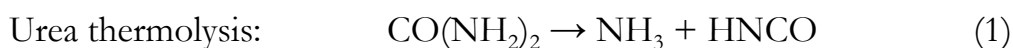
In fact, scattered information in the literature indicates that urea thermolysis itself is catalyzed on metal oxide and SCR catalysts [1, 39, 48, 58]. In chapter 6, catalytic urea thermolysis under steady-state conditions will be reported.

Larrubia et al. (2000) have studied the adsorption of urea onto a V_2O_5–MoO_3–TiO_2 SCR catalyst using transmission/absorption Fourier transform infrared spectroscopy [58]. They managed to adsorb gaseous urea on the

---

catalyst surface; however, NH_3 and CO_2 were the main species in the gas phase. Significantly better results were obtained when a mixture of solid urea and catalyst powder was heated under vacuum to remove non-adsorbed bulk urea. As a result of heating, a characteristic peak of bulk urea (1454 cm^{-1}) disappeared, which indicated that only adsorbed urea and decomposition products remained in the sample. The spectra of the adsorbed urea showed a strong new band at 1562-1552 cm^{-1}, which was attributed to the asymmetric OCN stretching mode of adsorbed urea. Hence, Larrubia et al. (2000) proposed that urea adsorbs in its anionic form, as shown in Fig. 5-1 [58].
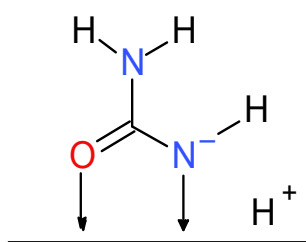
Fig. 5-1 Adsorbed urea in its anionic form, as proposed by Larrubia et al. (2000) [58].

In the present study, we recorded DRIFT spectra of urea adsorbed onto an anatase TiO_2 catalyst. DRIFT samples were prepared via the adsorption of high-purity gaseous urea onto the catalyst. Catalyst samples were washed, and the washing solutions were analyzed using HPLC to independently confirm urea adsorption. To investigate how urea adsorbs, we performed DFT calculations of urea adsorbed at the anatase TiO_2 (101) surface. The (101) surface was considered because it was found to be abundant based on high-resolution powder X-ray diffraction results (XRD) in another study [85].

5.2. Experimental and theoretical details

5.2.1. DRIFT samples and catalyst coating

DRIFT samples were prepared via three different methods:

- Adsorption of gaseous urea onto anatase TiO_2 catalyst powder (Crystal Global DT-51), see chapter 5.2.2. Abbreviation: "urea (g)".

- Additionally, NH_3 was adsorbed onto TiO_2. Before adsorbing NH_3, the TiO_2 sample was cleaned at 450°C inside the DRIFT cell, then the temperature was set to 60°C and the DRIFT cell was supplied with 200 ppm NH_3 in N_2 for 75 min.

- Mixing of urea solution with catalyst powder by sonication for 3 min, followed by drying under ambient conditions. Abbreviation: "urea (aq)". For comparison, TiO_2 samples with biuret, cyanuric acid, ammelide and melamine were prepared likewise. Ammelide was suspended at 0.1% concentration.

- Dry grinding of solid urea (Merck, ≥99.5% purity) with catalyst powder, CaF_2 (Sigma-Aldrich, puriss.), KBr (Fluka, >99% purity) or cordierite (Corning). Abbreviation: "urea (s)".

In addition to catalyst powders, gaseous urea was also adsorbed onto a TiO_2-coated cordierite monolith, which was prepared as described in chapter 2.6. The monolith was coated with 0.6 g of TiO_2 (including 10% wt% commercial silicate binder, Ludox AS-40).

5.2.2. Adsorption and thermolysis of gaseous urea on TiO_2

Gaseous urea was obtained by passing a carrier gas at 100°C and at atmospheric pressure through an inert cordierite monolith that was impregnated with urea. According to chapter 3, urea desorbed from the monolith in monomolecular form. The applied temperature of 100°C was expected to result in a urea concentration of 27 ppm in the gas phase (assuming saturation) [41, 43]. Because of the low temperature applied, non-catalytic urea decomposition was negligible (chapter 3).

To perform urea adsorption, a sample of TiO_2-catalyst powder was charged into a crucible and placed in the hot urea-containing carrier gas, as shown in Fig. 5-2. Because the TiO_2 catalyst was also exposed to the sublimation temperature of 100°C, urea had to adsorb onto the catalyst rather than condense into the bulk form. Notably, at the reactor exit, where the temperature was lower, the urea vapor condensed and formed needle-shaped crystals.
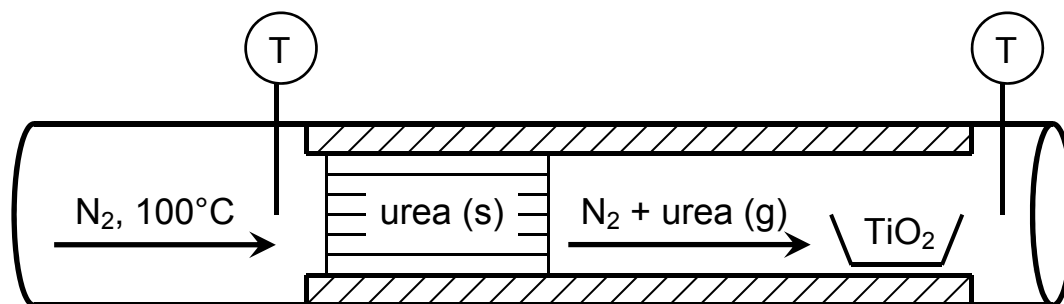

Fig. 5-2. Schematic of the experimental setup for urea evaporation and adsorption onto TiO_2.

Urea adsorption was performed in the TPD reactor described in chapter 2.4. An inert cordierite monolith (400 cpsi, 40 mm long, 17.5 mm wide and 12.4 mm high) was impregnated with 430 mg of urea by dipping it into 40 wt% urea solution. The impregnated monolith was inserted into a metal

adaptor and the metal adaptor was placed in the reactor. The N_2 carrier gas flow was set to 200 L/h at STP, which resulted in a GHSV of 23'000 h^{-1} through the impregnated monolith. The impregnated monolith was first dried inside the reactor at 70°C, and the crucible with ≈0.1 g of TiO_2 was subsequently placed in the metal adaptor, as shown in Fig. 5-2. In some of the experiments, a humid gas mixture composed of 3% H_2O, 10% O_2 and balance N_2 was used as the carrier gas instead of pure N_2. Because drying of the impregnated monolith catalyst was not necessary in this case, the catalyst powder was placed in the reactor at the beginning.

In addition, we performed urea adsorption at 100°C and urea thermolysis at 130°C on TiO_2-coated monoliths (20 mm long, other dimensions identical to those of the inert monolith) inserted into the metal adaptor instead of the crucible. Urea thermolysis on the TiO_2-coated monolith was performed with a flow of 10% O_2 in N_2 at a rate of 431 L/h at STP (GHSV = 98'000 h^{-1}).

5.2.3. HPLC analysis

To quantify the adsorbed urea and the eventual urea decomposition byproducts on the TiO_2 samples, we applied HPLC analysis using the method described in chapter 2.3. Liquid samples were obtained by washing a monolith or a sample of catalyst powder in the HPLC eluent overnight.

For the urea thermolysis experiment conducted at 130°C, gaseous urea and HNCO were absorbed out of the carrier gas by a liquid-quench probe (see chapter 2.2) and then quantified by HPLC. Three liquid samples were collected sequentially at intervals of 5 min. The results are given in the form "average ± standard deviation".

5.2.4. DRIFT measurements

DRIFT spectra were measured on a ThermoNicolet Nexus FTIR spectrometer at a resolution of 4 cm^{-1} using the Smart Collector and Environmental Chamber accessories. The Environmental Chamber is a heated DRIFT cell that is equipped with ZnSe windows and gas supply lines. The samples were placed in the sample holder and pressed and flattened with a spatula. The DRIFT cell was always purged with either pure N_2 (140 L/h at STP) or with a gas mixture composed of 3% H_2O, 10% O_2 and balance N_2 (200 L/h at STP).

DRIFT spectra were measured at various temperatures up to 300°C. The measurements were started at low temperature, and the temperature was increased step-wise. All of the shown spectra are subtraction spectra. Background spectra of urea-free samples were recorded under dry N_2 at the same temperatures as the actual samples.

5.2.5. Computational details[A]

The electronic structure of the $Ti_8O_{28}H_{24}$ cluster, which represents the (101) surface of anatase, and that of the urea adsorbates was calculated using *ab initio* DFT methods (StoBe code [24]). We chose to consider the (101) surface because it was found to be abundant based on high-resolution powder X-ray diffraction results (XRD) in another study [85]. The generalized gradient-corrected functionals according to Perdew, Burke and Ernzerhof (RPBE) were used to account for electron exchange and correlation [73, 74]. All Kohn–Sham orbitals were represented by linear combinations of atomic orbitals (LCAOs) with Gaussian basis sets for the

---

[A] The second author Izabela Czekaj carried out the DFT calculations.

atoms [86, 87]. The vibration frequencies were calculated by single-point energy calculations of the optimized geometries. The calculations of the vibrational frequencies were performed with harmonic approximations as well as with an anharmonicity fit in the Morse potential function, as implemented in the StoBe code [75].

5.3. Results and Discussion

5.3.1. Confirmation of urea adsorption by HPLC analysis

Gaseous urea was adsorbed onto TiO_2 at 100°C, as described in chapter 5.2.2. Non-catalytic urea decomposition was negligible at 100°C; however, urea may have decomposed on the catalyst. To confirm that urea was present on the TiO_2 powder samples and to determine whether byproducts were formed, we performed HPLC analysis of catalyst washing solutions. After the adsorption of urea onto TiO_2 powder, part of the sample was used for DRIFT measurements. The remaining sample was washed in the aqueous HPLC eluent, and the washing solution was analyzed by HPLC. In addition, TiO_2-coated monoliths with adsorbed urea were analyzed likewise. Finally, the inert cordierite monolith that had been impregnated with urea and used as a source of urea vapor, was analyzed after the experiment. Table 5-1 shows the results.

Table 5-1. HPLC analysis of catalyst and monolith washing solutions.

Sample	Carrier-gas	Duration, h	Urea/TiO_2, wt%	Composition of compounds in washing solution, wt%					
				Urea	Biuret	Triuret	HNCO	Cyanamide	CYA
TiO_2 powder	dry N_2	21.5	>1	94.0	5.9	0.1	0	0	0
TiO_2 monolith	dry N_2	20.5	4.3	73.9	21.7	1.5	1.8	0.69	0.18
TiO_2 monolith	3% H_2O	18	5.5	99.5	0.5	0	0	0	0.003
Inert monolith	dry N_2	21.5	110 mg	99.99	0	0.005	0	0	0.002

HPLC analysis of the catalyst washing solutions showed that urea was the main (water-soluble) constituent in all the TiO_2 samples. On the TiO_2 powder placed in the crucible and exposed under dry N_2, we found slightly more than 1 wt% of urea per TiO_2. In addition to 94% urea, 6% biuret was found in the washing solution. Apparently, some urea was catalytically thermolyzed on the TiO_2 surface to form HNCO, and the HNCO then reacted with intact urea to form biuret [1, 38, 46]. When a TiO_2-coated monolith was placed in the reactor instead of a crucible, more urea adsorbed onto the catalyst and more biuret (22%) was formed. Adsorption worked more efficiently on the monolith due to its significantly greater geometric surface area. The resulting greater surface coverage of urea on the TiO_2-coated monolith may explain the increased biuret yield compared to that obtained with the powder. Because of its low vapor pressure [46], biuret was accumulated on the catalyst surface during the complete exposure time at 100°C. In contrast to biuret, very little CYA was formed. Analogous results are reported in chapter 4.3.6, where we concluded that HNCO preferentially combines with urea rather than with biuret. Thermolysis produced significant amounts of CYA only when a catalyst-coated monolith was impregnated with biuret (chapter 4.3.6).

When urea was adsorbed from humid carrier gas, very little biuret was formed. In this case, HNCO hydrolyzed due to the presence of water instead of being consumed for biuret formation, or the formed biuret was hydrolyzed again [1, 45, 46, 48, 49]. Notably, the urea concentration of approximately 27 ppm was significantly lower than the water concentration of 30'000 ppm, and the catalyst still adsorbed a significant amount of urea. The adsorption of urea from the humid carrier gas indicated that urea adsorbs more strongly onto TiO_2 than does water.

Pure urea was found on the impregnated inert monolith that had been used as the source of urea vapor, which indicated that urea was stable at 100°C in the absence of a catalyst. Of the initial amount of 430 mg urea, 110 mg remained on the monolith after it was heated to 100°C for 21.5 h. Hence, 430 mg – 110 mg = 320 mg urea had evaporated during the experiment. Based on the vapor pressure of urea [41, 43], 310 mg of urea was expected to evaporate, which is in good agreement with the measured amount of remaining urea.

5.3.2. Quasi-stationary thermolysis of gaseous urea on a TiO_2-coated monolith

Quasi-stationary urea thermolysis over TiO_2 was performed at 130°C using an impregnated inert monolith as the source of gaseous urea. Instead of the crucible shown in Fig. 5-2, a TiO_2-coated monolith was placed in the reactor downstream of the inert monolith. After approximately 30 min of equilibration at 130°C, three liquid samples with absorbed product gas were collected during 3×5 min for HPLC analysis. For comparison, an analogous experiment was performed without a catalyst. Because of the catalytic activity of TiO_2, the HNCO yield increased from 5% to 35% (Table 5-2). The C-balance in both cases agreed fairly well, which indicated that the catalyst was under stationary conditions.

Table 5-2. Quasi-stationary decomposition of gaseous urea at 130°C. Carrier gas: 10% O_2 in N_2, 431 L/h at STP.

1st monolith (GHSV, h^{-1})	2nd monolith (GHSV, h^{-1})	Urea, ppm	HNCO, ppm	Total carbon, ppm
Inert (50'000)	TiO_2-coated (98'000)	119 ± 0.5	63 ± 2	181
Inert (50'000)	none	182 ± 9	8.6 ± 0.7	190

Table 5-2 shows the results from solvent-free, catalytic thermolysis of gaseous urea. These results support the findings about catalytic urea thermolysis under steady-state conditions at various temperatures over different metal oxide catalysts that will be presented in chapter 6. In the experiments presented in chapter 6, the existence of urea aerosols at the catalyst entrance could not be excluded with certainty and a solvent was always used to dose the urea.

5.3.3. DRIFT measurements at 80°C

Fig. 5-3 shows the DRIFT spectra of urea on TiO_2 recorded at 80°C. The temperature of 80°C was chosen to desorb weakly adsorbed water without inducing urea decomposition. The spectra of urea in CaF_2 and that of clean TiO_2 under humid gas are shown for comparison. The latter spectrum "clean TiO_2, 3% H_2O" was the "ads. urea on TiO_2" sample after in-situ cleaning by hydrolysis at 450°C. The bottom two spectra in Fig. 5-3 were recorded under humid model gas; all of the other spectra were recorded under dry N_2. The spectrum of urea in CaF_2 best represented bulk solid urea because it showed better-defined peaks compared to the spectra of urea in KBr or urea in cordierite powder (not shown). Furthermore, our spectrum of urea in CaF_2 agrees best with the spectrum of pure crystalline urea measured by Grdadolnik et al. (2002), who used attenuated total reflectance (ATR) spectroscopy [88].
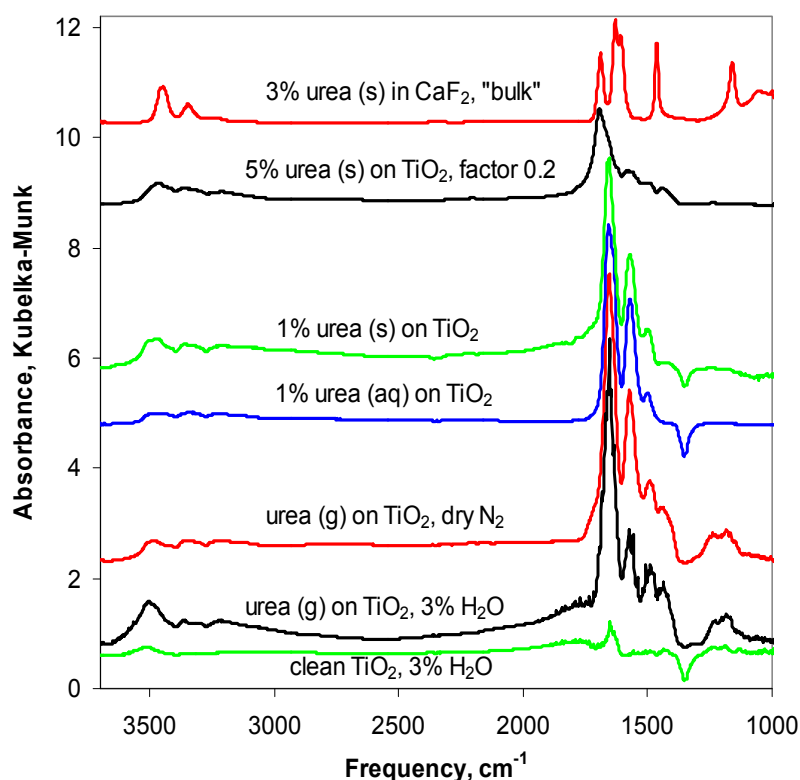
Fig. 5-3. DRIFT spectra of urea recorded at 80°C; the intensities of the "5% urea (s) on TiO$_2$" sample were multiplied by a factor of 0.2. Sample preparation methods: urea (g) = urea vapor adsorbed onto catalyst powder at 100°C; urea (aq) = aqueous urea solution mixed with catalyst powder by sonication, followed by drying under ambient conditions; urea (s) = solid urea mixed with catalyst powder by dry grinding.

We attributed the bands of our 3% urea in CaF$_2$ spectrum using the assignments of Grdadolnik et al. (2002) [88], see Table 5-3. In their study, the absorption bands were assigned based on a comparison of the spectra from different isotopomers of urea (urea with D and/or ^{13}C) [88]. Here, the bands at 1689 cm^{-1} and 1631 cm^{-1} were attributed to the NH$_2$ bending vibrations, the band at 1608 cm^{-1} was attributed to the C=O stretching vibration, the band at 1465 cm^{-1} was attributed to the CN stretching vibration, and the band at 1160 cm^{-1} was attributed to the NH$_2$ rocking vibration, see Table 5-3.

The spectra of adsorbed urea strongly differed from that of the bulk urea spectrum (see 1% urea (s) on TiO_2, 1% urea (aq) on TiO_2, urea (g) on TiO_2 vs. bulk urea in Fig. 5-3). In the 1% urea (aq) on TiO_2 spectrum, the two prominent peaks of bulk urea at 1465 cm^{-1} (CN stretching vibration) and at 1160 cm^{-1} (NH_2 rocking vibration) disappeared. On the other hand, new and/or shifted peaks appeared at 1657 cm^{-1}, 1573 cm^{-1} and 1501 cm^{-1}. This change in the urea spectrum is in good agreement with the results reported by Larrubia at al. (2000) [58]. The peak assignment of adsorbed urea is discussed in the next chapter 5.3.4.

Interestingly, the three different preparation methods for the urea on TiO_2 samples resulted in quite similar spectra (see 1% urea (s) on TiO_2, 1% urea (aq) on TiO_2 and urea (g) on TiO_2 in Fig. 5-3). Apparently, urea (aq) predominantly adsorbed onto the same sites of TiO_2 as did gaseous urea. Also, the grinding of solid urea with the catalyst seemed to provide sufficient energy to induce urea diffusion to the same energetically favored adsorption sites of TiO_2. However, a clearly different spectrum was obtained when 5 wt% instead of 1 wt% of urea was ground with TiO_2: the 5% urea (s) on TiO_2 spectrum appeared to be a transition from the spectrum of 1% urea on TiO_2 to that of bulk urea. The most intense peak in the spectrum of 5% urea (s) on TiO_2 was located at 1695 cm^{-1}, which matches well with the peak at 1689 cm^{-1} (NH_2 bending vibration) in the spectrum of bulk urea. The spectrum of 5% urea (s) on TiO_2 did not show other prominent peaks at wavenumbers less than 1800 cm^{-1}, but the two most intense peaks in the spectrum of the 1% urea (aq) on TiO_2 at 1655 cm^{-1} and 1575 cm^{-1} seemed to be present as shoulders in the spectrum of 5% urea (s) on TiO_2. The spectrum of 5% urea (s) on TiO_2 may be explained by the relatively high surface coverage.

The presence of water in the purge gas of the DRIFT cell (urea (g) on TiO$_2$, 3% H$_2$O in Fig. 5-3) caused the superposition of the urea spectrum with numerous small, narrow water signals. Apart from the small water signals, the urea spectrum did not appear to be influenced by the presence of water in the purge gas. We attempted to correct the urea spectrum by subtracting the spectrum of clean TiO$_2$ acquired under humid model gas but did not obtain a satisfactory result. Nonetheless, the humid purge gas substantially influenced the spectra when the temperature was increased greater than 100°C because the $^-$NCO band at 2200 cm^{-1} was suppressed by HNCO hydrolysis.

Although the spectra of urea (g) on TiO$_2$ and 1% urea (aq) on TiO$_2$ in Fig. 5-3 were quite similar, a closer look reveals some differences, see also Fig. 5-4. The spectrum of urea (g) showed small peaks at 1443 cm^{-1}, 1240 cm^{-1} and 1185 cm^{-1}, which were not observed in the urea (aq) samples (Fig. 5-4b). Since the urea (g) on TiO$_2$ sample was contaminated with biuret that had formed during urea adsorption at 100°C (see Table 5-1), the additional peaks in urea (g) might be attributed to biuret. Also, NH$_3$, which was not quantified by our HPLC method, may have contributed to the urea (g) on TiO$_2$ spectrum. However, the 0.5% biuret (aq) and the NH$_3$ on TiO$_2$ spectra (top two curves in Fig. 5-4b), did not show peaks at 1443 cm^{-1}, 1240 cm^{-1} or 1185 cm^{-1}, indicating that these peaks were attributed to adsorbed urea. We assume that the urea distribution on the catalyst surface was more uniform in the urea (g) on TiO$_2$ sample than in the urea (aq) on TiO$_2$ samples, which allowed the observation of additional peaks.
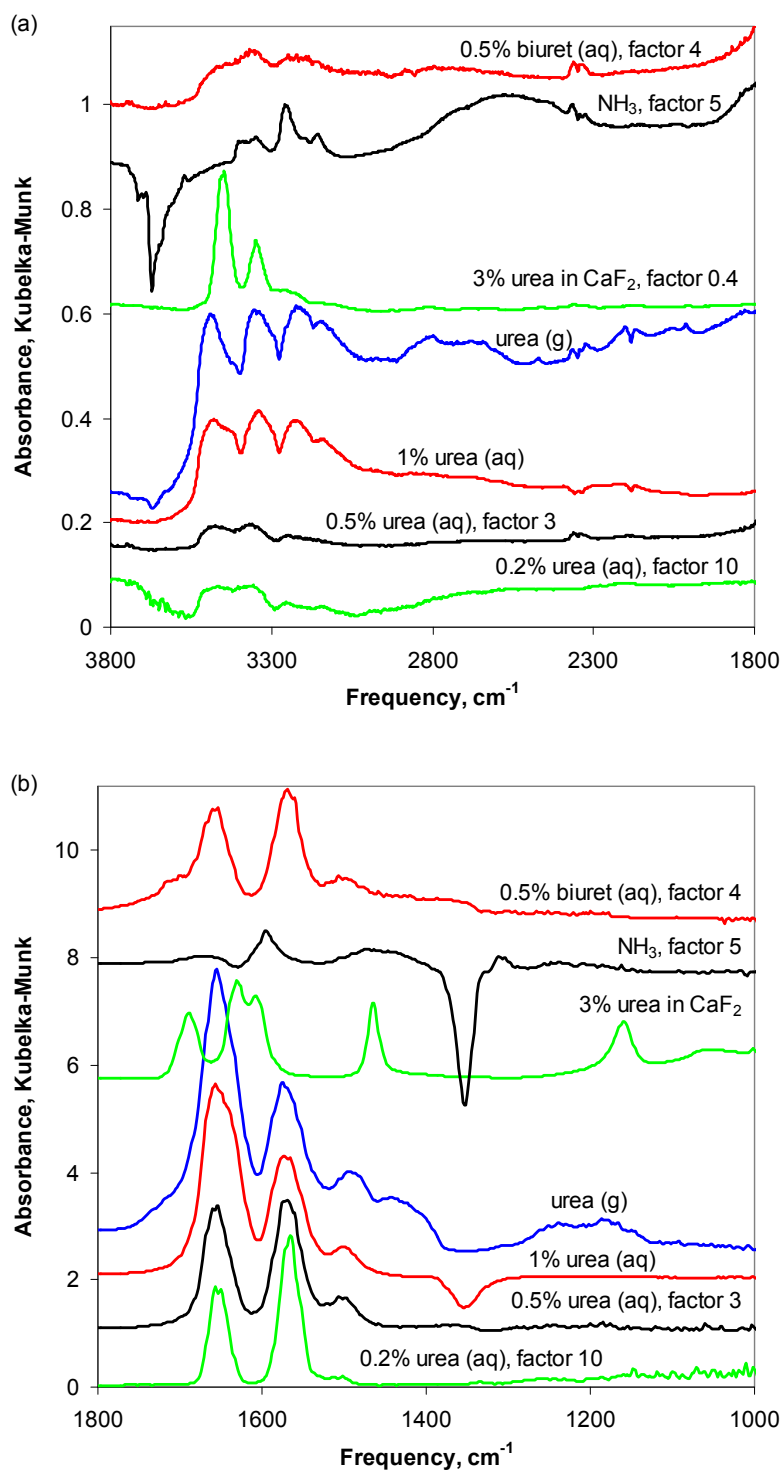
Fig. 5-4. DRIFT spectra of different urea on TiO₂ samples, of biuret on TiO₂ and of NH₃ on TiO₂. All spectra were recorded at 80°C. NH₃ was adsorbed onto TiO₂ by supplying the DRIFT cell with 200 ppm NH₃ in N₂ at 60°C for 75 min. The shown NH₃ on TiO₂ spectrum was recorded at 80°C, 20 min after switching to purging with N₂.

135

The negative peak at 1354 m^{-1} in the NH$_3$ on TiO$_2$ spectrum in Fig. 5-4b was attributed to a breaking of Ti-O-S bonds upon interaction with NH$_3$. Hauck et al. (2007) observed a similar negative peak at 1371 cm^{-1} [45]. Sulphate species are present in commercial TiO$_2$ because of its synthesis via the sulphate method, and the sulphate species show a characteristic band in this region due to their S=O stretching vibration [45]. Our 1% urea (aq) on TiO$_2$ spectrum in Fig. 5-4b and in Fig. 5-3 also showed a negative peak at the same position, but that peak was smaller.

Fig. 5-4 also compares urea (aq) on TiO$_2$ samples with different urea concentrations. Decreasing the urea concentration changed the relative intensities of the peaks. At 1% urea concentration, the peak at 1657 cm^{-1} was most intense, but at lower concentrations of 0.5%, 0.2% and 0.1% (0.1% not shown), the peak at 1569 cm^{-1} became most intense. Further, the relative intensity of the peak at 1501 cm^{-1} (compared to the most intense peak) decreased at low urea concentrations. Anyway, the peaks of urea (g) on TiO$_2$ at 1443 cm^{-1}, 1240 cm^{-1} and 1185 cm^{-1} were not observed in any of the urea (aq) on TiO$_2$ samples.

5.3.4. Comparison of DRIFT measurements with DFT calculations

Table 5-3 shows a comparison of the vibration frequencies of urea, measured in different environments, and the DFT-calculated frequencies. The TiO$_2$ cluster with adsorbed urea, shown in Fig. 5-5, was used for the DFT calculations.

Table 5-3. Comparison of the vibration frequencies [cm⁻¹] of urea in different samples with the DFT-calculated results (represented in italics) obtained in the present work (p.w.) or with results taken from the literature; *: most intensive peak; (in brackets): shoulder.

| Urea sample	v NH$_2$	δ NH$_2$	v CO	v$_{as}$ Ti-OCN-Ti	δ HN-C-NH	v CN	ρ NH$_2$	δ NH	Method, source
3% urea (s) in CaF$_2$, 80°C	3447, 3349	1689, 1631*	1608			1465, 1008	1160, 1051		DRIFT, p.w.
Crystalline urea	3437*, 3343	1682, 1624	1599			1466, 1003	1156, 1057		ATR, [88]
Adsorbed urea form A	*3603, 3479, 3465 3565, 3523*	*1638⁺*		*1578*	*1438*	*1002*	*1102*	*1198*	*DFT, p.w.*
Adsorbed urea form B	*(NH$_2$), 3423, 3393 (NH)*	*1638*		*1579*	*1375**	*966*	*1091*	*1221*	*DFT, p.w.*
Urea (g) on TiO$_2$, 80°C	3488, 3353, 3224	(1635)	1655*	1575 (1567), (1560)	1492, 1443	1240	1185	1240	DRIFT, p.w.
1% urea (aq) on TiO$_2$, 80°C	3480, 3341, 3231	(1637)	1657*,	1573, (1566), (1556)	1501				DRIFT, p.w.
0.5% urea (aq) on TiO$_2$, 80°C	3469, 3355, 3250	(1638)	1654	1569* (1560)	1506				DRIFT, p.w.
0.2% urea (aq) on TiO$_2$, 80°C			1657, (1651)	1566*, (1556)	1502				DRIFT, p.w.
0.1% urea (aq) on TiO$_2$, 80°C			1653	1568*	1507				DRIFT, p.w.
1% urea (aq) on V-Mo-TiO$_2$	3469, 3365, 3250		1652*	1562–1552					FTIR, [58]
Gaseous urea	*3584-3455*	*1624*	*1752**			*1372*			*DFT, [43]*
Gaseous urea	3540, 3437	1600	1773*			1392			FTIR, [43]
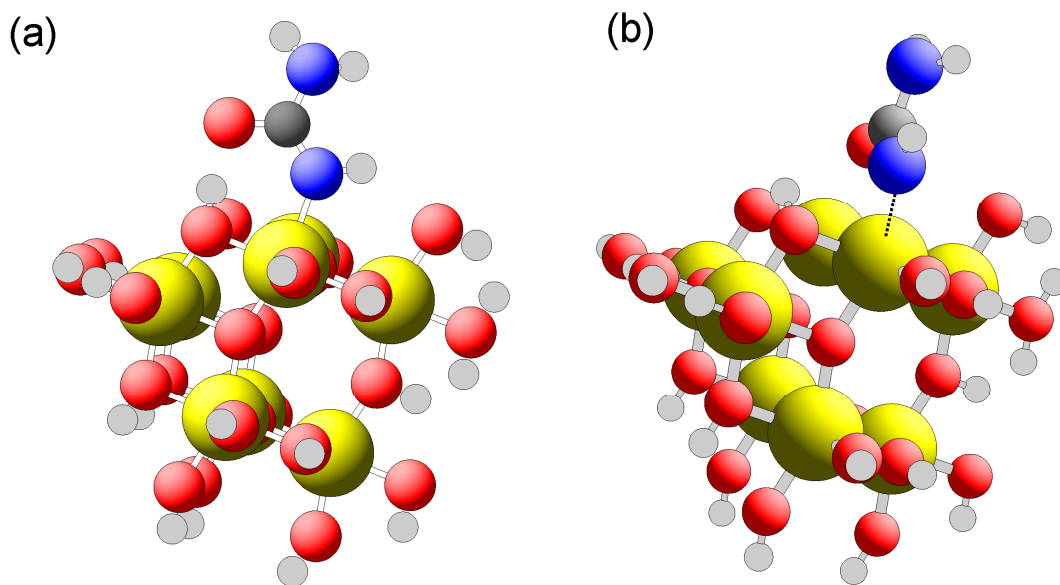
Fig. 5-5. Urea adsorbed onto the $Ti_8O_{28}H_{24}$ cluster, which represents the (101) TiO_2 surface; these results were used for the DFT calculations; these results were used for the DFT calculations; (a): adsorbed urea form A; (b): adsorbed urea form B.

Fig. 5-5 shows the two different adsorption positions of urea at the anatase TiO_2 (101) surface that were found to be most likely. Adsorbed urea A (Fig. 5-5a) was deprotonated to the anionic form, $HN^-C(O)NH_2$, by proton transfer to surface $O(2)$, and bound with the HN^- group at one Ti site with an adsorption energy of -0.26 eV. Adsorbed urea B (Fig. 5-5b) was similarly deprotonated and bound at two Ti sites with both the HN^- group and the double-bonded O, with an adsorption energy of -0.28 eV. Notably, adsorbed urea B corresponds to the scheme of adsorption proposed by Larrubia et al. (2000) [58]. We also considered zwitterionic urea, $H_2NC(O^+H)N^-H$, bound with the HN^- group at one Ti site with an adsorption energy of -0.78 eV. However, the zwitterionic form should have shown a strong OH stretching vibration band at 2539 cm^{-1}, which was not observed in the DRIFT spectra.
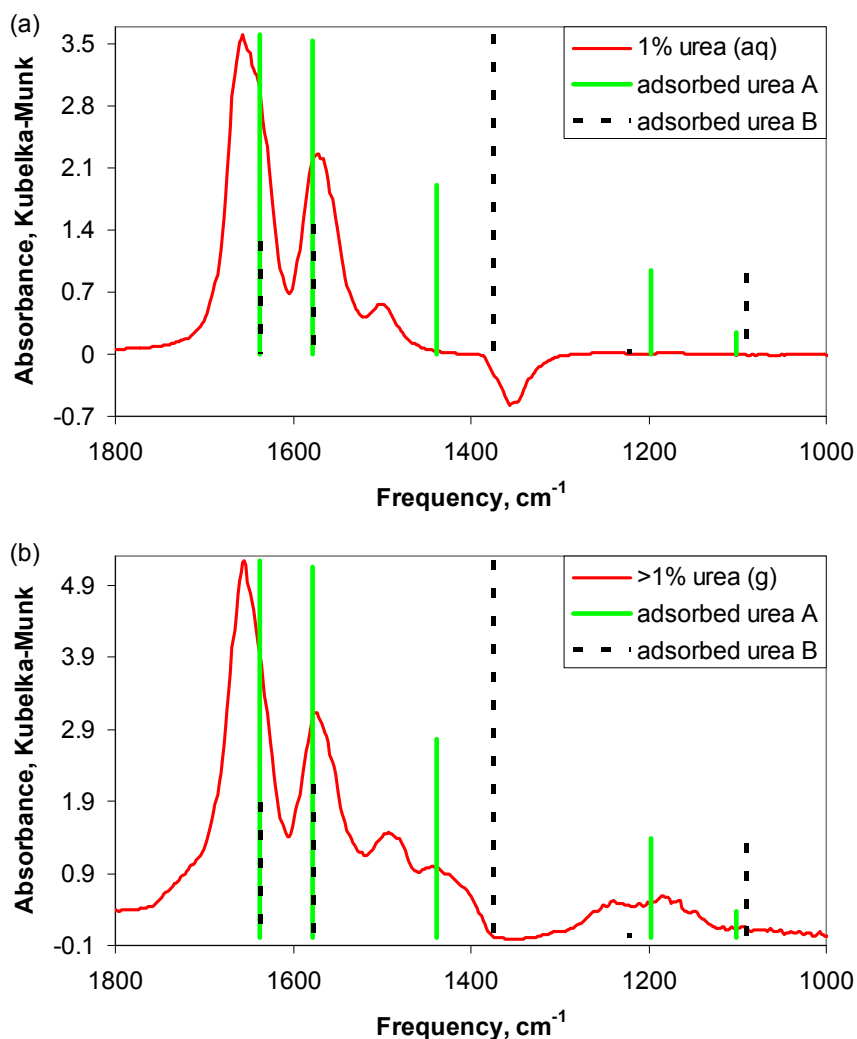
Fig. 5-6. Comparison of DRIFT spectra with DFT-calculated frequencies and intensities (vertical lines) for the two adsorbed states shown in Fig. 5-5. (a) 1% urea (aq), (b) >1% urea (g).

Fig. 5-6 shows a comparison between the experimental DRIFT spectra of urea adsorbed onto TiO_2 (with urea added in aqueous form in Fig. 5-6a and with urea in gaseous form in Fig. 5-6b) and the DFT-calculated frequencies. Fig. 5-6 focuses on the region below 1800 cm^{-1}, because both the experimental and the theoretical spectra showed only peaks with low intensity at higher wavenumbers. Comparison of the urea (g) on TiO_2 spectrum with the DFT-calculated spectra (Fig. 5-6b) indicates that the two

different adsorbed states of urea shown in Fig. 5-5 exist on TiO_2 simultaneously. The two most intense peaks in the experimental spectra are in good agreement with the DFT calculations.

A closer examination of the most intense peak in Fig. 5-6b at 1655 cm^{-1} reveals a shoulder at approximately 1635 cm^{-1}, which indicates two overlapping peaks. Based on the calculated intensities, we attributed the main peak to the NH_2 bending mode of adsorbed urea A (measured: 1655 cm^{-1}, calculated: 1638 cm^{-1}), and the shoulder to the NH_2 bending mode of adsorbed urea B (measured: 1635 cm^{-1}, calculated: 1638 cm^{-1}).

The second-most intense peak was measured at 1575 cm^{-1}. This peak was attributed to the asymmetric Ti-OCN-Ti stretching modes of adsorbed urea A and B, which were calculated to occur at 1578 cm^{-1} and 1579 cm^{-1}, respectively. Larrubia et al. (2000) observed a similar peak in the spectrum of urea on a V_2O_5–MoO_3–TiO_2 SCR catalyst at 1562–1552 cm^{-1}, which they considered to be characteristic for adsorbed urea [58]. They also assigned their peak at 1562–1552 cm^{-1} to the asymmetric Ti-OCN-Ti stretching mode [58].

The next most intense peaks in the urea (g) on TiO_2 spectrum (Fig. 5-6b) were measured at 1492 cm^{-1} and 1443 cm^{-1}. These peaks were attributed to the HN-C-NH scissoring modes of adsorbed urea A (measured: 1492 cm^{-1}, calculated: 1438 cm^{-1}) and of adsorbed urea B (measured: 1443 cm^{-1}, calculated: 1375 cm^{-1}). Further, the small peak at 1240 cm^{-1} was attributed to a combination of the NH bending of adsorbed urea A at 1198 cm^{-1} and to the CN stretching mode of adsorbed urea B at 1221 cm^{-1}. The nearby

peak at 1185 cm^{-1} was assigned to the NH$_2$ rocking modes of adsorbed urea A and B at 1102 cm^{-1} and 1091 cm^{-1}, respectively.

Notably, the peaks at 1443 cm^{-1}, 1240 cm^{-1} and 1198 cm^{-1} were not observed in the urea (aq) on TiO$_2$ (Fig. 5-6a) or in the urea (s) on TiO$_2$ (Fig. 5-3) spectra, which is tentatively explained by interaction between adsorbed urea molecules. Interactions between adsorbed molecules reduce their degree of freedom, which can suppress some theoretically observed vibrations like bending of NH groups. By contrast, only single molecules adsorbed onto the TiO$_2$ surface with full degree of freedom were considered in our DFT calculations, which corresponds to a small coverage and an even distribution of urea at surface. Apparently, the urea was uniformly distributed in the urea (g) on TiO$_2$ sample and its DRIFT spectrum could therefore be well represented by the DFT calculations (Fig. 5-6b).

5.3.5. Urea thermolysis followed by DRIFT spectroscopy

Fig. 5-7 shows DRIFT spectra measured during the decomposition of (a) 1% and (b) 5% urea on TiO$_2$. The urea was decomposed on the catalysts by increasing the temperature of the DRIFT cell stepwise (spectra were recorded at constant temperature). The spectra of the sample with the lower urea concentration of 1%, shown in Fig. 5-7a, remained substantially unchanged up to 150°C. At 200°C, most of the urea was decomposed. A close examination of the spectra (window with enlarged viewing in Fig. 5-7a reveals a tiny peak that appeared at 2202 cm^{-1} at 100°C, which was assigned to the asymmetric stretching vibrations of adsorbed $^-$NCO groups [45, 49, 55, 58] produced by the catalytic thermolysis of urea into HNCO and NH$_3$ [58, 62, 89]. The peak became more intense and shifted slightly to

2200 cm^{-1} at 120°C and to 2197 cm^{-1} at 150°C, where its intensity reached a maximum; however, the maximum-intensity peak was still significantly less intense than the peaks in the region of 1700-1500 cm^{-1}. After 9 min at 150°C, the intensity of the $^-$NCO peak decreased again, and it disappeared completely at 250°C. Possibly, only a small amount of $^-$NCO could build up at the catalysts surface because it was steadily hydrolyzed with adsorbed water.
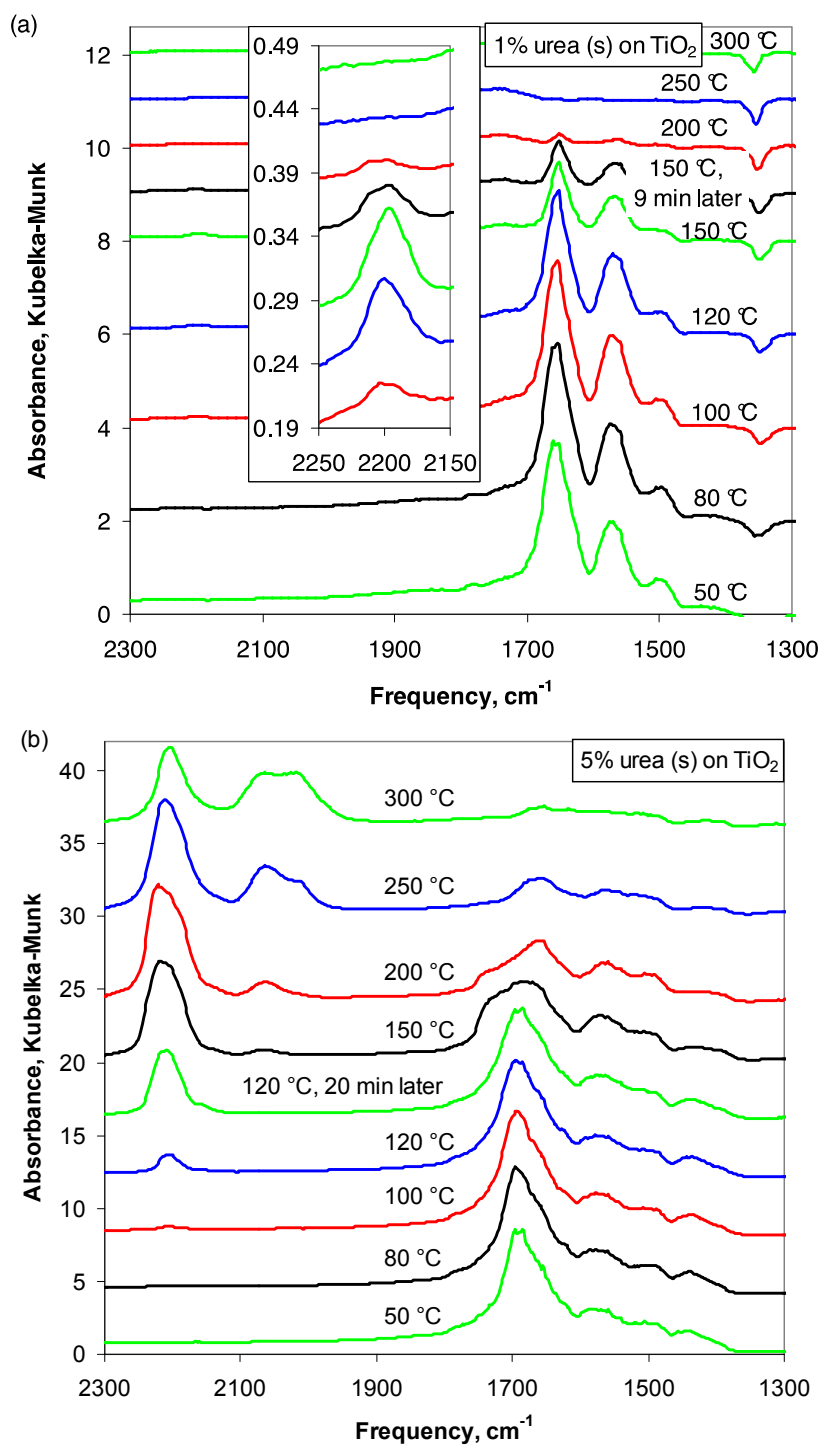
Fig. 5-7. DRIFT spectra measured during the decomposition of urea on TiO$_2$: (a) 1% urea and (b) 5% urea.

Fig. 5-7b shows DRIFT spectra measured during the decomposition of 5% urea on TiO_2. As previously mentioned in the discussion of Fig. 5-3, an increase in the urea concentration from 1% to 5% significantly changed the spectrum. We interpreted this behavior to be caused by a high surface coverage, which resulted in a spectrum with features of both bulk and adsorbed urea without simply being the sum of these two spectra. In analogy with the results reported by Larrubia et al. (2000) [58], heating the sample may desorb/decompose excessive urea so that a spectrum of adsorbed urea plus the decomposition products was observed at a certain temperature. Indeed, the three main peaks of adsorbed urea at 1657 cm^{-1}, 1573 cm^{-1} and 1501 cm^{-1} (Table 5-3) were observed in the spectrum of 5% urea on TiO_2 at 200°C, with small shifts to 1654 cm^{-1}, 1560 cm^{-1} and 1506 cm^{-1} (Fig. 5-7b). Biuret probably was present as well, the pure biuret spectrum showed peaks at 1653, 1570, 1506 cm^{-1} (Fig. 5-4b).

The decrease in the intensity of the largest peak at 1695 cm^{-1} (the NH_2 bending mode of bulk urea) upon heating was accompanied by the growth of several new peaks due to urea decomposition products and byproducts. Most importantly, isocyanate formation was observed at the catalyst surface that showed peaks at 2204-2222 cm^{-1}. The high intensity of the ^-NCO band (Fig. 5-7b), which is in contrast to the low-intensity band obtained with the 1% urea (s) on TiO_2 (Fig. 5-7a), was a consequence of the increased urea-to-water ratio. The use of 5% instead of 1% solid urea in the catalyst sample did not increase the amount of adsorbed water on the catalyst; hence, the major fraction of the HNCO could not be hydrolyzed.

At 150°C, a new band appeared at 2066 cm^{-1} in the DRIFT spectrum (see Fig. 5-7b and Fig. 5-8), which we assigned, based on the work of Hauck et

al. (2007) [45], to cyanamide adsorbed in the tautomeric and deprotonated form $^-$N=C=NH. Cyanamide is the monomer of melamine and can be formed by the disproportionation of HNCO into CO_2 and cyanamide [35]. Cyanamide was also detected by HPLC (Table 5-1).

Furthermore, a shoulder at 1740 cm^{-1} was observed in the spectra of 5% urea on TiO_2 at 150 and 200°C, which we tentatively assigned to the C=O stretching mode of cyanuric acid (IUPAC name: 1,3,5-triazinane-2,4,6-trione) in its trione tautomeric form. A DFT vibration analysis of gaseous cyanuric acid showed bands at 1778 cm^{-1}, 1766 cm^{-1} and 1764 cm^{-1} for this mode. The assignment of the shoulder at 1740 cm^{-1} to cyanuric acid is supported by the spectrum of cyanuric acid on TiO_2 shown in Fig. 5-8. Further, Fig. 5-8 suggests that ammelide (IUPAC name: 6-amino-1,3,5-triazine-2,4-diol) also contributed to the shoulder with its most intense peak at 1737 cm^{-1} (Fig. 5-8).
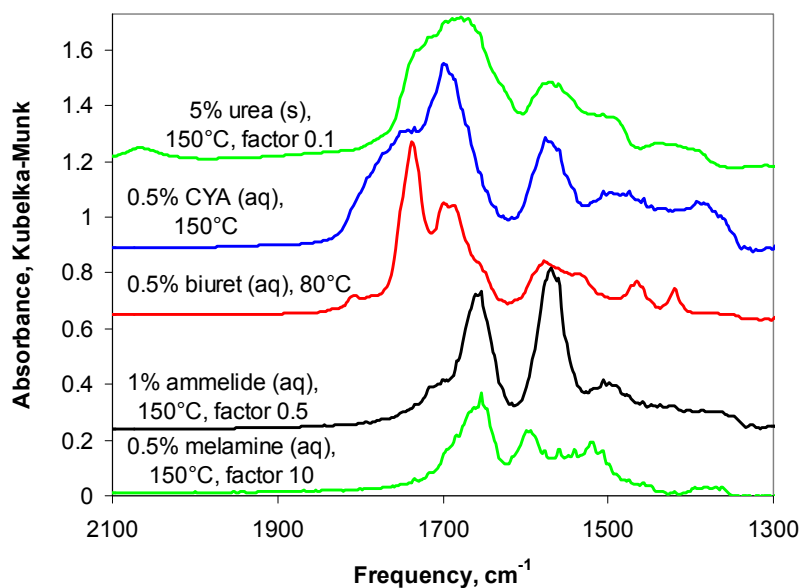
Fig. 5-8. Comparison between "5% urea (s) on TiO₂", taken from Fig. 5-7, and the spectra of the urea decomposition byproducts CYA, biuret, ammelide and melamine (from top to bottom) on TiO₂.

At 250°C, the band at 1740 cm^{-1} was no longer evident, which may be due to catalytic cyanuric acid de-polymerization into HNCO. This temperature is in fair agreement with the start of HNCO emissions between 250 and 275°C in a temperature programmed thermolysis experiment of cyanuric acid on TiO₂ [46]. Another possible explanation for the disappearance of the cyanuric acid shoulder (1740 cm^{-1}) at 250°C is the substitution of OH groups in cyanuric acid or ammelide with NH₃, which yields ammeline (IUPAC name: 4,6-diamino-1,3,5-triazin-2-ol) or melamine (IUPAC name: 1,3,5-triazine-2,4,6-triamine).

The disappearance of the cyanuric acid shoulder (1740 cm^{-1}) at 250°C was accompanied by the growth of a new band at 2019 cm^{-1}, which we could not assign.

5.4. Conclusions

Gaseous urea was found, using HPLC analysis and DRIFT spectroscopy, to adsorb onto anatase TiO_2 at 100°C. DFT calculations suggested two different adsorbed states of deprotonated urea, $HN^-C(O)NH_2$, to be present at the anatase (101) surface: in one state, urea bound at one Ti site with an adsorption energy of -0.26 eV, and in the other state, urea was rotated and bound at two Ti sites with an adsorption energy of -0.28 eV. Zwitterionic urea, $H_2NC(O^+H)N^-H$, was also considered but abandoned, because the expected OH vibration was not observed in the DRIFT spectra. The confirmation of urea adsorption supports our conclusions in the chapters 4 and 6 about catalytic urea decomposition.

6. Catalytic urea decomposition[A]

6.1. Symbols

a diffusion surface area

A pre-exponential factor in the Arrhenius equation

c volume fraction for gases; mass fraction for liquids

$c_{1,g}$ reactant concentration in the gas phase

d_g diffusion length

$D_{1.2}$ binary diffusion coefficient

$DaII$ second Damköhler-number

E_a apparent activation energy

r_{eff} effective reaction rate

k_1 apparent pseudo first-order reaction rate constant

k_g gas phase mass transport coefficient

η_{ext} efficiency factor, $\eta_{ext} = r_{eff} / r$

R gas constant

T actual temperature

T_0 temperature for the tabulated value of $D_{1,2}$

V^* total flow rate at the actual temperature and pressure

W catalyst weight

X relative conversion

6.2. Introduction

In the urea-SCR process, the dosed urea solution decomposes in the hot exhaust gas and on the catalyst to yield the actual reducing agent NH_3. According to the established mechanism, urea first thermolyzes into NH_3 and HNCO in a non-catalytic reaction (1) and the intermediately formed HNCO then hydrolyzes catalytically (2). HNCO is relatively stable in the gas phase, hence non-catalytic HNCO hydrolysis can be neglected [51]. However, a large fraction of the dosed urea remains intact before it enters the catalyst [14]. Therefore, catalytic urea thermolysis should also be considered. Yet, most studies on urea decomposition in the SCR process have either focused on non-catalytic thermolysis [8, 29, 30, 38, 40, 67-70, 90], or on catalytic HNCO hydrolysis [45, 49, 51, 52, 55-57, 76, 82]. Scattered information in the literature indicates that urea thermolysis (1) can be catalyzed as well [1, 39, 48, 58], but dynamic experiments, such as thermogravimetric analysis (TGA), have been prevailing so far. Dynamic experiments are difficult to use for kinetic evaluation due to mass and heat transfer phenomena. A theoretical study of Todorova et al. (2011) proposes catalytic urea thermolysis. These authors calculated the reaction energy barriers for the hydrolysis of guanidine on anatase TiO_2 (101) using DFT and found adsorbed urea as an intermediate on the TiO_2 surface [78]. From the adsorbed urea NH_3 can be eliminated, leaving HNCO on the catalyst surface. HNCO then hydrolyzes via carbamic acid as another intermediate [55, 78]. Interestingly, an additional reaction pathway was proposed, where water directly attacks the adsorbed urea rather than adsorbed HNCO [78]. In this more direct reaction (3), carbamic acid is formed as an intermediate as well, but the reaction step of intermediate HNCO formation is skipped. Fig. 6-1 illustrates the two reaction pathways. The term "urea

decomposition" is used to indicate any combination of reactions that consumes urea.

Urea thermolysis: $\qquad CO(NH_2)_2 \rightarrow NH_3 + HNCO \qquad$ (1)

HNCO hydrolysis: $\qquad HNCO + H_2O \rightarrow NH_3 + CO_2 \qquad$ (2)

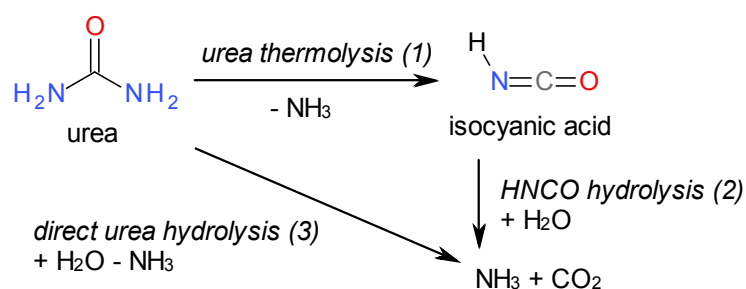Direct urea hydrolysis: $\quad CO(NH_2)_2 + H_2O \rightarrow 2\,NH_3 + CO_2 \quad$ (3)
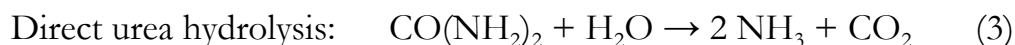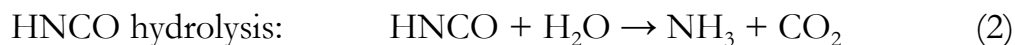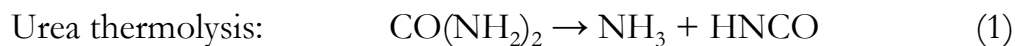

Fig. 6-1 Reaction scheme of catalytic urea decomposition.

In this chapter 6, water-free (dry) catalytic urea thermolysis (1) on different catalysts is compared with catalytic urea hydrolysis (wet). Additionally, urea thermolysis on all the catalysts tested and direct urea hydrolysis on ZrO_2 is analyzed by a pseudo first-order kinetic model.

6.3. Experimental

The tests were conducted using the spray reactor described in chapter 2.1. Table 6-1 shows the catalysts-coated monoliths used. The base feed of the reactor was composed of 10% O_2 and 0% or 5% H_2O in N_2, at a total flow rate of 500 L/h at STP.

Table 6-1 Catalyst-coated monoliths used (the GHSV was calculated at 500 L/h at STP).

Monolith name	cpsi	Active mass, mg	Length, cm	GHSV, h^{-1}	Loading, g/L
TiO_2	400	710	2	98'000	140
ZrO_2	400	610	2.1	93'000	110
Al_2O_3	400	740	2.1	93'000	140
V-SCR	400	700	2.1	93'000	130
Fe-Beta	400	530	2	97'000	100
TiO_2	600	45	2	91'000	8.3
TiO_2b	600	85	1.06	170'000	29
TiO_2c	600	540	6	30'000	33
TiO_2d	600	24	2	91'000	4.4
ZrO_2	600	52	2	91'000	9.4
Al_2O_3	600	64	2	91'000	12
H-ZSM-5	600	48	2	91'000	9.1
SiO_2	600	55	2	91'000	10

100 ppm urea in the gas phase was realized by spraying 4 wt% urea in EtOH (70.4 µL/min), 5 wt% urea in MeOH (56.3 µL/min) or 15 wt% urea in water solution (14.5 µL/min). Dosing of the organic solvents resulted in gas phase concentrations of 0.31% EtOH or 0.36% MeOH. In the first screening with 400 cpsi monoliths, 32.5 wt% urea solution was dosed at 31.5 µL/min, resulting in 500 ppm urea. In the biuret hydrolysis experiments, 2% biuret (Fluka, p.a.) in de-ionized water solution was dosed at 95.3 µL/min, resulting in 50 ppm biuret.

We did not observe catalyst deactivation or deposit formation in most of our experiments. Only dry experiments with the H-ZSM-5 catalyst induced slight deactivation. Non-catalytic urea decomposition could be neglected because very little urea conversion was observed in the empty reactor up to 200°C (Fig. 6-2) and most of the data points considered for the Arrhenius analyses were below 200°C.
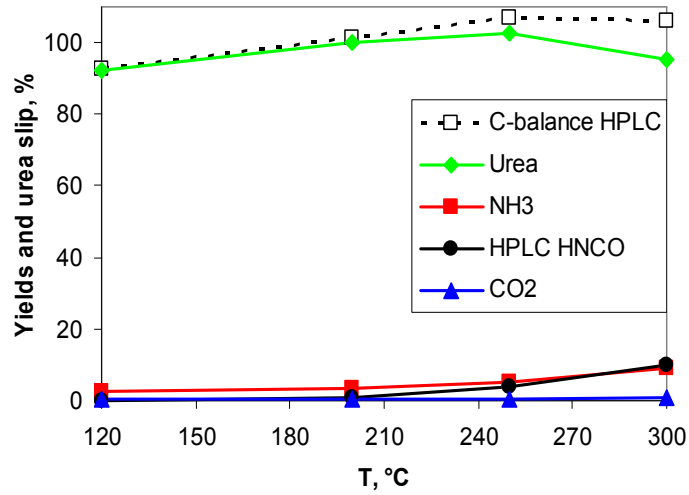
Fig. 6-2. Urea conversion in the empty reactor.

The C-balance could usually be closed within ±5% accuracy by summing up the HNCO, urea and CO_2 amounts. The CO_2 yield in the dry experiments due to hydrolysis by water traces was mostly below 5%.

6.3.1. Calculation of product yields and urea conversions

The yields of the reaction products NH_3, HNCO and CO_2 were calculated based on the N- or C-balance. Using the concentrations was allowed, as all species were diluted to ≤200 ppm in the model exhaust gas matrix:

NH_3 yield = $c(NH_{3,out})$ / $(2 \times c(urea_{in}))$

$HNCO$ yield = $c(HNCO_{out})$ / $c(urea_{in})$

CO_2 yield = $c(CO_{2,out})$ / $c(urea_{in})$

urea slip = $c(urea_{out})$ / $c(urea_{in})$

Urea conversion (X) was always calculated according to

$X = 2 \times NH_3$ yield $- CO_2$ yield

Although it would have been easiest to calculate the urea conversion based on the urea slip, the equation $X = 2 \times NH_3$ yield $- CO_2$ yield was used

because of the following reasons: a) NH_3 and CO_2 could be measured more precisely than urea, b) a moderate relative measuring error of the large urea slip at low conversions would have resulted in a large relative error of the conversion rates, required for the Arrhenius analyses, c) the urea conversion is still indicated irrespectively of the presence of water (see explanation in the next two paragraphs) and d) urea condensation in the reactor would have indicated wrong urea conversion.

For the dry experiments, it would have been acceptable to calculate the conversion based on the HNCO yield alone. However, intermediately formed HNCO, which is hydrolyzed due to water traces, is missing in the HNCO yield. A "true" HNCO yield, which is corrected for the HNCO missing due to HNCO hydrolysis, can be calculated by adding the CO_2 yield to the HNCO yield (provided that there is no direct urea hydrolysis). The HNCO quantification by FTIR spectroscopy is highly sensitive, but more vulnerable to systematic errors than the quantification of the other compounds because calibration of the reactive HNCO is difficult. The HNCO quantification by HPLC is rugged, but time consuming and less sensitive than the quantification by FTIR spectroscopy. Hence, it was the better option to use the NH_3 yield to calculate the yield of the NH_3 produced by urea thermolysis alone (thermolysis-NH_3 yield), which is in principle equivalent to the "true" HNCO yield.

"true" HNCO yield: *HNCO yield + CO_2 yield*
thermolysis-NH_3 yield: *$2 \times NH_3$ yield − CO_2 yield*

If only urea thermolysis takes place, the HNCO yield, the "true" HNCO yield and the thermolysis-NH_3 yield are identical except for measuring errors. In the wet experiments, the chosen definition of the urea conversion

based on the thermolysis-NH_3 yield is valid as well. In fact, the thermolysis-NH_3 yield indicates the urea conversion irrespectively of the product selectivity. Even if direct urea hydrolysis (3) takes place, the thermolysis-NH_3 yield correctly indicates the urea conversion, but, of course, without indicating anymore how much NH_3 was produced by urea thermolysis. Anyway, if CO_2 is produced with very high selectivity, the best option is to simply base the urea conversion on the CO_2 yield. We tested using the CO_2 yield to analyze urea hydrolysis on ZrO_2, but the result was very close to the result based on the thermolysis-NH_3 yield. Hence, we chose to use only one definition of the urea conversion. Using a uniform definition of the urea conversion is simple and provides excellent comparability between the results obtained under different conditions (dry or wet and different catalysts).

6.4. Results and Discussion

6.4.1. Catalyst screening with 400 cpsi monoliths and high loadings[A]

A first screening was carried out with 400 cpsi monoliths, high catalyst loadings of about 0.6 g, 120 g/L and a high urea dosing rate of 500 ppm (Fig. 6-3). Under these conditions, both, the ZrO_2 and the TiO_2 catalyst showed high hydrolysis activity. The advantage of ZrO_2 over TiO_2, which was expected based on the HNCO hydrolysis activities reported by [57], was only small.

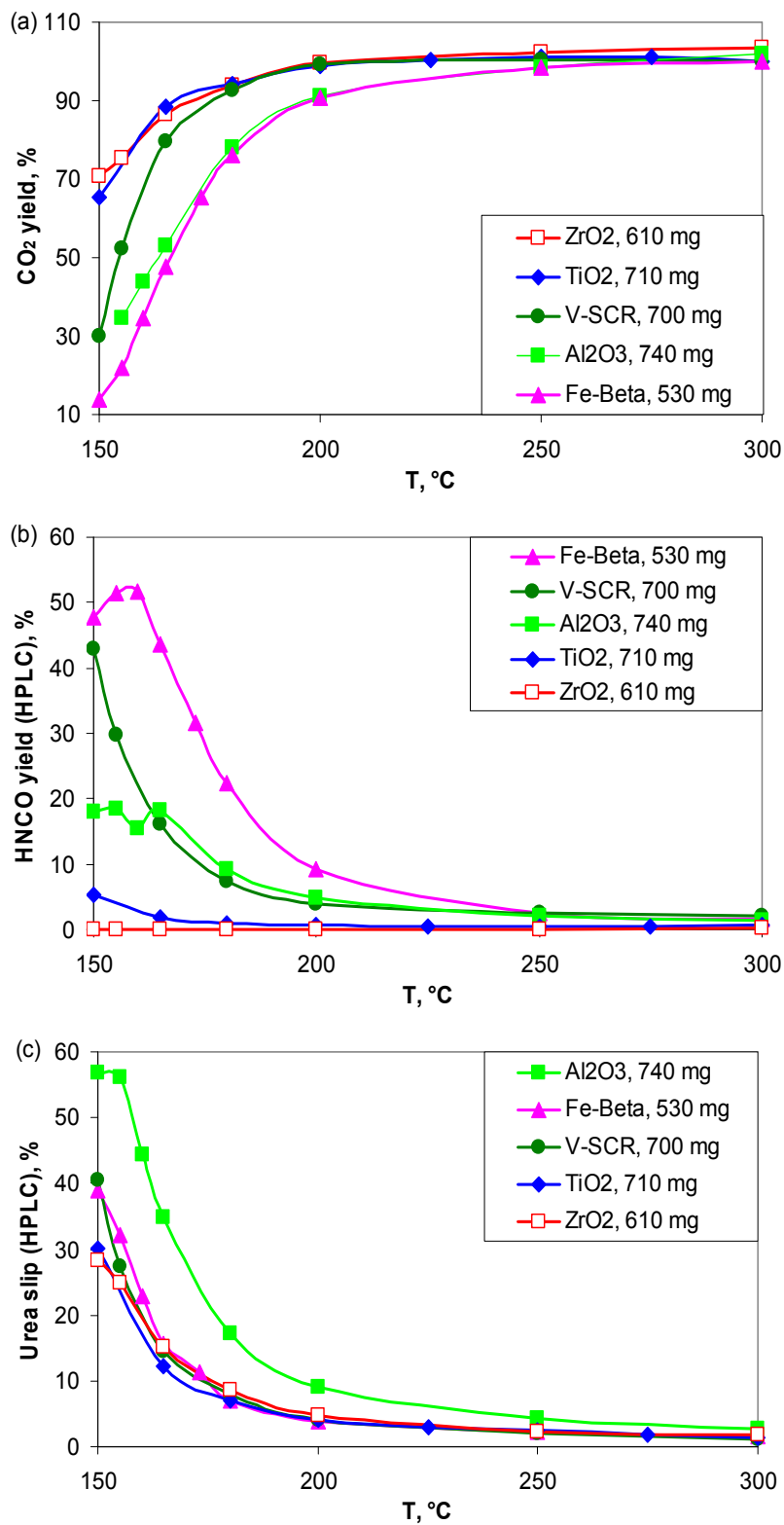[A] This chapter is based on results that were not used for a peer-reviewed publication.

Fig. 6-3. Catalyst screening for urea hydrolysis activity; model gas: 500 ppm urea, 10% O_2, 5% H_2O, in N_2, gas flow = 500 L/h at STP, GHSV ≈ 100'000 h^{-1}, 32.5% urea solution.

It is important to mention that two different ZrO_2 catalysts were used in this study: The 400 cpsi monoliths were coated with the ZrO_2 with a BET surface of 39 m^2/g, whereas the 600 cpsi monoliths were coated with 67 m^2/g ZrO_2. All the catalysts used are listed in Table 2-5 on page 70.

The V_2O_5/WO_3-TiO_2 (2.2% V_2O_5) SCR catalyst showed moderate hydrolysis activity. The decreased hydrolysis activity of V_2O_5/WO_3-TiO_2 compared to pure TiO_2 is in agreement with analogous results on the HNCO hydrolysis reported elsewhere [51, 52]. Piazzesi et al. (2006) concluded that the hydrolysis activity of the catalysts is inversely correlated with their stronger acidity [52], whereas the moderate strength Lewis acid sites of pure TiO_2 are well suited for HNCO hydrolysis [57]. The results shown in Fig. 6-3 indicate that the same correlation applies for urea hydrolysis.

Both the Fe-Beta and the V_2O_5/WO_3-TiO_2 SCR catalysts showed high HNCO yields below 200°C (Fig. 6-3b), while the urea conversion was almost as high as on the TiO_2 catalyst (Fig. 6-3c). Apparently, the stronger acidity of the SCR catalysts decreased their hydrolysis activity, but not their thermolysis activity. The Al_2O_3 catalyst showed the lowest urea conversion (Fig. 6-3c). In conclusion, the results from this first screening provided additional evidence for the known suitability of TiO_2 as a dedicated urea hydrolysis catalyst. Unlike TiO_2, Al_2O_3 is not sufficiently active to be recommended as a dedicated hydrolysis catalyst; still, Al_2O_3 may be suitable for anti-deposit coatings [54].

Fig. 6-4 shows urea hydrolysis on TiO_2 at different urea concentrations. The relative CO_2 yields shown in Fig. 6-4 indicate a first-order dependence with respect to urea at temperatures above 150°C. At 150°C, the relative

CO_2 yield decreased only slightly with increasing urea dosing rates, hence the reaction order was still almost first-order. By contrast, the absolute CO_2 yields were quite constant at 130°C and 120°C, which points at a zero-order dependence. Notably, the experiments at 130°C and 120°C were influenced by urea condensation, since the C-balance decreased with increasing urea concentration (dashed lines in Fig. 6-4).
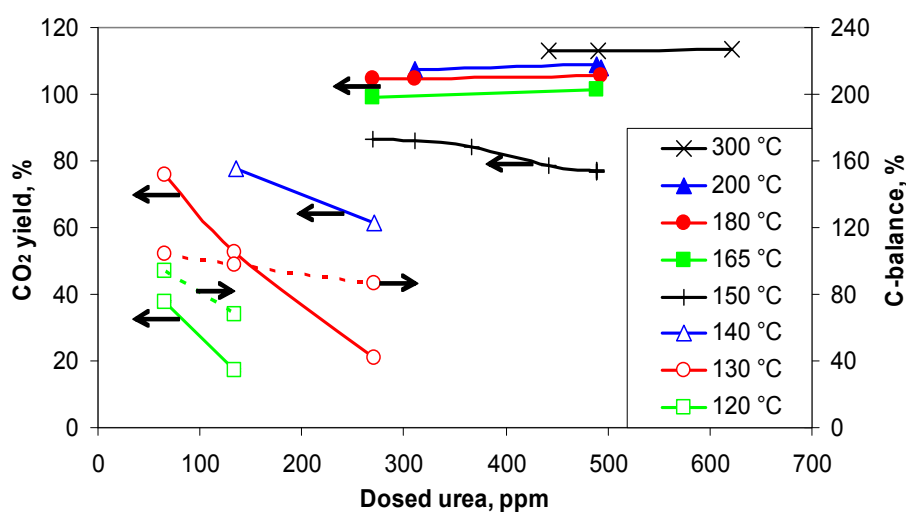
Fig. 6-4. Urea hydrolysis at different urea dosing rates. Solid lines show the relative CO_2 yield and dashed lines show the C-balance. Parameters: 710 mg TiO_2, GHSV = 98'000 h^{-1}, 10% O_2, 5% H_2O, in N_2, gas flow = 500 L/h at STP.

Fig. 6-5a shows the correlation between the TiO_2 catalyst loading and the hydrolysis activity. Interestingly, the lowest catalyst loading of 120 mg showed a local maximum in the HNCO yield at 165°C (Fig. 6-5b). Local maxima of intermediate compounds are typical for sequential reactions. Even more pronounced local maxima in the HNCO yields were observed in the second catalyst screening with low catalyst loadings, see the next chapter 6.4.2. We attempted to use the urea conversions obtained with the 400 cpsi monoliths for Arrhenius analyses, but the result was unsatisfying because of diffusion limitation.
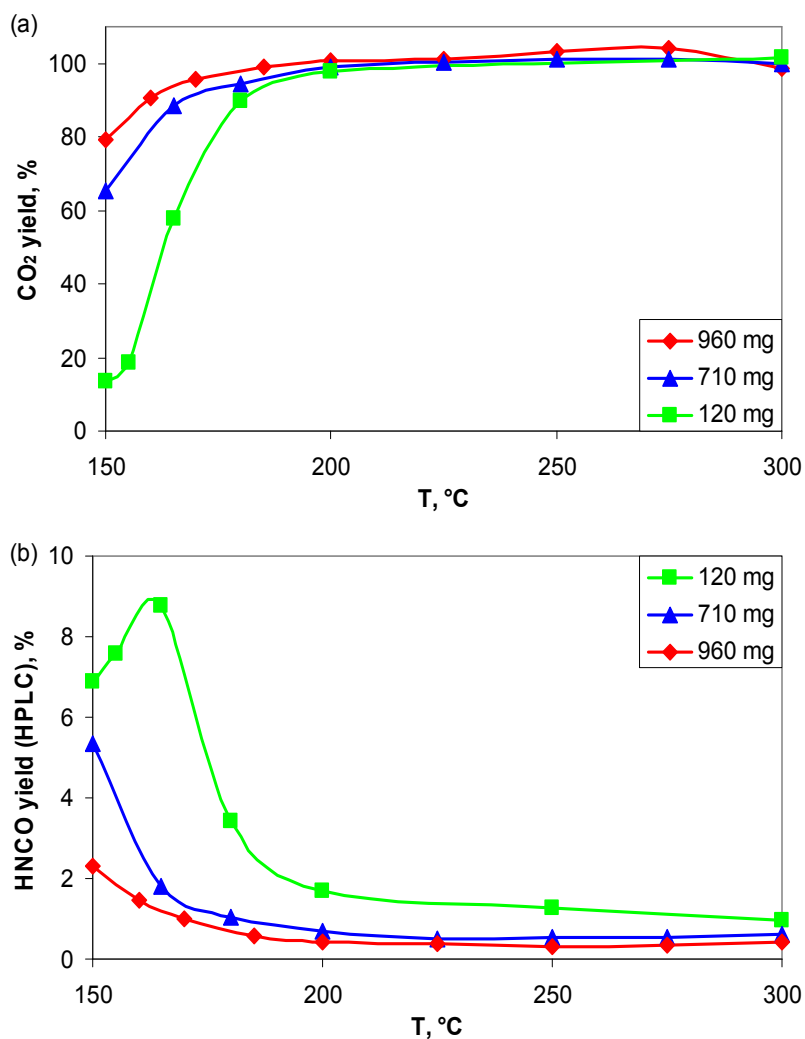
Fig. 6-5. Urea hydrolysis on TiO₂ with different active masses.

6.4.2. Catalyst screening with 600 cpsi monoliths and low loadings

Catalytic urea decomposition is a fast reaction. The goal of this second screening was to realize reaction conditions with little diffusion limitation. Hence, small amounts of the catalyst powders were coated on cordierite monoliths with a high cell density of 600 cpsi. The typical catalyst loading of about 50 mg corresponded to only 9 g/L, which is about 20 times lower than in a real application in exhaust gas aftertreatment. Also, we chose a rather low urea concentration of 100 ppm in the gas phase to allow

measurements at low temperatures around 150°C without urea condensation.

Fig. 6-6 shows the results of a catalyst screening for dry urea thermolysis (a-b) and urea hydrolysis in the presence of 5% water (c-d). Dry conditions, required for studying urea thermolysis without hydrolysis, were realized by using EtOH and MeOH solutions of urea. Fig. 6-6a-b also compare urea thermolysis in the presence of EtOH (solid lines) with thermolysis in the presence of MeOH (dashed lines). Changing the solvent from EtOH to MeOH influenced the thermolysis reaction only slightly, indicating that these water-free, polar solvents are suitable for studying the urea thermolysis only. In both cases, no compounds originating from side-reactions due the presence of the solvent could be detected by FTIR spectroscopy or HPLC analysis and the mass balance could often be closed more precisely than in the hydrolysis experiments.
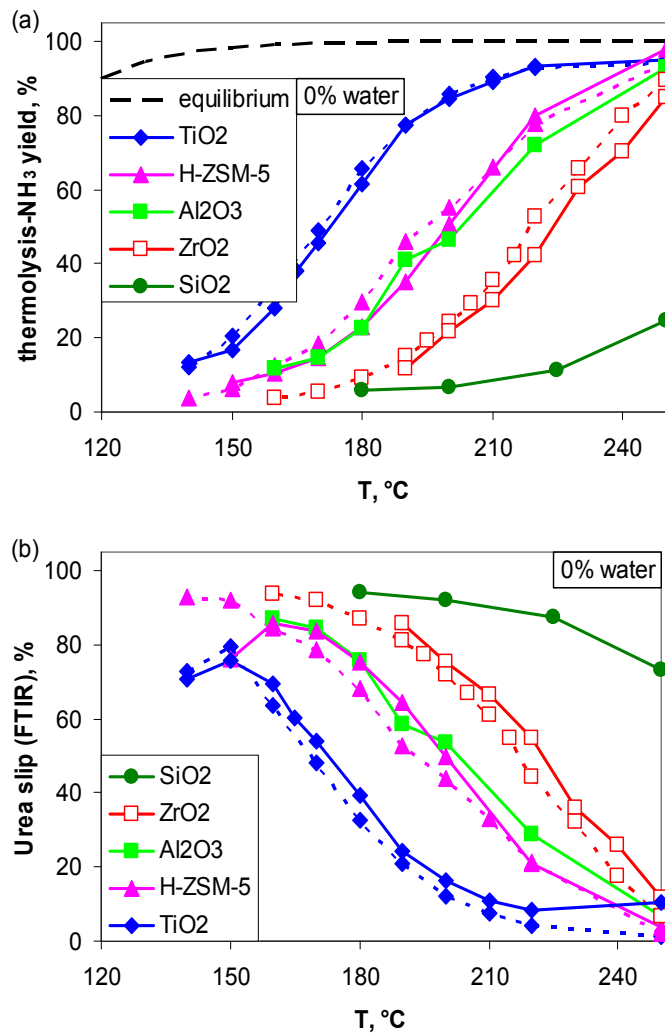
Fig. 6-6 (a-b). Catalysts screening for urea thermolysis. Solid lines: EtOH, dashed lines: MeOH. Parameters: 100 ppm urea, 0% H_2O, 10% O_2 in N_2; total gas flow = 500 L/h at STP; GHSV = 91'000 h^{-1}; active masses ≈ 50 mg. Fig. 6-6a includes the NH_3 yield according to the thermodynamic equilibrium of the urea thermolysis reaction [37].
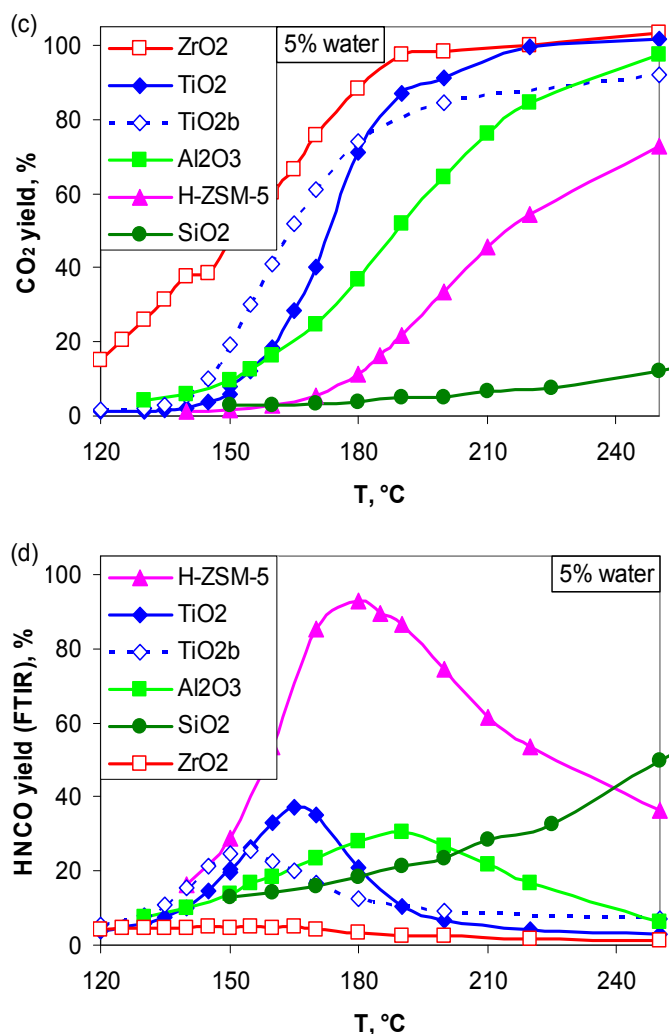
Fig. 6-6 (c-d). Catalysts screening for urea hydrolysis. Parameters: 100 ppm urea, 5% H_2O, 10% O_2 in N_2; total gas flow = 500 L/h at STP; GHSV = 91'000 h^{-1}; active masses ≈ 50 mg.

In the absence of water (Fig. 6-6a-b), the urea thermolysis products NH_3 and HNCO were formed with high selectivity. Adding the urea slip (Fig. 6-6b) to the NH_3 or HNCO yield usually allowed for closing the mass balance. Only at the lowest temperatures, the urea slip decreased due to urea condensation.

Under hydrolysis conditions (Fig. 6-6c-d), NH_3 and CO_2 were the final products, however, only ZrO_2 always showed high selectivity for CO_2. By

contrast, TiO_2, Al_2O_3 and H-ZSM-5 showed significant local maxima in the HNCO yield at 165°C, 180°C and 190°C, respectively. SiO_2 showed poor thermolysis and even lower hydrolysis activity. The hydrolysis activity was so low that even in the presence of water the HNCO yield increased steadily with increasing temperature (Fig. 6-6d).

In the light of the very high HNCO hydrolysis rates on anatase TiO_2 reported by Hauck et al. (2007) [56], the intermediate HNCO peaks in Fig. 6-6d were surprising. Fig. 6-7 shows the hydrolysis of 100 ppm HNCO on some of the previously tested catalysts for urea hydrolysis. Indeed, we found HNCO hydrolysis to be very fast on TiO_2 and even much faster on ZrO_2. The HNCO slip on TiO_2 at 165°C was only 3%, whereas a local maximum of 37% HNCO yield was observed at 165°C during urea hydrolysis on the same TiO_2-coated monolith (Fig. 6-6d). Apparently, HNCO hydrolysis was strongly inhibited by the presence of urea.
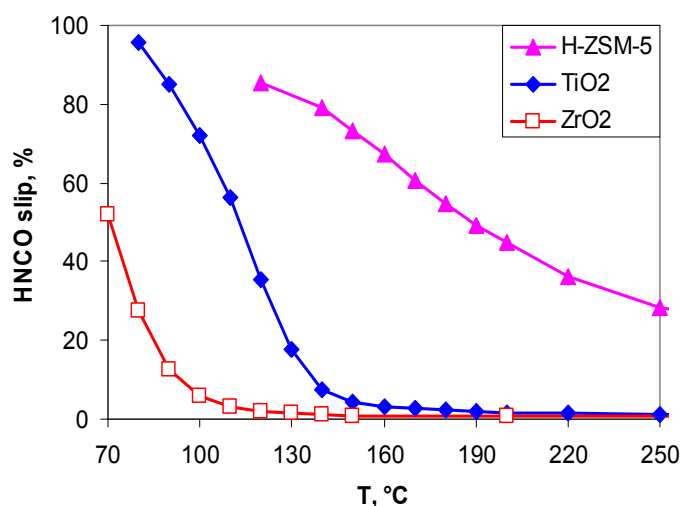
Fig. 6-7. HNCO hydrolysis, using the same catalyst-coated monoliths as were used for the experiments shown in Fig. 6-6. Parameters: 100 ppm HNCO, 5% H_2O, 10% O_2 in N_2; total gas flow = 500 L/h at STP; GHSV = 91'000 h^{-1}.

Fig. 6-8 shows a comparison of the HNCO yields observed in the presence of water and without water. To indicate the urea conversion irrespectively of the product selectivity, Fig. 6-8 also shows the thermolysis-NH_3 yield (dashed lines). If only urea thermolysis takes place, the HNCO yield and the thermolysis-NH_3 yield are identical except for measuring errors. Due to the strong inhibition of the HNCO hydrolysis reaction by the presence of urea, the HNCO yield obtained on TiO_2 under hydrolysis conditions was only slightly lower than the HNCO yield without water up to 160°C (Fig. 6-8a). Above 165°C, the HNCO yield decreased again due to HNCO hydrolysis. On ZrO_2, the HNCO yield was much higher without water at most temperatures; however, at the lowest temperature investigated (160°C), the difference was small (without water: 6%, with water: 5% HNCO yield, see Fig. 6-6).
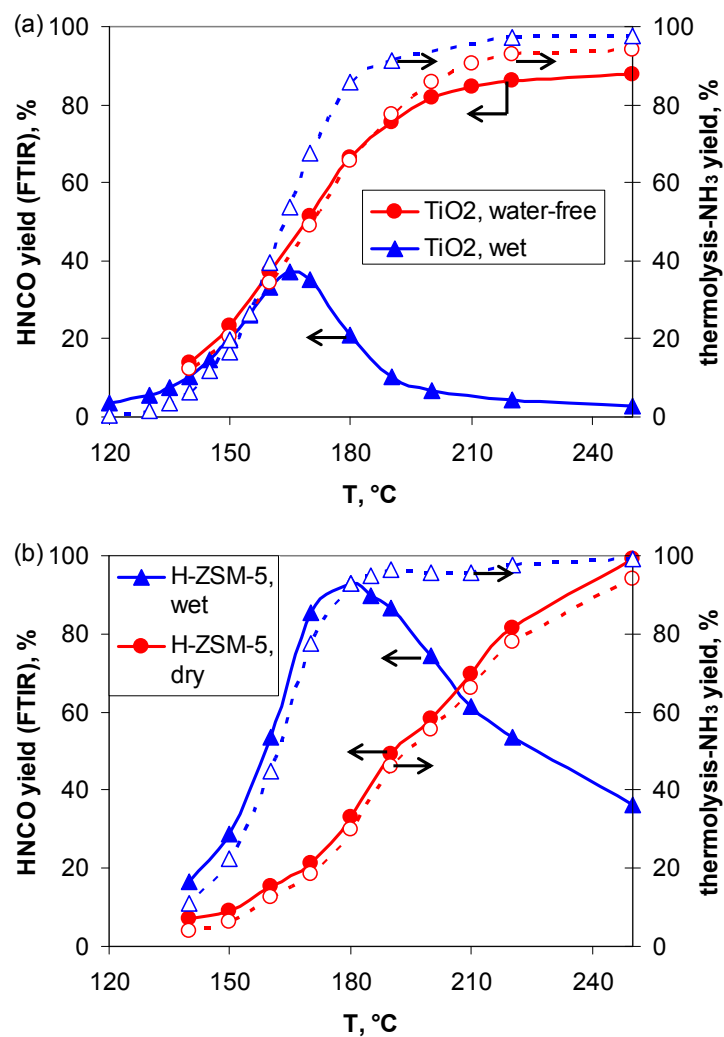
Fig. 6-8 (a-b). Dry and wet urea decomposition on (a) TiO$_2$ and (b) H-ZSM-5. The data are from the same experiments as those shown in Fig. 6-6. Dashed lines and empty symbols represent the NH$_3$-yield by thermolysis, solid lines and filled symbols show the FTIR data for HNCO. The dry experiments were conducted with urea in methanol solution.
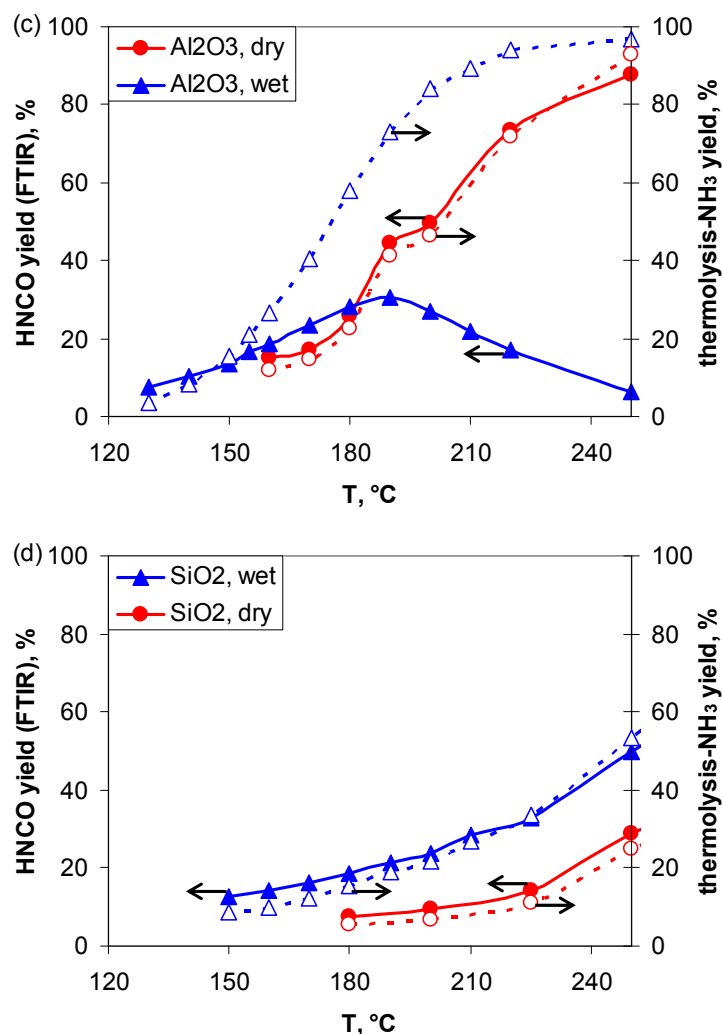
Fig. 6-8 (c-d). Dry and wet urea decomposition on (c) Al₂O₃ and (d) SiO₂. The data are from the same experiments as those shown in Fig. 6-6. Dashed lines and empty symbols represent the NH₃-yield by thermolysis, solid lines and filled symbols show the FTIR data for HNCO. The dry experiments were conducted with urea in ethanol solution.

Surprisingly, the HNCO yields obtained on the H-ZSM-5 (Fig. 6-8b) and on the Al_2O_3 (Fig. 6-8c) catalyst were higher in the presence of water than without water at some temperatures. On H-ZSM-5 at 180°C, the HNCO yield increased dramatically from 33% without water to 93% with water. On SiO_2, the HNCO yield was higher with water over the whole temperature range (Fig. 6-8d).

The simplest explanation for the low HNCO yields in the dry experiments would be inhibition of urea thermolysis by the organic solvent used to dose the urea. However, it is plausible that the adsorption strength of the solvents on the metal oxide catalysts decreases with their polarity in the order H_2O > MeOH > EtOH. Moreover, the concentration of the organic solvents was about 15 times lower than the water concentration (H_2O: 5%, MeOH: 0.36%, EtOH: 0.31%). Hence, the organic solvents are likely to inhibit urea adsorption less strongly than does water.

Another potential effect of the organic solvents that has to be checked is the presence or absence of side-reactions like condensation into ethers or substitution of their OH group with NH_3. Our results show that the organic solvents did not induce side-reactions, since the CO_2 yields were low. If condensation reactions had occurred, higher CO_2 yields would have been found due to released water. Also, we did not observe solvent-related byproducts by FTIR spectroscopy or HPLC analysis. Even at high magnification of the FTIR spectra, no byproducts were found [89].

Possibly, the presence of water on the catalyst surface accelerated the urea thermolysis by facilitating proton transfer reactions. This assumption of water assisting in the urea thermolysis is supported by a theoretical study by Alexandrova et al. (2007) that suggests water to act as a proton shuttle for the formation of the zwitterionic intermediate $H_3N^+C(O)N^-H$ in the mechanism for urea thermolysis in aqueous solution [91].

Table 6-2 summarizes the catalyst activity results from Fig. 6-6 and Fig. 6-7. Interestingly, ZrO_2, which showed the highest hydrolysis activity, showed only low thermolysis activity (see also Fig. 6-10b). The high hydrolysis activity of the ZrO_2 catalyst in spite of its low thermolysis activity indicates

that urea hydrolyzed directly on the ZrO_2 surface (3) without intermediate HNCO formation. Alternatively, if HNCO was formed on ZrO_2 during urea hydrolysis as a short lived intermediate, the low thermolysis activity of ZrO_2 might be due a low proton transfer capability of the dry ZrO_2 surface. Anyway, since urea hydrolysis on the ZrO_2 catalyst always produced CO_2 with a high selectivity, a kinetic model with only one rate-determining step should be sufficient to describe urea hydrolysis on ZrO_2.

Table 6-2. Qualitative summary of the catalyst activities shown in Fig. 6-6 and Fig. 6-7.

Catalyst	Urea thermolysis	Urea hydrolysis	HNCO hydrolysis
TiO_2	high	high	high
ZrO_2	low	very high	very high
H-ZSM-5	moderate	low	low
Al_2O_3	moderate	moderate	$<TiO_2$ [50, 57]
SiO_2	very low	very low	very low [50, 57]

6.4.3. Kinetics

For comparison of the urea conversions on the different catalysts, we calculated pseudo first-order rate constants (k_1) using the equation

$$k_1 = -\frac{V^*}{W}\ln(1-X), \quad cm^3 g^{-1} s^{-1}$$

where V^* is the actual gas volume flow rate, W is the catalyst weight and X is the urea conversion. By using this equation, we assume a first-order dependency with respect to urea, whereas all the other reaction orders are approximated by zero. The same approach was used by Kleemann et at. (2000) [51] to calculate pseudo first-order rate constants of the HNCO hydrolysis (first-order with respect to HNCO, water present in excess). Fig. 6-4 (page 157) suggested that urea hydrolysis on TiO_2 is indeed a first-order reaction at temperatures above 150°C. At the lowest temperatures

investigated, the actual reaction order may have been closer to zero-order than to first-order. Still, pseudo first-order rate constants are suitable for comparing the activities of different catalyst materials. Fig. 6-9 shows the resulting Arrhenius plot of the urea thermolysis data presented in Fig. 6-6a.
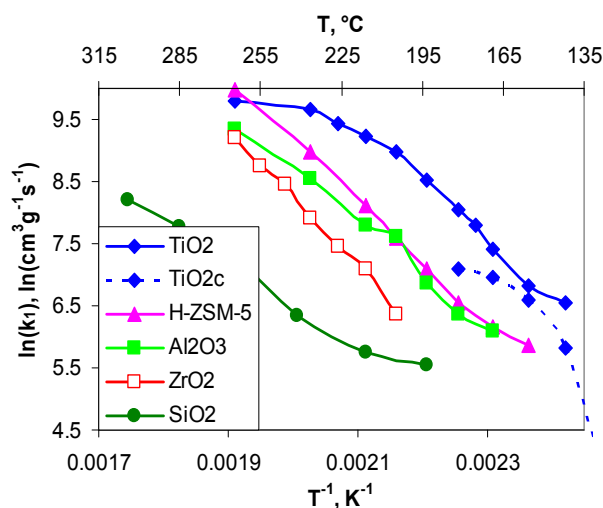
Fig. 6-9. Arrhenius analysis of the urea thermolysis experiments presented in Fig. 6-6a.

To experimentally confirm that the urea conversion on the most active catalyst in our screening, TiO_2, was not limited by the thermodynamic equilibrium of the urea thermolysis reaction, we performed an experiment with increased active mass. As expected, increasing the active mass from 45 mg (curve "TiO_2" in Fig. 6-9) to 540 mg (curve "TiO_2c" in Fig. 6-9) on the monolith increased the HNCO yield from 22% to 56%, respectively. Since the pseudo first-order rate constants shown in Fig. 6-9 are normalized to the active mass, the rates for the "TiO_2c"-monolith were below those of the "TiO_2"-monolith. Still, the pseudo first-order rate constants at 150°C were quite similar for the two TiO_2-coated monoliths due to the higher urea conversion on the "TiO_2c"-monolith. Below 150°C, the pseudo first-order rate constants from the "TiO_2c"-monolith were probably lowered

due to urea condensation, whereas, above 150°C, they were lowered due to mass transport limitation.

To test the presence or absence of mass transfer limitation in the Arrhenius plot (Fig. 6-9), we calculated $\eta_{ext}DaII$ values using the equation

$$\eta_{ext}DaII = \frac{r_{eff}}{k_g(T) \cdot ac_{1,g}} \quad \text{with} \quad k_g(T) \approx \frac{D_{1,2}}{d_G} \cdot \left(\frac{T}{T_0}\right)^{3/2}, \quad cm \cdot s^{-1} \text{ [92]}$$

where r_{eff} is observed reaction rate, k_g is gas phase mass transport coefficient, a is the geometric monolith surface area, T is the actual temperature and T_0 is the temperature for the tabulated value of the binary diffusion coefficient ($D_{1,2}$).

The $\eta_{ext}DaII$ value is a measure of the external mass transport limitation of a reaction (diffusion of gaseous urea in the monolith channels). A $\eta_{ext}DaII$ value below 0.1 means the mass transport limitation is insignificant [92]. The calculation of the $\eta_{ext}DaII$ values was based on the following assumptions:

− complete evaporation and mixing of the dosed urea with the model gas
− laminar gas flow
− diffusion length (d_g) = ¼ channel width
− The binary diffusion coefficient ($D_{1,2}$) of urea in the model gas was approximated by the binary diffusion coefficient of SO_2 in air: $D_{urea, model\ gas} \approx D_{SO2,\ air} = 0.122$, cm^2s^{-1} at 298 K [92]. The values for slightly different gas matrices do not differ significantly. The binary diffusion coefficient of SO_2 was chosen for the calculations with urea due to the quite similar molecular mass and due to the not completely different geometry.

– conversion at the catalyst exit used for calculating the concentration of gaseous urea ($c_{1,g}$)

Please note that using the conversion at the catalyst exit for calculating $c_{1,g}$ means making a worst case assumption, because the low $c_{1,g}$ at the catalyst exit leads to the assumption of a small urea concentration gradient. Another assumption made has to be discussed: the assumption of complete urea evaporation. Unfortunately, we could not directly measure if and where the urea aerosols evaporate in our reactor. However, the vapor pressure of urea is more than high enough to allow for complete urea evaporation at the conditions applied, see chapter 3. Indeed, several indications suggest that the high spray quality in our setup allowed for quantitative urea evaporation upstream of the catalyst:

– Fig. 6-6c shows the CO_2 yield obtained by urea hydrolysis in long ("TiO_2") and short ("TiO_2b") TiO_2-coated monoliths. The shorter monolith with the higher amount of the catalyst showed a higher CO_2 yield at low temperatures up to 180°C, as expected for gaseous urea but not for urea aerosols. If evaporation of the urea aerosols would not have been complete upstream of the monolith, aerosols would have preferably slipped through the channels of the short monolith resulting in a lower conversion at all temperatures.

– During method development, the performance of the SCR reaction with respect to NO_x reduction and NH_3 emissions at the reactor exit was found to be almost the same with sprayed urea solution as with NH_3 gas over a very broad parameter range, when the distance between nozzle and catalyst was properly chosen, see chapter 2.1.9.

– In a first series of urea hydrolysis experiments, we placed a catalyst-coated monolith in a larger distance from the spray nozzle. Then we placed an inert cordierite foam between the spray nozzle and the catalyst. Neither of these measures increased the urea conversion, see chapter 2.1.11. If the urea aerosols evaporated slowly, an inert structure upstream of the catalyst should have improved the urea evaporation, which should also have increased the urea conversion on the catalyst.

These observations suggest that most of the urea aerosols dosed by the spray nozzle evaporated upstream of the catalyst. If the urea aerosols did not evaporate, at least the aerosol slip through the catalyst-coated monoliths was insignificant.

6.4.4. Determination of apparent activation energies

Fig. 6-10a shows an Arrhenius plot of the urea thermolysis on anatase TiO_2 and the calculated $\eta_{ext}DaII$ values for this experiment. An $\eta_{ext}DaII$ value below 0.1 indicates insignificant mass transport limitation [92]. The pseudo first-order rate constants of the urea hydrolysis were calculated likewise and plotted in Fig. 6-10a, too. We are aware of the fact that the simple kinetic model is not applicable for the two-step urea hydrolysis on TiO_2, where a significant amount of the intermediate HNCO can desorb into the gas phase. However, due to the definition of the conversion as $X = 2 \times NH_3$ yield - CO_2 yield, the NH_3 produced by HNCO hydrolysis is subtracted and only the NH_3 produced by urea thermolysis is taken into account. Therefore, the pseudo first-order rate constants obtained for hydrolysis conditions (5% water) should be suitable for comparison. Comparison of the pseudo first-order rate constants shows that the hydrolysis was somewhat slower than thermolysis below 150°C, whereas the hydrolysis

was faster above 160°C. Maybe, the hydrolysis was slower below 150°C due to competitive adsorption of urea and water, whereas the hydrolysis was faster above 160°C because the surface coverage was lowered by HNCO hydrolysis or because adsorbed water accelerated the thermolysis by acting as a proton shuttle.
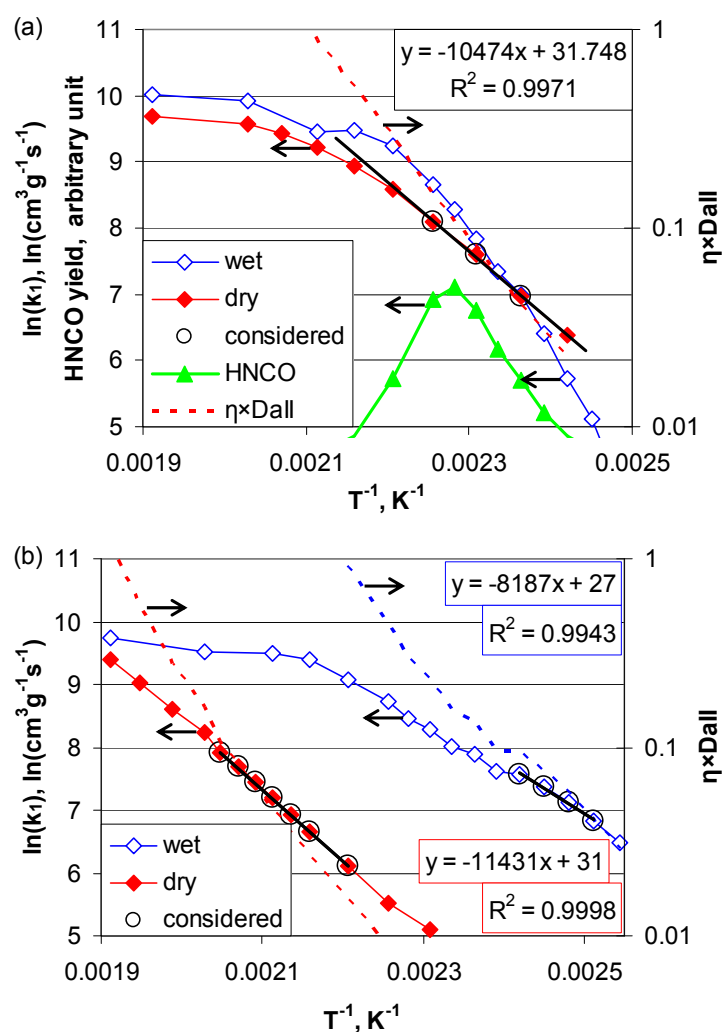

Fig. 6-10. Arrhenius analyses of urea decomposition on (a) anatase TiO$_2$ and (b) ZrO$_2$. Urea in MeOH solution was used for the dry experiments.

Based on the $\eta_{ext}DaII$ values and on the apparent linearity of the Arrhenius plots in the temperature range between 150°C and 170°C, the urea

thermolysis data points in this temperature range were used for a linear regression (highlighted in Fig. 6-10a). From the obtained regression line an apparent activation energy (E_a) of 90 kJ/mol and a pre-exponential factor (A) of $6 \cdot 10^{13}$ s^{-1} were calculated for urea thermolysis on TiO_2 (Fig. 6-10a).

The activity of the ZrO_2 catalyst (Fig. 6-10b) was analyzed likewise. If urea hydrolyzes in one step on ZrO_2 according to reaction (3) as proposed in chapter 6.4.2, the kinetic model used for the urea thermolysis can be applied for urea hydrolysis on ZrO_2 as well. The corresponding values derived from Fig. 6-10b are E_a = 100 kJ/mol, A = $4 \cdot 10^{13}$ s^{-1} for the thermolysis (considering the data points at 180, 190, 195, 200, 205, 210 and 215°C) and E_a = 70 kJ/mol, A = $8 \cdot 10^{11}$ s^{-1} for the hydrolysis (considering the data points at 125, 130, 135 and 140°C).

6.4.5. Biuret hydrolysis

Byproduct formation was not observed in the experiments reported in this chapter 6, however, byproducts may have accumulated slowly, which could cause catalyst deactivation after long-term operation. The most probable byproducts are biuret, CYA, triuret and ammelide, see chapter 4. Since only biuret has a significant solubility in water, 2% aqueous biuret solution was used in this study to investigate byproduct decomposition.
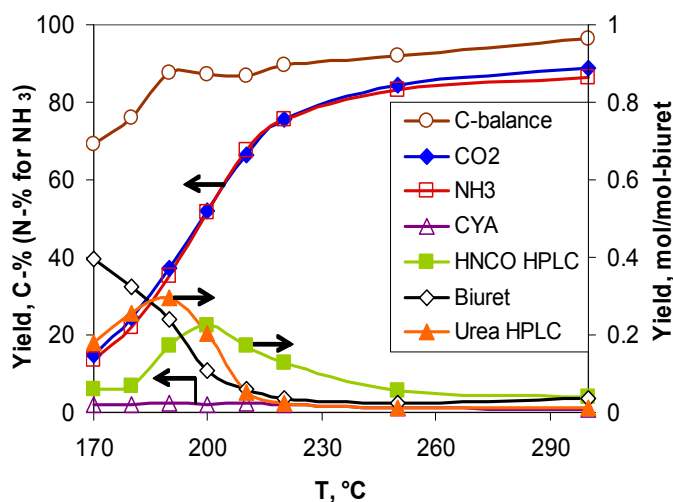
Fig. 6-11. Biuret hydrolysis on the TiO$_2$d-monolith sample. Parameters: 50 ppm biuret, 5% H$_2$O, 10% O$_2$ in N$_2$; total gas flow = 500 L/h at STP; GHSV = 91'000 h^{-1}; active mass: 24 mg.

Fig. 6-11 shows the product distribution of biuret hydrolysis on TiO$_2$. Biuret hydrolyzed fairly well in a three-step reaction, showing local maxima of the formed intermediates urea and HNCO. The urea yield peaked at 190°C and 0.29 mol/mol-biuret, whereas HNCO peaked at 200°C and 0.23 mol/mol-biuret. When the water concentration in the gas phase was decreased from 5% to 1.4%, the urea peak increased to 0.36 mol/mol-biuret, whereas the HNCO peak shifted to 210°C and increased to 0.52 mol/mol-biuret (not shown).

In the empty reactor, higher biuret conversions were observed (not shown) than urea conversions shown in Fig. 6-2. This result is surprising because biuret is more stable against non-catalytic decomposition than urea [38]. The high biuret conversion in the empty reactor was probably caused by the low vapor pressure of biuret: Unlike urea, which seemed to evaporate quickly and completely in our experiments, part of the biuret may have stuck to the reactor wall until it decomposed. In other words, the residence

time and the heat transfer from the reactor wall to the reactant were increased for biuret compared to urea. The decomposition products urea, HNCO and NH_3 have higher vapor pressures than biuret and could therefore easily leave the reactor. As mentioned, the biuret conversion in the empty reactor was quite high. Still, the TiO_2 catalyst largely increased the biuret conversion: At 190°C, where the urea yield with the TiO_2 catalyst peaked at 0.29 mol/mol-biuret, the yield in the empty reactor was only 0.08 mol/mol-biuret, which strongly indicates catalytic biuret decomposition. Catalytic byproduct decomposition activity is a highly welcome feature of a urea hydrolysis catalyst in an SCR system, because byproducts that may form during low temperature operation will quickly hydrolyze at elevated temperatures.

6.5. Conclusions

Experiments on the catalytic hydrolysis of 100 ppm urea to NH_3 and CO_2 in the gas phase showed the following order of hydrolysis activities:

$ZrO_2 > TiO_2 > Al_2O_3 > $ H-ZSM-5 $ > SiO_2$
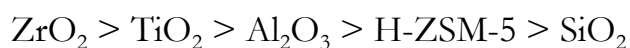
Dry experiments on the thermolysis of urea to HNCO and NH_3 revealed a different activity order:

$TiO_2 > $ H-ZSM-5 $ \approx Al_2O_3 > ZrO_2 > SiO_2$

For the most active catalysts TiO_2 and ZrO_2 the activation energies for hydrolysis and thermolysis were determined by means of an Arrhenius analysis of the apparent pseudo first-order rate constants:

Urea thermolysis on TiO_2: $E_a = 90$ kJ/mol

Urea thermolysis on ZrO_2: $E_a = 100$ kJ/mol

Urea hydrolysis on ZrO_2: $E_a = 70$ kJ/mol
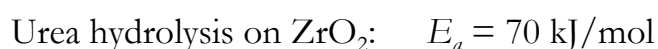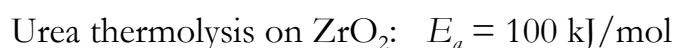
The found activation energies for the thermolysis of urea are larger than the activation energy of 73 kJ/mol reported for the hydrolysis of HNCO on anatase TiO_2 by Hauck et al. (2007) [56]. Also, the HNCO hydrolysis rates reported by [56], as well as those found in our own measurements, were significantly higher than the urea thermolysis rates (Fig. 6-6 vs. Fig. 6-7). Consequently, our results clearly show that urea thermolysis must be the rate-determining step in catalytic urea decomposition in the SCR process.

On TiO_2, the urea conversion in the absence of water was quite similar to the urea conversion with water (Fig. 6-10a). The main effect of the presence of water was a changed selectivity of the overall reaction due to HNCO hydrolysis. By contrast, the ZrO_2 catalyst showed a much lower urea conversion in the absence of water than with water (Fig. 6-10b), which indicates that urea hydrolyzes on ZrO_2 according to a different mechanism, in which water directly attacks adsorbed urea rather than adsorbed HNCO as proposed in [78].

7. Conclusions and Outlook

7.1. Conclusions

Urea was found to evaporate from an inert cordierite monolith at atmospheric pressure (chapter 3). The large geometric surface area of the monolith and the high gas flow rate relative to the amount of urea present on the monolith allowed urea evaporation to be faster than decomposition. At a later stage, a method was developed to quantify gaseous urea by FTIR spectroscopy. With respect to the urea-SCR application, our results suggest that considering gaseous urea should improve CFD models used for designing urea SCR systems. In fact, two recent theoretical studies [29, 30] on the evaporation and decomposition of urea solution droplets achieved good agreement with experimental data by considering urea evaporation. These two recent studies plus the results presented here in the chapters 2.1.8, 2.1.11, 3, 5 and 6 strongly indicate that urea evaporation is relevant to the urea-SCR process.

Urea decomposition, including the formation and decomposition of byproducts, was investigated on anatase TiO_2, where complete urea hydrolysis could be achieved (chapter 4). In the absence of water, TiO_2 was found to catalyze urea thermolysis into NH_3 and HNCO. At 125°C, the formed HNCO preferentially combined with urea to form biuret rather than CYA. If, however, biuret was used as the starting material instead of urea, CYA was the main solid reaction product at 100°C, 125°C and 150C°. In the presence of water, biuret could be converted into urea by direct partial hydrolysis at 100°C and 114°C. Urea was the main solid product, but smaller amounts CYA were formed in spite of the presence of water. Melamine was found to hydrolyze on TiO_2 in a multi-step reaction via the

intermediates ammeline, ammelide and CYA. CYA was most stable against hydrolysis among the compounds tested. CYA hydrolysis on TiO_2 started at about 200°C, whereas CYA thermolysis started at about 250°C. The high hydrolysis activity of TiO_2 for urea decomposition byproducts indicates that TiO_2, used as a dedicated hydrolysis catalyst, is resistant to urea-induced deactivation. Even if byproducts are formed on the catalyst at low temperature, or if byproduct-containing aerosols are deposited on the catalyst, these byproducts will be easily hydrolyzed at higher temperature.

High-purity gaseous urea from an inert cordierite monolith was used to adsorb urea onto TiO_2-catalyst samples (chapter 5). Urea adsorption was independently confirmed by HPLC analysis and by DRIFT spectroscopy. DFT calculations and DRIFT spectra indicated that two different adsorbed states of deprotonated urea existed simultaneously: in one adsorbed state, urea bound with its HN^- group at one Ti site. In the other adsorbed state, urea was rotated and bound with both its HN^- group and its O group at two Ti sites.

A catalyst screening under stationary conditions showed urea hydrolysis activities in the order $ZrO_2 > TiO_2 > Al_2O_3 >$ H-ZSM-5 $> SiO_2$ (chapter 6). The thermolysis activities exhibited a different order $TiO_2 >$ H-ZSM-5 $\approx Al_2O_3 > ZrO_2 > SiO_2$. The high urea hydrolysis activity of ZrO_2 in spite of its low thermolysis activity indicated that urea hydrolyzed directly on ZrO_2 without intermediate HNCO formation. In agreement with this assumption of direct urea hydrolysis on ZrO_2, ZrO_2 showed by far the highest selectivity towards CO_2 under hydrolysis conditions, whereas the TiO_2, Al_2O_3, H-ZSM-5 catalysts showed significant local maxima in the HNCO slip at 165°C, 180°C and 190°C, respectively. Local maxima of

intermediates are typical for two-step reactions. Still, the local maxima in the HNCO slip were surprising, because the hydrolysis of pure HNCO, reported in [56], is much faster than urea hydrolysis. We performed hydrolysis of pure HNCO on the same catalyst-coated monoliths as used for the urea hydrolysis experiments and found very high HNCO hydrolysis rates, too. In the light of the very high HNCO hydrolysis rates, the observed local maxima in the HNCO slip under urea hydrolysis conditions can only be explained by urea inhibition of the HNCO hydrolysis reaction. Thus, catalytic urea thermolysis into NH_3 and HNCO must be the rate-determining step on TiO_2, Al_2O_3 and H-ZSM-5.

7.2. Outlook

Starting with the catalyst screening presented in chapter 6.4.2, a logical next step would be determining the reaction orders. The reaction order with respect to water appears to be most interesting, but its determination would bring along experimental difficulties. An organic solvent would have to be used at low water concentrations to avoid the presence of excess water due to the solvent. Hence, it may be necessary to determine the reaction order with respect to the organic solvent, too. It would also be interesting to extend the screening to commercial SCR catalysts. However, using an organic solvent may not work with SCR catalysts because of side-reactions.

The study could be further developed towards either more basic or more application-related research.

On the basic side, more evidence for direct urea hydrolysis on ZrO_2 should be found. In addition to determining the reaction orders, DFT calculations may be applied for simulating the adsorption, thermolysis and hydrolysis of

urea on ZrO_2. Combining activity measurements, DRIFT spectroscopy and DFT calculations should decisively improve the understanding of the high CO_2 selectivity of the ZrO_2 catalyst. The previously performed DRIFT spectroscopy experiments may be upgraded into in-situ experiments with conversion of gaseous urea in a plate reactor, equipped with a window and operated in differential mode. To avoid urea condensation on the window, two windows may be used, with a gap that is purged with hot nitrogen. Further, the turn over frequency (TOF) may be determined. The high pre-exponential factors obtained from the Arrhenius analyses indicate that a high number of active sites is present on the catalysts [56]. Yet, the determination of the number of active sites is outstanding. A rough estimate may be obtained from NH_3 adsorption experiments. Unfortunately, the actual reactant urea is likely to prove unpractical for adsorption experiments, because the temperature window, where urea has both significant vapor pressure and stability on the catalyst, is narrow. Adsorption experiments with a model compound may be the better option. Methanamide appears to be a promising model compound, as it is more stable and more volatile than urea. Also methanamide adsorption itself is of interest, since methanamide is considered as an alternative NH_3 precursor compound [26].

On the application-related side, a kinetic model of urea hydrolysis on TiO_2 and/or on a commercial SCR catalyst may be developed. The model could be extended to include mass transport phenomena. The extended model may use experimental data from the lab-scale spray reactor with high catalyst loadings and low cell densities as input. In a final step, the kinetic model may be combined with the CFD model of AdBlue® sprays obtained in the framework of the NADiP CCEM project. The NADiP project aims

at developing an improved CFD model of AdBlue® sprays, based on experiments that apply laser particle analysis techniques. The NADiP project has been running in parallel with the presented thesis, but it is still in an early stage.

An idea that could be worth testing is mixing a commercial zeolite SCR catalyst with a small amount of TiO_2 to improve its hydrolysis activity. Commercial zeolite SCR catalysts typically show a smaller HNCO slip than V_2O_5-based SCR catalysts, which indicates that zeolites exhibit higher hydrolysis activity. On the other hand, zeolite catalysts are more vulnerable to deactivation by urea decomposition byproducts. Placing a dedicated TiO_2 hydrolysis catalyst in front of the SCR catalyst improves urea hydrolysis and should therefore avoid urea-induced deactivation of the SCR catalyst. However, as a rule of thumb, increasing the size of the SCR catalyst results in a higher SCR performance than adding a dedicated hydrolysis catalyst. Also, the manufacturers usually dislike adding a catalyst, because it adds complexity and cost to the exhaust aftertreatment system. Mixing a zeolite SCR catalyst with TiO_2 might be a cost-effective solution to improve both its urea hydrolysis activity and its resistance against urea-induced deactivation.

8. References

1. M. Eichelbaum, R. J. Farrauto, M. J. Castaldi "The impact of urea on the performance of metal exchanged zeolites for the selective catalytic reduction of NOx: Part I. Pyrolysis and hydrolysis of urea over zeolite catalysts" *Appl. Catal., B* **97**, 90 (2010).

2. M. Radojevic "Reduction of nitrogen oxides in flue gases" 1st International Nitrogen Conference 1998, Noordwijkerhout, Netherlands (1998).

3. D. Fowler, C. Flechard, U. Skiba, M. Coyle, J. N. Cape "The atmospheric budget of oxidized nitrogen and its role in ozone formation and deposition" *New Phytol.* **139**, 11 (1998).

4. S. K. Hoekman, C. Robbins "Review of the effects of biodiesel on NOx emissions" *Fuel Process. Technol.* **96**, 237 (2012).

5. S. C. Hill, L. Douglas Smoot "Modeling of nitrogen oxides formation and destruction in combustion systems" *Prog. Energy Combust. Sci.* **26**, 417 (2000).

6. J. Hu, Y. Wu, Z. Wang, Z. Li, Y. Zhou, H. Wang, X. Bao, J. Hao "Real-world fuel efficiency and exhaust emissions of light-duty diesel vehicles and their correlation with road conditions" *J. Environ. Sci.* **24**, 865 (2012).

7. Y. Wada, K. Yamatsuta. (1977).

8. T. J. Wang, S. W. Baek, S. Y. Lee, D. H. Kang, G. K. Yeo "Experimental investigation on evaporation of urea-water-solution droplet for SCR applications" *AIChE J.* **55**, 3267 (2009).

9. R. O. McClellan, T. W. Hesterberg, J. C. Wall "Evaluation of carcinogenic hazard of diesel engine exhaust needs to consider revolutionary changes in diesel technology" *Regul. Toxicol. Pharm.* **63**, 225 (2012).

10. M. Koebel, M. Elsener, G. Madia "Recent Advances in the Development of Urea-SCR for Automotive Applications" International Fall Fuels and Lubricants Meeting and Exposition, San Antonio, Texas (2001).

11. K. O. Lee, J. Zhu, J. Song "Effects of exhaust gas recirculation on diesel particulate matter morphology and NOx emissions" *Int. J. Engine Res.* **9**, 165 (2008).

12. A. Traebert, L. Zimmermann, R. Frey, T. Johansson "Investigation of a Combined Exhaust After-Treatment System for Commercial Vehicles", Berlin, Germany (2010).

13. B. K. Yun, M. Y. Kim "Modeling the selective catalytic reduction of NOx by ammonia over a vanadia-based catalyst from heavy duty diesel exhaust gases" *Appl. Therm. Eng.* **50**, 152 (2013).

14. M. Koebel, M. Elsener, M. Kleemann "Urea-SCR: a promising technique to reduce NOx emissions from automotive diesel engines" *Catal. Today* **59**, 335 (2000).

15. L. J. Alemany, F. Berti, G. Busca, G. Ramis, D. Robba, G. P. Toledo, M. Trombetta "Characterization and composition of commercial V2O5-WO3-TiO2 SCR catalysts" *Appl. Catal., B* **10**, 299 (1996).

16. D. M. Chapman "Behavior of titania-supported vanadia and tungsta SCR catalysts at high temperatures in reactant streams: Tungsten and vanadium oxide and hydroxide vapor pressure reduction by surficial stabilization" *Appl. Catal., A* **392**, 143 (2011).

17. J. H. Kwak, R. G. Tonkyn, D. H. Kim, J. n. Szanyi, C. H. F. Peden "Excellent activity and selectivity of Cu-SSZ-13 in the selective catalytic reduction of NOx with NH3" *J. Catal.* **275**, 187 (2010).

18. O. Kröcher, M. Devadas, M. Elsener, A. Wokaun, N. Söger, M. Pfeifer, Y. Demel, L. Mussmann "Investigation of the selective catalytic reduction of NO by NH3 on Fe-ZSM5 monolith catalysts" *Appl. Catal., B* **66**, 208 (2006).

19. O. Kröcher, M. Elsener "Chemical deactivation of V2O5/WO3-TiO2 SCR catalysts by additives and impurities from fuels, lubrication oils, and urea solution: I. Catalytic studies" *Appl. Catal., B* **77**, 215 (2008).

20. M. Koebel, E. A. Strutz "Thermal and hydrolytic decomposition of urea for automotive selective catalytic reduction systems: Thermochemical and practical aspects" *Ind. Eng. Chem. Res.* **42**, 2093 (2003).

21. D. Peitz, A. Bernhard, O. Kröcher "Ammonia storage and release in SCR systems for mobile applications" in *Urea-SCR technology for deNOx aftertreatment of Diesel exhausts,* (Springer, accepted).

22. R. A. Perry, D. L. Siebers "Rapid reduction of nitrogen oxides in exhaust gas streams" *Nature* **324**, 657 (1986).

23. D. L. Siebers, J. A. Caton "Removal of nitric oxide from exhaust gas with cyanuric acid" *Combust. Flame* **79**, 31 (1990).

24. J. Thompson, J. Op De Beeck, E. Joubert, T. Wilhelm "Case Studies of Urea SCR Integration on Passenger Cars Monitoring of Urea Inside the Tank During Hot and Cold Environment Test Missions" *SAE Technical Paper* **2008-01-1181**, (2008).

25. O. Kröcher, M. Elsener, E. Jacob "A model gas study of ammonium formate, methanamide and guanidinium formate as alternative ammonia precursor compounds for the selective catalytic reduction of nitrogen oxides in diesel exhaust gas" *Appl. Catal., B* **88**, 66 (2009).

26. D. Peitz "Investigation on the catalytic decomposition of guanidinium formate, ammonium formate and methanamide as NH3-precursors for the selective catalytic reduction of NOx" Dissertation at ETH Zurich, Switzerland, Thesis No. 20568 (2012).

27. F. Birkhold, U. Meingast, P. Wassermann, O. Deutschmann "Modeling and simulation of the injection of urea-water-solution for automotive SCR DeNOx-systems" *Appl. Catal., B* **70**, 119 (2007).

28. H. Ström, A. Lundström, B. Andersson "Choice of urea-spray models in CFD simulations of urea-SCR systems" *Chem. Eng. J.* **150**, 69 (2009).

29. E. Abu-Ramadan, K. Saha, X. Li "Modeling the depleting mechanism of urea-water-solution droplet for automotive selective catalytic reduction systems" *AIChE J.* **57**, 3210 (2011).

30. A. Lundström, B. Waldheim, H. Ström, B. Westerberg "Modelling of urea gas phase thermolysis and theoretical details on urea evaporation". Paper presented at the Proceedings of the Institution of Mechanical Engineers, Part D: Journal of Automobile Engineering, October 1, 2011, 2011.

31. G. Della Gatta, D. Ferrq "Enthalpies of fusion and solid-to-solid transition, entropies of fusion for urea and twelve alkylureas" *Thermochim. Acta* **122**, 143 (1987).

32. V. N. Emel'yanenko, G. J. Kabo, S. P. Verevkin "Measurement and Prediction of Thermochemical Properties: Improved Increments for the Estimation of Enthalpies of Sublimation and Standard Enthalpies of Formation of Alkyl Derivatives of Urea" *J. Chem. Eng. Data.* **51**, 79 (2005).

33. D. Ferro, G. Barone, G. Della Gatta, V. Piacente "Vapour pressures and sublimation enthalpies of urea and some of its derivatives" *J. Chem. Thermodyn.* **19**, 915 (1987).

34. V. Ebrahimian, Nicolle, A. and Habchi, C. "Detailed modeling of the evaporation and thermal decomposition of urea-water solution in SCR systems" *AIChE J.* **58**, 1998 (2012).

35. A. Schmidt "Herstellung von Melamin aus Harnstoff bei Atmosphärendruck" *Chem. Ing. Tech.* **38**, 1140 (1966).

36. F. Fadul, A. Nelli, A. Fakheri "Urea mixing in selective catalytic reduction systems" ASME International Mechanical Engineering Congress and Exposition, Proceedings, Seattle, WA (2008).

37. HSC Chemistry 7. Computer program by Outokupu Research.

38. P. A. Schaber, J. Colson, S. Higgins, D. Thielen, B. Anspach, J. Brauer "Thermal decomposition (pyrolysis) of urea in an open reaction vessel" *Thermochim. Acta* **424**, 131 (2004).

39. H. L. Fang, H. F. M. DaCosta "Urea thermolysis and NOx reduction with and without SCR catalysts" *Appl. Catal., B* **46**, 17 (2003).

40. A. Lundström, B. Andersson, L. Olsson "Urea thermolysis studied under flow reactor conditions using DSC and FT-IR" *Chem. Eng. J.* **150**, 544 (2009).

41. A. P. Krasulin, A. A. Kozyro, G. Y. Kabo "Saturation vapor pressure of urea in the temperature range 329-403 K" *J. Appl. Chem. USSR* **60**, 96 (1987).

42. J. Langer, B. Schrader, V. Bastian, E. Jacob "Infrared-spectra and force-constants of urea in the gaseous-phase" *Fresenius J. Anal. Chem.* **352**, 489 (1995).

43. A. M. Bernhard, I. Czekaj, M. Elsener, A. Wokaun, O. Kröcher "Evaporation of Urea at Atmospheric Pressure" *J. Phys. Chem. A* **115**, 2581 (2011).

44. S. Kontin, A. Höfler, R. Koch, H.-J. Bauer "Heat and Mass Transfer accompanied by Crystallisation of single Particles containing Urea-water-solution" 23rd Annual Conference on Liquid Atomization and Spray Systems, Brno, Czech Republic (2010).

45. P. Hauck, A. Jentys, J. A. Lercher "On the quantitative aspects of hydrolysis of isocyanic acid on TiO2" *Catal. Today* **127**, 165 (2007).

46. A. M. Bernhard, D. Peitz, M. Elsener, A. Wokaun, O. Kröcher "Hydrolysis and thermolysis of urea and its decomposition byproducts biuret, cyanuric acid and melamine over anatase TiO2" *Appl. Catal., B* **115-116**, 129 (2012).

47. H. Dong, Shuai, S., and Wang, J. "Effect of Urea Thermal Decomposition on Diesel NOx-SCR Aftertreatment Systems" *SAE Technical Paper* **2008-01-1544**, (2008).

48. A. Lundström, T. Snelling, P. Morsing, P. Gabrielsson, E. Senar, L. Olsson "Urea Decomposition and HNCO Hydrolysis Studied over Titanium dioxide, Fe-Beta and [gamma]-Alumina" *Appl. Catal., B* **106**, 273 (2011).

49. G. Piazzesi, O. Kröcher, M. Elsener, A. Wokaun "Adsorption and hydrolysis of isocyanic acid on TiO2" *Appl. Catal., B* **65**, 55 (2006).

References

50. I. Czekaj, O. Kröcher "Decomposition of Urea in the SCR Process: Combination of DFT Calculations and Experimental Results on the Catalytic Hydrolysis of Isocyanic Acid on TiO2 and Al2O3" *Top. Catal.* **52**, 1740 (2009).

51. M. Kleemann, M. Elsener, M. Koebel, A. Wokaun "Hydrolysis of isocyanic acid on SCR catalysts" *Ind. Eng. Chem. Res.* **39**, 4120 (2000).

52. G. Piazzesi, M. Devadas, O. Kröcher, M. Elsener, A. Wokaun "Isocyanic acid hydrolysis over Fe-ZSM5 in urea-SCR" *Catal. Commun.* **7**, 600 (2006).

53. M. Eichelbaum, A. B. Siemer, R. J. Farrauto, M. J. Castaldi "The impact of urea on the performance of metal-exchanged zeolites for the selective catalytic reduction of NOx--Part II. Catalytic, FTIR, and NMR studies" *Appl. Catal., B* **97**, 98 (2010).

54. Z. Zhan, M. Müllner, J. A. Lercher "Catalytic hydrolysis of s-triazine compounds over Al2O3" *Catal. Today* **27**, 167 (1996).

55. I. Czekaj, O. Kröcher, G. Piazzesi "DFT calculations, DRIFT spectroscopy and kinetic studies on the hydrolysis of isocyanic acid on the TiO2-anatase (1 0 1) surface" *J. Mol. Catal. A: Chem.* **280**, 68 (2008).

56. P. Hauck, A. Jentys, J. A. Lercher "Surface chemistry and kinetics of the hydrolysis of isocyanic acid on anatase" *Appl. Catal., B* **70**, 91 (2007).

57. G. Piazzesi "The Catalytic Hydrolysis of Isocyanic Acid (HNCO) in the Urea-SCR Process" Dissertation at ETH Zurich, Switzerland, Thesis No. 16693 (2006).

58. M. A. Larrubia, G. Ramis, G. Busca "An FT-IR study of the adsorption of urea and ammonia over V2O5-MoO3-TiO2 SCR catalysts" *Appl. Catal., B* **27**, L145 (2000).

59. T. Sekiya, S. Kurita "Defects in Anatase Titanium Dioxide" in *Nano-and Micromaterials-Advances in Materials Research,* (2008), vol. 9, pp. 121-141.

60. DuPont™ Ti-Pure®. http://www2.dupont.com/Titanium_Technologies/de_US/tech_info/literature/Plastics/PL_B_Polymers_Light_Science.pdf

61. J.-M. Sohier (TOTAL France), M. Jermann (PSI), A. Wokaun (PSI). (2008).

62. A. M. Bernhard, D. Peitz, M. Elsener, T. Schildhauer, O. Kröcher "Catalytic urea hydrolysis in the selective catalytic reduction of NOx: Catalyst screening and kinetics on anatase TiO2 and ZrO2" *Catal. Sci. Technol.*, DOI: 10.1039/C2CY20668D.

References

63.   A. M. Bernhard, I. Czekaj, M. Elsener, O. Kröcher "Adsorption and catalytic thermolysis of gaseous urea on anatase TiO2, studied by HPLC analysis, DRIFT spectroscopy and DFT calculations" *Appl. Catal., B*, DOI: 10.1016/j.apcatb.2013.01.009.

64.   D. Peitz, A. Bernhard, M. Elsener, O. Kröcher "Laboratory test reactor for the investigation of liquid reducing agents in the selective catalytic reduction of NOx" *Rev. Sci. Instrum.* **82**, 084101 (2011).

65.   C. Livingston, P. Rieger, A. Winer "Ammonia emissions from a representative in-use fleet of light and medium-duty vehicles in the California South Coast Air Basin" *Atmos. Environ.* **43**, 3326 (2009).

66.   M. Koebel, M. Elsener "Determination of urea and its thermal decomposition products by high-performance liquid chromatography" *J. Chromatogr. A* **689**, 164 (1995).

67.   H. Aoki, T. Fujiwara, Y. E. Morozumi, T. Miura "Measurements of urea thermal decomposition reaction for NO selective non-catalytic reduction" Proceedings of Fifth International Conference on Technologies and Combustion for a Clean Environment, Lisbon, Portugal (1999).

68.   S. D. Yim, S. J. Kim, J. H. Baik, I. S. Nam, Y. S. Mok, J. H. Lee, B. K. Cho, S. H. Oh "Decomposition of urea into NH3 for the SCR process" *Ind. Eng. Chem. Res.* **43**, 4856 (2004).

69.   E. F. Zanoelo "A lumped model for thermal decomposition of urea. Uncertainties analysis and selective non-catalytic reduction of NO" *Chem. Eng. Sci.* **64**, 1075 (2009).

70.   O. Carp "Considerations on the thermal decomposition of urea" *Rev. Roum. Chim.* **46**, 735 (2001).

71.   F. Birkhold, U. Meingast, W. Peter, O. Deutschmann "Analysis of the Injection of Urea-water-solution for automotive SCR DeNOx-Systems: Modeling of Two-phase Flow and Spray/Wall-Interaction" *SAE Int.* **2006-01-0643**, (2006).

72.   J. Y. Kim, S. H. Ryu, J. S. Ha "Numerical prediction on the characteristics of spray-induced mixing and thermal decomposition of urea solution in SCR system" ASME Internal Combustion Engine Division, Long Beach, California USA (2004).

73.   B. Hammer, L. B. Hansen, J. K. Nørskov "Improved adsorption energetics within density-functional theory using revised Perdew-Burke-Ernzerhof functionals" *Phys. Rev. B: Condens. Matter* **59**, 7413 (1999).

74.   J. P. Perdew, K. Burke, M. Ernzerhof "Generalized Gradient Approximation Made Simple" *Phys. Rev. Lett.* **77**, 3865 (1996).

References

75. C. Friedrich "Geometrische, elektronische und vibronische Eigenschaften der reinen und defektbehafteten V2O5(010)-Oberfläche und deren Wechselwirkung mit Adsorbaten: Theoretische Untersuchungen" Dissertation at FU Berlin, Germany, (2004).

76. G. Piazzesi, D. Nicosia, M. Devadas, O. Kröcher, M. Elsener, A. Wokaun "Investigation of HNCO adsorption and hydrolysis on Fe-ZSM5" *Catal. Lett.* **115**, 33 (2007).

77. A. Masunov, J. J. Dannenberg "Theoretical Study of Urea. I. Monomers and Dimers" *J. Phys. Chem. A* **103**, 178 (1998).

78. T. Todorova, D. Peitz, O. Kröcher, A. Wokaun, B. Delley "Guanidinium Formate Decomposition on the (101) TiO2-Anatase Surface: Combined Minimum Energy Reaction Pathway Calculations and Temperature-Programmed Decomposition Experiments " *J. Phys. Chem. C* **115**, 1195 (2011).

79. M. Koebel "Comperative Study on the Use of Various Selective Reducing Agents in Automotive DeNOx Systems" (1999).

80. P. M. Schaber, J. Colson, S. Higgins, E. Dietz, D. Thielen, B. Anspach, J. Brauer "Study of the urea thermal decomposition (pyrolysis) reaction and importance to cyanuric acid production" *American Laboratory* **August**, 13 (1999).

81. B. Bann, S. A. Miller "Melamine And Derivatives Of Melamine" *Chem. Rev.* **58**, 131 (1958).

82. O. Kröcher, M. Elsener "Materials for thermohydrolysis of urea in a fluidized bed" *Chem. Eng. J.* **152**, 167 (2009).

83. A. Nishioka, Y. Sukegawa, K. Katogi, H. Mamada, T. Kowatari, T. Mukai, H. Yokota "A Study of a New Aftertreatment System (2): Control of Urea Solution Spray for Urea-SCR" *SAE Int.* **2006-01-0644**, (2006).

84. C. He, Y. Wang, Y. Cheng, C. K. Lambert, R. T. Yang "Activity, stability and hydrocarbon deactivation of Fe/Beta catalyst for SCR of NO with ammonia" *Appl. Catal., A* **368**, 121 (2009).

85. I. Czekaj, G. Piazzesi, O. Kröcher, A. Wokaun "DFT modeling of the hydrolysis of isocyanic acid over the TiO2 anatase (1 0 1) surface: Adsorption of HNCO species" *Surf. Sci.* **600**, 5158 (2006).

86. N. Godbout, D. R. Salahub, J. Andzelm, E. Wimmer "Optimization of Gaussian-type basis sets for local spin density functional calculations. Part I. Boron through neon, optimization technique and validation" *Can. J. Chem.* **70**, 560 (1992).

References

87. J. K. Labanowski, J. W. Anzelm (Eds.) *Density Functional Methods in Chemistry*. (Springer, New York, 1991).

88. J. Grdadolnik, Y. Maréchal "Urea and urea-water solutions – an infrared study" *J. Mol. Struct.* **615**, 177 (2002).

89. A. M. Bernhard, D. Peitz, M. Elsener, O. Kröcher "Quantification of gaseous urea by FTIR spectroscopy and its application in catalytic urea thermolysis" Submitted to *Top. Catal.*

90. A. Schmidt "Verfahrenstechnische Probleme bei der Herstellung von Melamin aus Harnstoff bei Atmosphärendruck" *Oesterr. Chem. Ztg* **6**, 175 (1967).

91. A. N. Alexandrova, W. L. Jorgensen "Why Urea Eliminates Ammonia Rather than Hydrolyzes in Aqueous Solution" *J. Phys. Chem. B* **111**, 720 (2007).

92. M. Baerns, H. Hofmann, A. Renken *Chemische Reaktionstechnik*. (Georg Thieme Verlag Stuttgart, ed. 2. durchgesehene Auflage, 1992), vol. Band 1.

List of publications

Peer-reviewed articles as the first author

1. A. M. Bernhard, I. Czekaj, M. Elsener, A. Wokaun, O. Kröcher „Evaporation of Urea at Atmospheric Pressure" *J. Phys. Chem. A* **115**, 2581 (2011).

2. A. M. Bernhard, D. Peitz, M. Elsener, A. Wokaun, O. Kröcher „Hydrolysis and thermolysis of urea and its decomposition byproducts biuret, cyanuric acid and melamine over anatase TiO_2" *Appl. Catal., B.* **115-116**, 129 (2012).

3. A. M. Bernhard, D. Peitz, M. Elsener, O. Kröcher "Quantification of gaseous urea by FTIR spectroscopy and its application in catalytic urea thermolysis" Submitted to *Top. Catal.*

4. A. M. Bernhard, D. Peitz, M. Elsener, T. Schildhauer, O. Kröcher "Catalytic urea hydrolysis in the selective catalytic reduction of NO_x: Catalyst screening and kinetics on anatase TiO_2 and ZrO_2" *Catal. Sci. Technol.* DOI: 10.1039/C2CY20668D.
    Related to this article, we supplied a **cover artwork**, which was chosen to feature the outside front cover of the issue in which this article will be published. The same arwork is featuring the outside front cover of the presented thesis.

5. A. M. Bernhard, I. Czekaj, M. Elsener, O. Kröcher „Adsorption and catalytic thermolysis of gaseous urea on anatase TiO_2 studied by HPLC analysis, DRIFT spectroscopy and DFT calculations" *Appl. Catal., B.* DOI: 10.1016/j.apcatb.2013.01.009.

Posters

1. A. Bernhard, O. Kröcher, M. Elsener, D. Peitz „Investigation on Urea Decomposition in the SCR Process" *EMPA PhD Symposium*, Dübendorf, Switzerland (November 19th 2009).

2. A. Bernhard, D. Peitz, M. Elsener, O. Kröcher „Investigation of the catalytic urea decomposition in the SCR process" *APAC 2010 International Symposium*, Cracow, Poland (September 8th-11th 2010).

3. A. M. Bernhard, M. Elsener, O. Kröcher „Behavior of urea decomposition byproducts on TiO_2-anatase" *1st Swiss Heterogeneous Catalysis Meeting*, Grindelwald, Switzerland (June 16th-17th 2011).

4. A. M. Bernhard, M. Elsener, D. Peitz, O. Kröcher „Behavior of urea decomposition byproducts on TiO_2-anatase" *EuropaCat X*, Glasgow, Scotland (August 28th – September 2nd 2011).

5. A. M. Bernhard, D. Peitz, M. Elsener, O. Kröcher (presenting) „Catalytic thermolysis of urea into ammonia and HNCO" *15th International Congress on Catalysis*, Munich, Germany, (July 1st-6th, 2012).

6. A. M. Bernhard, D. Peitz, M. Elsener, O. Kröcher „Novel details of catalytic urea decomposition" *Ninth International Congress on Catalysis and Automotive Pollution Control*, Brussels, Belgium, (August 29th-31st 2012).

Other publications

1. D. Peitz, A. Bernhard, M. Elsener, O. Kröcher „Laboratory test reactor for the investigation of liquid reducing agents in the selective catalytic reduction of NO_x" *Rev. Sci. Instrum.* **82**, 084101 (2011).

2. M. Casapu, A. Bernhard, D. Peitz, M. Mehring, M. Elsener, O. Kröcher „A Niobia-Ceria based multi-purpose catalyst for selective catalytic reduction of NO_x, urea hydrolysis and soot oxidation in diesel exhaust" *Appl. Catal., B.* **103**, 79 (2011).

3. M. Elsener, O. Kröcher, D. Peitz, A. Bernhard „Ammonia generator converting liquid ammonia precursor solutions to gaseous ammonia for denox applications using selective catalytic reduction of nitrogen oxides" *Patent application EP11153417, 2011P01935WO*, 2011.

4. D. Peitz, A. M. Bernhard, M. Elsener, O. Kröcher "Liquid-phase catalytic decomposition of novel ammonia precursor solutions for the selective catalytic reduction of NO_x" Submitted to *Top. Catal.*

5. D. Peitz, A. Bernhard, O. Kröcher „Ammonia storage and release" in *SCR systems for mobile applications in Urea-SCR technology for deNO$_x$ aftertreatment of Diesel exhausts* (Springer, accepted).

6. D. Peitz, A. M. Bernhard, M. Mehring, M. Elsener and O. Kröcher „Urea hydrolysis for the selective catalytic reduction of NO_x: comparison of liquid phase and gas phase decomposition" *Chem. Ing. Tech.* DOI: 10.1002/cite.201200183.
    This article is written in German, but the title and the abstract are available in English as well.

Curriculum vitae

Name: Andreas Manuel Bernhard

Date of birth: 29.04.1984

Place of birth: Biel, Switzerland

Nationality: Swiss

Professional education

02/2009 – 11/2012   PhD thesis in the Catalysis for Energy Group at the Paul Scherrer Institut in Villigen, Switzerland under the supervision of Prof. Dr. A. Wokaun at ETH Zurich

03/2008 – 11/2008   Master thesis in the group of Dr. M. Amman at the Paul Scherrer Institut in Villigen, Switzerland under the supervision of Dr. M. Schwikowski at University of Berne

09/2007 – 01/2009   Master studies of Chemistry and Molecular Sciences at University of Berne

04/2007 – 06/2007   Bachelor thesis in the group of Prof. Dr. J. Hulliger at University of Berne

10/2004 – 07/2007   Bachelor studies of Chemistry and Molecular Sciences at University of Berne